ENGINEERING OF RECOMBINANT FORTILIN PROTEIN FOR STRUCTURE ACTIVITY STUDIES

by

Maranda S. Cantrell

A dissertation

submitted in partial fulfillment

of the requirements for the degree of

Doctor of Philosophy in Biomolecular Sciences

Boise State University

August 2021

BOISE STATE UNIVERSITY GRADUATE COLLEGE

DEFENSE COMMITTEE AND FINAL READING APPROVALS

of the dissertation submitted by

Maranda S. Cantrell

Dissertation Title: Engineering of Recombinant Fortilin Protein for Structure Activity Studies

Date of Final Oral Examination: 18 June 2021

The following individuals read and discussed the dissertation submitted by student Maranda S. Cantrell, and they evaluated the student's presentation and response to questions during the final oral examination. They found that the student passed the final oral examination.

Owen M. McDougal, Ph.D.	Co-Chair, Supervisory Committee
Lisa R. Warner, Ph.D.	Co-Chair, Supervisory Committee
Cheryl L. Jorcyk, Ph.D.	Member, Supervisory Committee
Matthew King, Ph.D.	Member, Supervisory Committee
Xinzhu Pu, Ph.D.	Member, Supervisory Committee

The final reading approval of the dissertation was granted by Marie S. Curie, Ph.D., Chair of the Supervisory Committee. The dissertation was approved by the Graduate College.

ACKNOWLEDGMENTS

I need to first and foremost acknowledge my committee co-chairs, Drs. Owen McDougal and Lisa Warner. Dr. McDougal encouraged me to go out of my comfort zone and always provided a gentle nudge in the right direction when I needed it. Without his guidance in verbal communication, I would still be in tears when it came time for me to give public talks. He has helped me in so many ways to overcome my fear of public speaking. My written communication skills have also improved immensely under his guidance, being an amazing scientific writer himself. Owen has been an exceptional mentor and has always encouraged me to not only perform my best but understood that being my best also meant taking breaks and asking if I "went outside/ went on a hike/ went mountain biking" today, because I probably hadn't been outside. Likewise, Dr. Warner has always encouraged me to know when to take a break, for example when a particular sample is bringing out violent tendencies. Lisa has been an excellent mentor, especially in the realm of data analysis and understanding concepts. She is so intelligent when it comes to explaining concepts, I often wonder in awe at her in how she can be so knowledgeable, yet so humble and easy going. She is an example of someone I would like to be when, and if, I ever do grow up.

I would also like to acknowledge my committee members Dr. Jorcyk, Dr. King and Dr. Pu. Dr. Jorcyk is always one to ask the tough questions during a talk and it was for that reason I asked her to be on my committee. Those tough, sit-and-think-about-it questions are the best for expanding your knowledge set and her questions have forced

me to expand my thinking beyond just what I do in the lab. Dr. King is always kind and willing to lend a hand when it comes to my computational work and was invaluable for the work done in Chapter 4 of my dissertation. He is always helpful and around even if It's just for a chat in the chemistry hallway. Dr. Pu was critical to obtaining all of the mass spectrometry data and worked so diligently during the pandemic to get me the final mass spec data I needed for my publications, and for that I must thank him immensely. He is always willing to lend a helpful hand.

Lastly, I would like to acknowledge the family, friends, BMOL cohorts and lab mates for the support along the way. You know who you are.

ABSTRACT

Cardiovascular disease (CVD) is the leading cause of death worldwide affecting approximately 40% of all adults over the age of 20 and is responsible for an economic burden upwards of $3 billion annually. Treatments for CVD are limited to either hypertension medication to treat symptoms, and/or statin-based drugs to reduce low-density lipoprotein (LDL) cholesterol formation. However, recent studies suggest that approximately 50% of patients diagnosed with CVD have normal to low LDL cholesterol levels. Therefore, a critical need exists to develop new treatments for CVD that are independent of cholesterol lowering statins. Fortilin, also known as translationally controlled tumor protein (TCTP), is a 19kDa, 172 amino acid cytosolic protein ubiquitously expressed in all cell types, at all stages of life. Fortilin overexpression in arterial walls has been shown to propagate atherosclerotic plaque formation, a major component of CVD. Fortilin is therefore a promising target for the rational design of drugs to prevent formation of new plaques.

For a structure-based drug development process, recombinant protein is required to characterize potential protein-drug interactions. Recombinant expression and purification of fortilin has proven to be effectual, provided any affinity tag used for purification is not cleaved. Here, we designed several constructs of recombinant fortilin fusion protein and were the first to successfully cleave the affinity tag, making structural activity studies more meaningful due to greater semblance to the native protein. Our new construct, GGS-fortilin, can be produced in high yield with greater than 85% tag

cleavage, but still contains the three amino acid linkers at the N-terminus. To determine whether these three amino acids, Gly-Gly-Ser interfered with small molecule inhibitor (SMI) binding, loop constructs were designed, wherein the affinity tag, a Strep-Tactin peptide with the sequence WSHPQFEK, was placed at either the C terminal side of Arg37, Ser46 or Gly56 within the flexible loop of fortilin's highly conserved structure and activity validated via calcium titration. Structural analysis and SMI binding studies were performed for the loop constructs using circular dichroism (CD) and nuclear magnetic resonance (NMR) spectroscopy.

NMR spectroscopy is a dynamic tool used in structure-based drug development to characterize the structure of recombinantly expressed protein and to determine binding sites for SMIs. The results presented here portend to the development of novel fortilin constructs and structural studies with SMIs. Structural integrity was validated for the loop constructs using CD and NMR, and activity validated with an NMR calcium binding assay. Binding studies were also attempted using differential scanning fluorimetry (DSF) and NMR.

TABLE OF CONTENTS

LIST OF TABLES

LIST OF FIGURES

LIST OF ABBREVIATIONS

6His	6-histidine
ADAMTS7	a disintegrin and metalloproteinase with thrombospondin motifs TS7
AICAR	aminoimidazole-4-carboxamide ribonucleotide transformylase
AMPK	5'-adenosine monophosphate-activated protein kinase
ASK1	apoptosis signal-regulating kinase-1
BMP	bone morphogenic proteins
CAD	coronary artery disease
CD	circular dichroism
CHFR	checkpoint with forkhead and ringfinger domain
CV	column volume
CVD	cardiovascular disease
cyt C	cytochrome C
D_2O	deuterium oxide
d-DTT	deuterated dithiothreitol
DHA	dihydroartemisinin
DHFR	dihydrofolate reductase
DNA	deoxyribonucleic acid
DSF	differential scanning fluorimetry
EGFR	epidermal growth factor receptor

eIF1A	elongation factor 1A
ER	endoplasmic reticulum
ERE1α	inositol-requiring enzyme 1α
FACS	fluorescent assisted cell sorting
FDA	Food & Drug Administration
GAMPMS	genetic algorithm managed peptide mutant screening
GGS	glycine-glycine-serine
GST	glutathione S-transferase
GWAS	genome wide association studies
HA	hemagglutinin
HMG-Co-A	3-hydroxy-3-methyl-gutaryl-Co-A
HRF	histamine release factor
HRV 3C	human rhinovirus 3C
HSQC	heteronuclear spin quantum correlation
HTS	high throughput screening
JNK	Jun N-terminal
IL-1R	interleukin-1 receptor
IL-1β/1/6	interleukin-β/1/6
IP3	inositol triphosphate receptor
IPTG	isopropyl-β-d-1-thiopyranogalactoside
LB	Luria Bertani
LDL	low-density lipoprotein
LTA_4H	leukotriene A_4 hydrolase

Mφ	macrophage
MBP	maltose binding protein
mPTP	mitochondrial permeability transition pore
Mss4	mitochondrial permeability transition pore
Mst1	mammalian sterile twenty-1
MyD88	myeloid differentiation response protein 88
nAChR	nicotinic acetylcholine receptor
NaCl	sodium chloride
NADPH	nicotinamide adenine dinucleotide phosphate
NaF	sodium fluoride
NETs	networks of chromatin granules
NFκB	nuclear factor κB
NKEF	natural killer enhancing factors
NIH	National Institutes of Health
NMR	nuclear magnetic resonance
NO	nitric oxide
OSM	oncostatin M
oxLDL	oxidized LDL
PAH	pulmonary arterial hypertension
PBS	phosphate buffered saline
PCR	polymerase chain reaction
PD	Parkinson's disease
PDB	Protein Data Bank

PES	polyethersulfone
PLK1	polo-like kinase-1
PRX-1	peroxiredoxin-1
PTM	post-translational modification
RNA	ribonucleic acid
ROS	reactive oxygen species
SBDD	structure based drug design
SMI	small molecule inhibitor
SNP	single nucleotide polymorphism
SPIDR	small molecule peptide influenced drug repurposing
SPR	surface plasmon resonance
SSDBD	single-stranded DNA binding domain
TCEP	tris(2-carboxyethyl)phosphine
TCTP	translationally controlled tumor protein
TEV	tobacco etch virus
TNF-α	tumor necrosis factor α
TSP	trimethylsilylpropanoic acid
UMLS	Unified Medical Language System
UPR	unfolded protein response
XBP1	X-box binding protein-1

CHAPTER ONE: INTRODUCTION

1.1 The Drug Discovery Process: Drug Repurposing in Cardiovascular Disease

Section 1.1 published in *Pharmaceuticals* (Open Access)

Maranda S. Cantrell[1,2], Alejandro Soto-Avellaneda[1,3], Jackson D. Wall[2], Aaron D. Ajeti[2], Brad E. Morrison[3], Owen M. McDougal[1] and Lisa R. Warner[1]

[1]Biomolecular Sciences Ph. D. Program, Boise State University,

[2]Department of Chemistry and Biochemistry, Boise State University

[3]Department of Biology, Boise State University

1.1.1 Introduction

Drug development is a long, labor-intensive process with no guarantee of success. On average, it takes 10 years and 2.6 billion dollars to develop a new drug, with success rates averaging only about 12%.[1] One way to mitigate the barriers of drug development is to repurpose Food and Drug Administration (FDA) approved drugs for the treatment of different diseases. Drug repurposing is the practice of finding new uses for existing drugs at any stage of development. The benefit of drug repurposing is that the risk of failure is significantly lower than drug development, which permits more effective use of resources to optimize drug efficacy for treatment of the desired ailment. Much of the primary research regarding repurposed drug safety, mechanism, and dosage has already been completed at the time the drug was first studied.[2] For example, a drug that demonstrated efficacy in animal models with low side effects but failed in human clinical trials to perform its intended purpose, may be a good candidate for use as a therapeutic for a

different disease. Drugs with potential to be repurposed have progressed through many of the steps required to meet regulatory safety and potency benchmarks, allowing for an accelerated and abbreviated path to FDA approval. A few representative examples of successful drugs that have been repurposed include amantadine, acetylsalicylic acid, mecamylamine, minoxidil, and tamoxifen (**Table 1**).[3] Repurposed drugs are generally screened by computer search algorithms from databases of therapeutics that may or may not have been sufficiently effective in providing treatment for the pathology that served as their original target. For example, some drugs lack sufficient drug-like qualities to warrant further investigation for treatment of an intended illness, but modification of the molecular scaffold or functional groups attached to the drug template may afford attributes and activity suitable for therapeutic viability. The therapeutic index for a repurposed drug requires investigation into dosage recommendations for maximal benefit to counter the illness, while minimizing detrimental side-effects to the patient.

Table 1.1 Examples of some FDA-approved repurposed drugs.

Drug	Original purpose	Repurposed use	Reference
Amantadine	Parkinson's disease	Influenza A	4
Acetylsalicylic acid	Inflammation, pain relief	Anti-platelet	5
Cyclosporine	Rheumatoid arthritis	Transplant rejection, psoriasis, chronic dry eye	6
Minoxidil	Hypertension	Alopecia	7
Imatinib	Chronic myelogous leukemia	Gastrointestinal stromal tumor	8

1.1.1.a Technology to repurpose drugs

Computational screening of previously marketed drugs to identify drug repurposing candidates can lead researchers to initiate new clinical trials for treatment of alternative ailments. Multiple computational strategies have emerged to identify potential candidates

for drug repurposing. Of these, four strategies have gained popularity in recent years and will be discussed in brief. These strategies are side effect similarity mapping, genome-wide association studies (GWAS), small-molecule peptide-influenced drug repurposing (SPIDR), and computational high throughput screening (HTS).[9–11]

In side-effect similarity mapping, existing drugs are categorized by their side effects using the Unified Medical Language System (UMLS) ontology for medical symptoms. Developed by Campillos et al. (2008), 746 marketed drugs were organized according to their listed phenotypic side effect similarities rather than a chemical similarity, and 20 of these marketed drugs were confirmed through *in vitro* assays to indicate that side effect similarity may be indicative of common protein targets. Using this strategy, prediction of the likelihood that two drugs had the same target based on their side effects was demonstrated.[12] This study describes a process by which drugs marketed for different targets could be identified as having potential for repurposing.

GWAS identify single nucleotide polymorphisms (SNPs) and their associated phenotypes for individuals with a given disease. GWAS is performed by genotyping individuals which share a common disease and determining whether a genetic variant is shared to statistical significance among this population. Experimental validation by chromatin precipitation is then performed and variants are associated by phenotypic effects.[13] This technique has been used to identify many novel variants to trait associations in a variety of diseases such as macular degeneration, anorexia nervosa, depression, coronary artery disease and diabetes mellitus, and can be used to determine novel drug targets as well.[13,14] For example, GWAS have been used to identify SNPs for Parkinson's disease (PD) and determined that estradiol may protect dopaminergic neurons in PD. This

supported previous evidence that estradiol may be protective against PD because men are more likely to be diagnosed.[15] The neuroprotective role of estradiol was later confirmed in *in vivo* studies. At present, estradiol is still not an approved treatment for PD, but efficacy studies are ongoing.[2,16,17] Another example of GWAS being useful for determining novel drug targets was the identification of a gene encoding a disintegrin and metalloproteinase with thrombospondin motifs TS7 (ADAMTS7), a gene implicated in coronary artery disease (CAD) for its presence in angiographic CAD patients and role in smooth muscle cell migration, a finding that supports the idea of genetically inherited CAD.[18,19] Using GWAS, it is possible to identify new potential targets based on SNPs.

SPIDR is a recently developed computational screening technique to identify drugs that can target a specific receptor by looking at its peptide ligand conformational space.[11] This method was integrated into the free program DockoMatic v 2.1, making this process accessible to lower resourced institutions.[20] This technique works by first utilizing the genetic algorithm managed peptide mutant screening (GAMPMS) to search for peptide mutants with high binding affinity to the receptor, and then this population of peptides is moved over to the SimSearcher utility to identify the best small molecules analogous to the peptide population for binding to the isoform.[11] SPIDR was developed and used to find 12 small molecules computationally predicted to bind with high affinity to a nicotinic acetylcholine receptor (nAChR) isoform associated with Alzheimer's and PD, by looking at α-conotoxin MII peptide analogs that would bind favorably to the receptor isoform specifically.[11] Following this publication, a qualitative assay to detect dopamine release by ligand action on nAChRs was developed with the intent to assess bioactivity of molecules that may act on different nAChR isoforms for drug development. This assay was created

using a luminescence-based assay and validated with known nAChR binders: acetylcholine, nicotine and cytosine.[21] The PC-12 cell-based assay was intended to be used to test the small molecules found in the SPIDR development publication for nAChR activity as an *in vitro* validation for the SPIDR methodology.

Additionally, small molecule compound screens can be used to identify drugs amenable to being repurposed. Computational programs such as AutoDock Vina are often used to screen molecular library databases like ZINC, chEMBL, pubchem, DrugBank, and others.[22–24] Computational screens of small molecule databases are an ideal starting point for any drug discovery project to narrow down a list of compounds that may bind a biological target with high affinity. However, wet lab experimentation needs to be conducted, which can be done with commercially available libraries of drugs using *in vitro* cell-based assays. Researchers study whether a drug induces a phenotypic effect in cell-based assays, which are usually performed in cell culture or on a model organism whereas a target-based screen can be performed *in vitro* using techniques like enzyme-linked immunosorbent assay (ELISA), surface plasmon resonance (SPR) or nuclear magnetic resonance (NMR) spectroscopy. Many reviews have been recently published on the topic of drug repurposing in either CVD or neurodegeneration.[25–31] However, there is little explored in the realm of drugs that may be repurposed to target inflammatory processes which link these two diseases. In this article we will briefly discuss strategies for repurposing drugs and examples of drugs that are being repurposed for treatment of cardiovascular disease and neurodegenerative disorders. Specifically, we will cover those conditions that affect both cardiovascular and neurodegenerative disease such as inflammatory pathways, which are intimately connected in both heart and brain disease.

Currently, repurposed drugs are being used in studies associated with two cardiovascular related diseases that include endothelial dysfunction and pulmonary arterial hypertension. In neurodegenerative diseases, repurposed drugs are being studied for the treatment of autophagy and neuroinflammation (**Table 2)**.

Table 1.2. Examples of drug or drug targets that have been identified using computational methods.

Drug or target	Target pathology	Research method	Reference
kinase inhibitors	Alzheimer's disease	machine learning	
dopaminergic agonists	Parkinson's disease	machine learning	26
beta-secretase 1 inhibitors	Alzheimer's diseases	data mining	32
GIST-T1 cells	Gastrointestinal stromal tumor	high throughput synergy screening	33

1.1.2 Targeting endothelial dysfunction in cardiovascular diseases

Cardiovascular diseases include atherosclerosis, coronary artery disease and arrhythmias that eventually lead to myocardial infarction and/or stroke. Ischemic events such as these are the leading cause of death in the world.[34] Pharmacological intervention of cardiovascular diseases is provided by statins, beta-blockers, and angiotensin converting enzyme inhibitors. In more advanced cases, surgical intervention may be necessary. The medications for cardiovascular disease target high cholesterol and low-density lipoprotein levels, and hypertension. There is an emerging field of research to discover small molecule inhibitors for alternative pathways aimed at the disruption of heart disease progression.[35] There is a robust market for pharmaceutical companies to synthesize drugs to treat disorders, but the potential for repurposing already FDA-approved drugs constitutes a desirable alternative to discovery since these medications have been deemed safe enough for patient use and thus make clinical trials for novel use

less trivial.

The endothelium is characterized by the cells of the tissue lining the various organs of the body, including the arteries and lymphatic system. The endothelium plays a major role in blood flow and constriction by facilitating the synthesis and degradation of vasodilating factors, such as nitric oxide (NO), arachidonic acid metabolites and reactive oxygen species (ROS).[36] Endothelial dysfunction occurs when the endothelium fails to function properly. Namely, that the endothelium dysfunctions in the formation of vasodilating factors. Endothelial dysfunction is especially important in cardiovascular disease because it is a leading contributor to cardiac events. Endothelial dysfunction is a component of atherosclerosis, which is characterized by the hardening and narrowing of the arterial walls, and hyperlipidemia, or high lipid concentrations in the blood.

Three drugs investigated for their potential to treat diseases of endothelial dysfunction that will be discussed here include colchicine, which has been traditionally used to treat gout, methotrexate, an immunosuppressant and chemotherapy drug, and tocilizumab, an immunosuppressant used to treat severe rheumatoid arthritis.

1.1.2.a Colchicine

Colchicine is a secondary metabolite from the plants *Gloriosa superba* and *Colchicum autumnale,* that is known to be toxic when ingested.[37] Its current approved use is to treat gout, an inflammatory form of arthritis common in people with high levels of uric acid in their blood. Due to its anti-inflammatory properties, colchicine is currently under investigation as a potential endothelial dysfunction drug. Endothelial dysfunction is a characteristic of cardiovascular disease that leads to an increase in macrophages, T

lymphocytes and growth factors that contribute to atherosclerotic lesion formation associated with atherosclerosis.[38–41] The same inflammation inhibition mechanism that permits colchicine to be effective against gout, may also be applicable to the treatment of patients with early stages of atherosclerosis.[42,43]

Colchicine prevents inflammation by binding to tubulin, preventing tubulin polymerization and function (see **Figure 1.1**).[18] As a result, colchicine halts mitotic cells in metaphase. Colchicine also concentrates in neutrophils and prevents chemotaxis via the release of crystal-derived chemotactic factor, and inhibits monosodium urate induced loss of myeloid inhibitory C-type lectin-like receptor in neutrophils and interleukin-8 formation.[44] Myeloid inhibitory C-type lectin-like receptor and interleukin-8 are important in immune homeostasis and inflammatory response.[45,46]

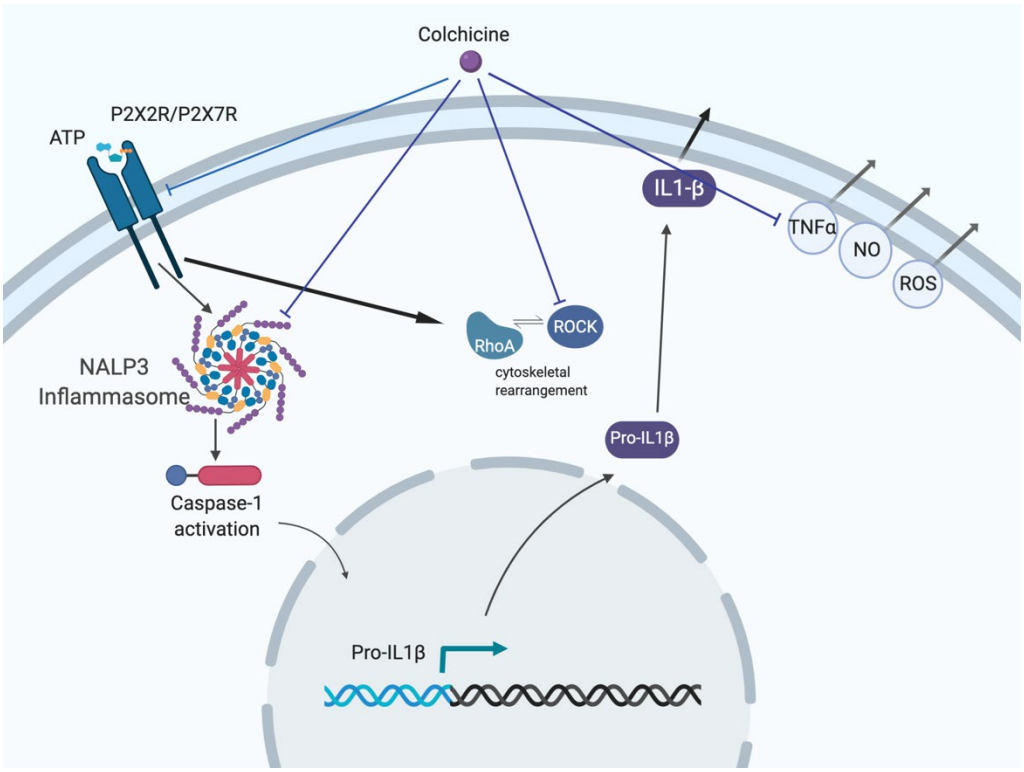

Figure 1.1. Inhibitory pathway of colchicine. Colchicine inhibits activation of purinergic P2X2/P2X7 receptors and blocks cation uptake and subsequent pro-inflammatory signaling cascades without affecting cell death. Colchicine also inhibits the NALP3 inflammasome pathway, the Rho/ROCK pathway via cytoskeleton rearrangement, and inhibits release of ROS, NO and TNF□. Figure 1.1 was created using BioRender.com (adapted from 44).

Cell adhesion is the process by which cells adhere to one another through the action of proteins, electrostatic interactions, and hydrophobic interactions. Adhesion is important because cells can use physical contact with one another to communicate via signal transduction. Colchicine interferes with cell adhesion by inducing the shedding of neutrophil adhesion molecules, which are important in neutrophil function.[44] These neutrophil adhesion molecules include selectins and counter receptors which partake in signal transduction. Selectins are single-chain transmembrane glycoproteins organized by leukocyte (L), endothelial (E) and platelet/endothelial (P) selectins. They are characterized by their similar homology in both sequence, structure and sugar ligands.

Colchicine reduces endothelial expression of selectins by acting on leukocytes in coronary artery disease.[43]

Nidorf et al. reviewed ongoing clinical trial results and experimental evidence that supported the use of colchicine as an anti-inflammatory drug with promising efficacy toward the treatment of atherosclerosis.[42] First, they describe the mechanisms by which colchicine acts on the various inflammatory pathways including the production of pro-inflammatory cytokines, such as interleukin (IL)-1ß, reduction of platelet leukocyte interactions that lead to atherothrombosis and suppressing the growth of fibroblasts and osteophytes. At lower doses, colchicine was found to have no reported side effects on patients with liver and/or kidney disease.[42] The authors concluded that colchicine could be repurposed for treatment of inflammation associated with atherosclerosis.

1.1.2.b Methotrexate

In the 1960's, the National Institutes of Health reported that methotrexate (**Figure 1.2**) was effective at treating rheumatoid arthritis and psoriatic arthritis. However, the rheumatology field at the time maintained a fidelity for corticosteroids to treat rheumatic syndromes, which stifled the use of methotrexate. Subsequent studies were conducted, establishing evidence that methotrexate was effective in the treatment of rheumatoid arthritis.[47]

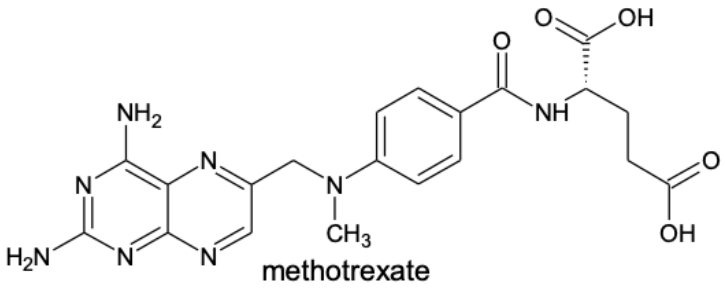

Figure 1.2. Chemical structure of methotrexate.

Methotrexate is a synthetic disease-modifying anti-rheumatic drug that is a structural analog of folic acid.[48] Methotrexate was originally used as a cancer drug but has recently been investigated for its use in inflammation associated with endothelial dysfunction. In a study of 673 patients, methotrexate was used for the treatment of rheumatoid arthritis, and was determined that under proper dosing and use, it could be a beneficial drug to treat arthritis with 1.7% adverse side effect frequency and 0.15% mortality.[49] Methotrexate was identified as a good candidate for use to treat inflammatory diseases, including endothelial dysfunction.

Methotrexate exerts a multitude of biochemical and biological perturbations when administered to patients. While the exact or primary mechanism of action is not completely understood, multiple modes of activity have been characterized that reveal how methotrexate functions (**Figure 1.3**). First, methotrexate diminishes the immune response by increasing the rate of T cell apoptosis. Methotrexate binds dihydrofolate reductase, causing an increase in nitric oxide synthase uncoupling through the prevention of the conversion of dihydrobiopterin to tetrahydrobiopterin (**Figure 1.3a**). Second, methotrexate suppresses inflammation and the immune response by promoting the release of adenosine. Metabolites of methotrexate inhibit aminoimidazole-4-carboxamide ribonucleotide (AICAR) transformylase, causing an increase in the concentration of

intracellular AICAR and thus more adenosine release (**Figure 1.3b**). Third, methotrexate increases the expression of long intergenic non-coding RNA p21, a mediator and regulator of a variety of pro-apoptotic processes (**Figure 1.3c**).[50]

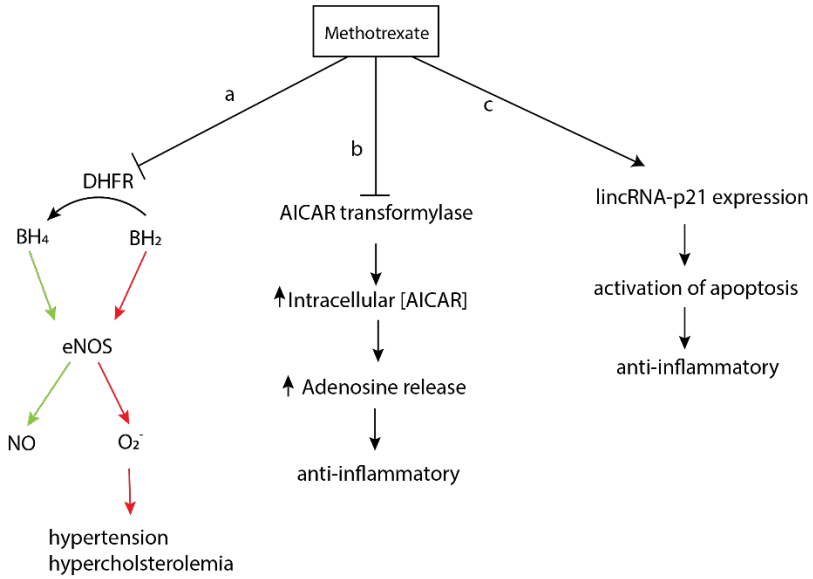

Figure 1.3. Metabolic pathways of methotrexate. a) Methotrexate inhibits dihydrofolate reductase (DHFR) and prevents conversion of dihydrobiopterin (BH2) to tetrahydrobiopterin (BH4), leading to uncoupling of NO synthase. b) Methotrexate inhibits AICAR transformylase, leading to increased adenosine levels and subsequent anti-inflammatory responses. c) Methotrexate stimulates lincRNA-p21 expression, leading to increased apoptotic gene expression and subsequent anti-inflammatory responses.

There is increasing evidence that the 5′-adenosine monophosphate-activated protein kinase (AMPK) is beneficial to the endothelium by protecting against apoptosis, oxidative stress and increases NO production in the endothelium, which reduces cholesterol efflux activity.[48] Stimulation of AMPK as a treatment for endothelial dysfunction is under investigation. One study showed that application of methotrexate on perivascular adipose tissue from Sprague-Dawley rats increased AMPK activity under basal and inflammatory conditions when treated with a negative control, palmitic acid.[48] A positive control using aminoimidazole-4-carboxamide ribonucleotide, a known AMPK

agonist, was also able to stimulate AMPK activity.[48] This study similarly showed that methotrexate stimulated adiponectin mRNA expression and suppressed the pro-inflammatory molecules nuclear factor kappa B (NFκB) p-65, tumor necrosis factor alpha (TNF-α), and interleukin-6 (IL-6) activity.[48] At the time of this review, only studies of methotrexate on perivascular adipose tissue taken from sacrificed mice and *in vitro* studies in cell culture have been performed, necessitating investigation into more physiologically relevant in vivo model systems.

Contrarily, other studies have indicated that methotrexate may contribute to vascular endothelial dysfunction by causing endothelial damage.[51] Methotrexate is a direct competitor with folic acid for the active site of human serum albumin, and indeed folic acid supplements are often provided in conjunction with methotrexate to prevent folic acid deficiency.[52] A study performed in Wistar rats, by Sankrityayan in 2016, showed that when administered with methotrexate, *ex vivo* vascular reactivity in the aorta was significantly reduced.[51] Vascular reactivity is the phenomenon responsible for both vasoconstriction and vasodilation, and those responses to various stimuli implicated in vasculature. Methotrexate has also been implicated in the reduction of NO, leading to increased oxidative stress and hindering of bioavailability of tetrahydrobiopterin by oxidizing it to dihydrobiopterin in the aorta.[53,54] This leads to hypertension, hyperlipidemia and induces endothelial dysfunction, because tetrahydrobiopterin is necessary as a cofactor required for synthesis of NO.[55]

There is contradicting evidence for methotrexate use as an endothelial dysfunction drug. On one hand, there is data that suggests methotrexate reduces inflammation, while

on the other hand, methotrexate appears to lead to endothelial dysfunction. Therefore, more studies must be performed to determine the true mechanism of action for methotrexate on the vascular endothelium if it is to be used to treat endothelial dysfunction. There are currently 2140 clinical trials listed under the National Library of Medicine's clinical trial database with methotrexate being evaluated for treatment of everything from ectopic pregnancy, to schizophrenia, to alopecia, and cancer. It appears that in many pathologies where inflammation is a principal concern, or where immunomodulation is of utility, methotrexate may provide benefit.

1.1.2.c Tocilizumab

Tocilizumab (TCZ) is an IL-6 inhibitor and recombinant monoclonal antibody used in rheumatoid arthritis treatment since obtaining FDA approval in 2010.[56] TCZ binds IL-6 and blocks JAK/STAT signaling to prevent the production of pro-inflammatory molecules.[56,57] It is currently being investigated for the treatment of endothelial dysfunction due to its anti-inflammatory properties. This is because RA is often listed as a co-morbidity in approximately 39-50% of atherosclerosis-related deaths, with endothelial dysfunction presented in many RA patients.[58] One hypothesis is that the release of networks of chromatin and granules (NETs) into the extracellular space, a common occurrence in both RA and endothelial function. TCZ was found to alleviate symptoms in endothelial dysfunction in a human clinical study.[57]

1.1.3 Targeting Pulmonary Arterial Hypertension

Pulmonary arterial hypertension (PAH) is a relatively rare condition, affecting approximately 10-52 people per million population, characterized by the narrowing of the pulmonary arteries.[59,60] Left untreated, pulmonary arterial hypertension leads to the

buildup of pressure on the right side of the heart when blood vessels in the lungs are diseased, causing the arteries to become increasingly narrow with time, and right-sided heart failure, often resulting in premature death.[61,62] While the direct cause of pulmonary arterial hypertension is unknown, a set of factors including liver disease, HIV infection, intravenous drug use, autoimmune disorders, and others are suspected to be culpable. For pulmonary arterial hypertension, there are several drugs under investigation for use in PAH in clinical trials and are discussed in detail.[63] Of these, two drugs, Anakinra and Tadalafil, target inflammatory processes specifically.

1.1.3.a Anakinra

Anakinra was approved for use in rheumatoid arthritis by the FDA in 2001. Anakinra is currently under investigation and has undergone Phase I clinical trial studies for novel use in PAH.[63,64] Anakinra, an interleukin-1 (IL-1) receptor protein antagonist analogue, is recombinantly expressed in *E. coli* and is administered via subcutaneous injection. The proposed mechanism of action for PAH, done in mice, is such that anakinra blocks perivascular macrophage recruitment in pulmonary artery smooth muscle cells.[65] In an inflammatory response pathway, IL-1β binds to IL-1 receptor (IL-1R) and recruits the myeloid differentiation primary response protein 88 (MyD88) and induces IL-1 synthesis via NFκB activation. In this study, the goal was to investigate whether this pathway played a role in the progression of PAH.[65] First, it was determined that in both the lung tissue taken of patients with PAH as well as mice with PAH, there were increased expression levels of both IL-1R and MyD88. In IL-1R$^{-/-}$ and MyD88$^{-/-}$ mice, severity of PAH was not significantly different between the two but were significantly lower in severity than hypoxic wild-type mice. Hypoxic wild-type mice treated with

anakinra (20 mg/kg per day) were shown to have lower severity in PAH symptoms, namely, right ventricular systolic presser and hypertrophy, than untreated mice. It was also observed than in both IL-1R$^{-/-}$ and MyD88$^{-/-}$ hypoxic mice as well as wild-type mice treated with anakinra, there was no significant fold change in IL-1β levels when compared to wild-type untreated mice with hypoxia over 48 hours. These findings suggest that anakinra is a good potential treatment for PAH in that IL-1β is not having to be expressed as an emergency measure for PAH. Furthermore, the pilot Phase I clinical study (clinicaltrials.gov: NCT03057028) done with treatment of PAH by anakinra found promising results by inducing IL-1 blockade.

1.1.3.b Tadalafil

Tadalafil is currently used to treat erectile dysfunction and benign prostatic hyperplasia, and was approved by the FDA in 2009 for treatment of pulmonary arterial hypertension.[63,66]Tadalafil is a phosphodiesterase type-5 (PDE5) inhibitor.[67] PDE5 mRNA levels are mostly found in the cerebellum, kidney, pancreas, and rat lung tissues, which may be indicative of human mRNA localization.[68] The result, here, is such that cyclic guanosine monophosphate (cGMP) concentrations are elevated and thus facilitate the NO pathway, namely vasodilation.[69] In brief, cGMP binds to PDE5 and increases catalytic activity approximately 10-fold, leading to a decrease in protein kinase G (PKG) stimulation and ultimately affecting vascular tone and growth in erectile dysfunction.[70] The inhibition of PDE5 leads to elevated cGMP and NO levels.

The 16-week, double-blind, phase III clinical trial that led to FDA approval of tadalafil for pulmonary arterial hypertension treatment consisted of 405 patients diagnosed with PAH. The patients were given a prescribed dosage of tadalafil or placebo,

and their performance to walk for 6-minutes was evaluated based on the distance they covered.[69] The findings of the study identified that an oral dosage of 40 mg per day of tadalafil could improve exercise capability by an average of 33 m in patients with pulmonary arterial hypertension versus the placebo patients. Dosage was weight-dependent, though all patients weighed an average of 75 ± 22 kg in this study. Of the 357 patients that participated in a long-term study with tadalafil, 295 of them continued treatment. While this study, along with other clinical trials, showed vast improvements in patients with pulmonary arterial hypertension, the molecular mechanism by which tadalafil acts as a therapeutic has yet to be elucidated.

1.1.4 Conclusion

The benefit of repurposing drugs that have previously been FDA approved removes many of the time and financial barriers for bringing a drug to market. FDA approval is a good indication of a drug's effectiveness and safety in clinical trials, which is indicative of a good outcome for the use of a drug for a different purpose. Because a drug can take anywhere from 8-12 years to go from initial discovery to the market, drug repurposing can cut this time significantly.[1] The repurposing of drugs to treat cardiovascular and neurodegenerative diseases is an emerging and promising field of study. Treatments for inflammatory diseases including vascular endothelial dysfunction, pulmonary arterial hypertension, multiple sclerosis, Parkinson's and Alzheimer's, using repurposed drugs like colchicine, methotrexate, tocilizumab, felodipine, lonafarnib, dimethyl fumarate and exemestane may prove to be an effective strategy to address the treatment gap for untreatable ailments.

1.2 A Review of Fortilin: Cellular Pathways, Functionality and Current Research Efforts

1.2.1 Introduction

Fortilin, also known as p21, p23, histamine release factor (HRF), and translationally controlled tumor protein (TCTP) is a cytosolic protein ubiquitously expressed in all cell types and is prevalent during all stages of life.[71] Since its initial characterization in 2001, fortilin has been implicated in many diseases including many cancers, malaria, CVD, pulmonary arterial hypertension (PAH), diabetes, and even some developmental disorders.[35] While fortilin has become recently recognized for its anti-apoptotic function in the progression of disease, fortilin is also required for optimal cell growth, cell proliferation, and cell cycle progression.[72]

Reviews to date focus on fortilin dysregulation in disease rather than the qualities that make fortilin unique. Here, we discuss the structure of fortilin across different species as well as the known cellular pathways of fortilin. We separate the known pathways into anti-apoptotic and pro-survival for the reason that fortilin not only prevents programmed cell death, but also contributes to cell proliferation during early development. We conclude by outlining current research efforts for targeting fortilin function in disease. The structure of fortilin is characterized by the N and C termini in close proximity to one another, a hydrophobic core split into an α-helical region and a β sheet region, and a flexible loop section (**Figure 1.4**).

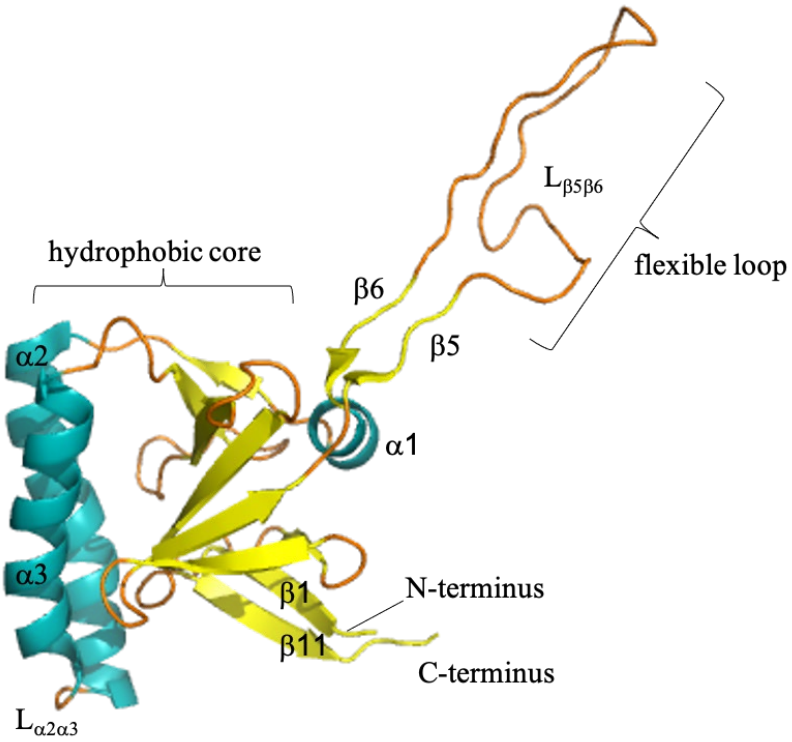

Figure 1.4. Structure of fortilin. The structure of fortilin consists of 172 amino acids encompassing 3 □ helices (aqua), 3 anti-parallel □ sheets consisting of 11 □ strands (yellow) and several non-structured loops (orange) that connect the protein. The flexible loop exists from T39 to V66. The N and C termini of fortilin are proximal in location and form part of the □ barrel comprised of □ strands 1-4 and 8-11.

1.2.2 Structure of Fortilin: Characteristics and Cross-Species Homology

Fortilin is unique in both structure and sequence because it does not belong to any classified family of proteins, though one study has shown that fortilin has some structural similarity to guanine nucleotide-free chaperone protein Mss4 (**Figure 1.5**).[73] As shown in **Figure 1.4**, fortilin consists of 3 alpha helices and 11 beta sheets, of which 9 form a rigid beta barrel. The structure of fortilin is quite rigid, with a flexible loop domain between residues T39 and V66 in human fortilin. Fortilin also consists of a highly conserved protein sequence across species and is found in all eukaryotic organisms, with a molecular weight ranging from 19 to 23 kDa.[74] Its taxonomic lineage can be traced

among all domains of life, and cellular localization of fortilin is largely found in the cytosol, though fortilin is also found in the nucleus.[71] A representation of the sequence homology is shown in **Figure 1.6**. This protein sequence homology corresponds to physical structural conserved relationships amongst different species, namely the flexible loop domain, for which a role in functionality has not yet been determined.

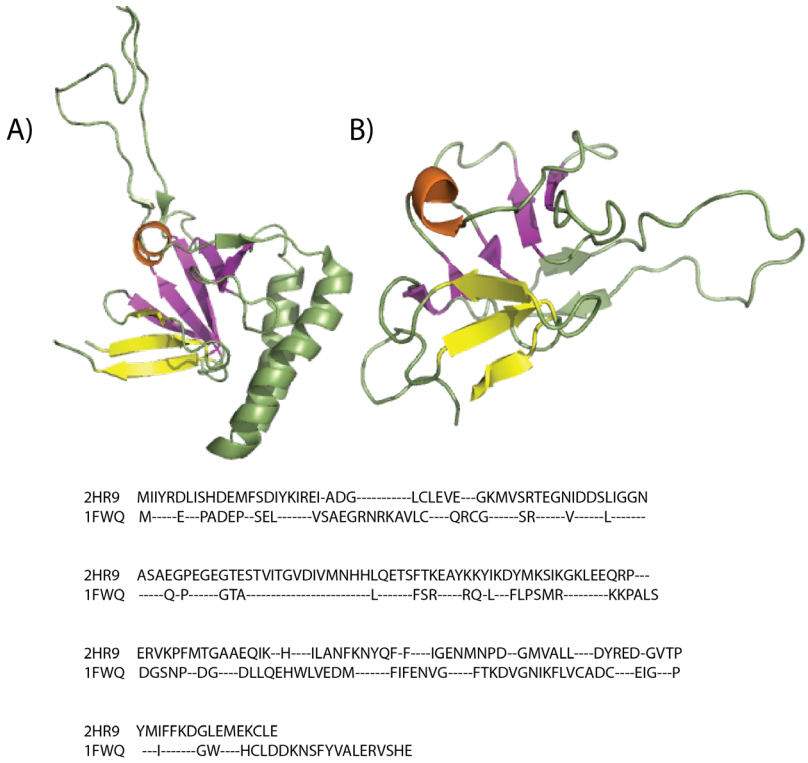

Figure 1.5. Structural similarities of fortilin and Mss4. Structural similarities highlighted between A) human fortilin (PDB 2HR9) and B) human Mss4 (PDB 1FWQ) protein. Primary similarities include the α helix (orange), and beta sheets (purple and yellow). Below is the protein sequence alignment for human fortilin and human Mss4. Mss4 has approximately 23.8% sequence homology to fortilin using LALIGN.[75]

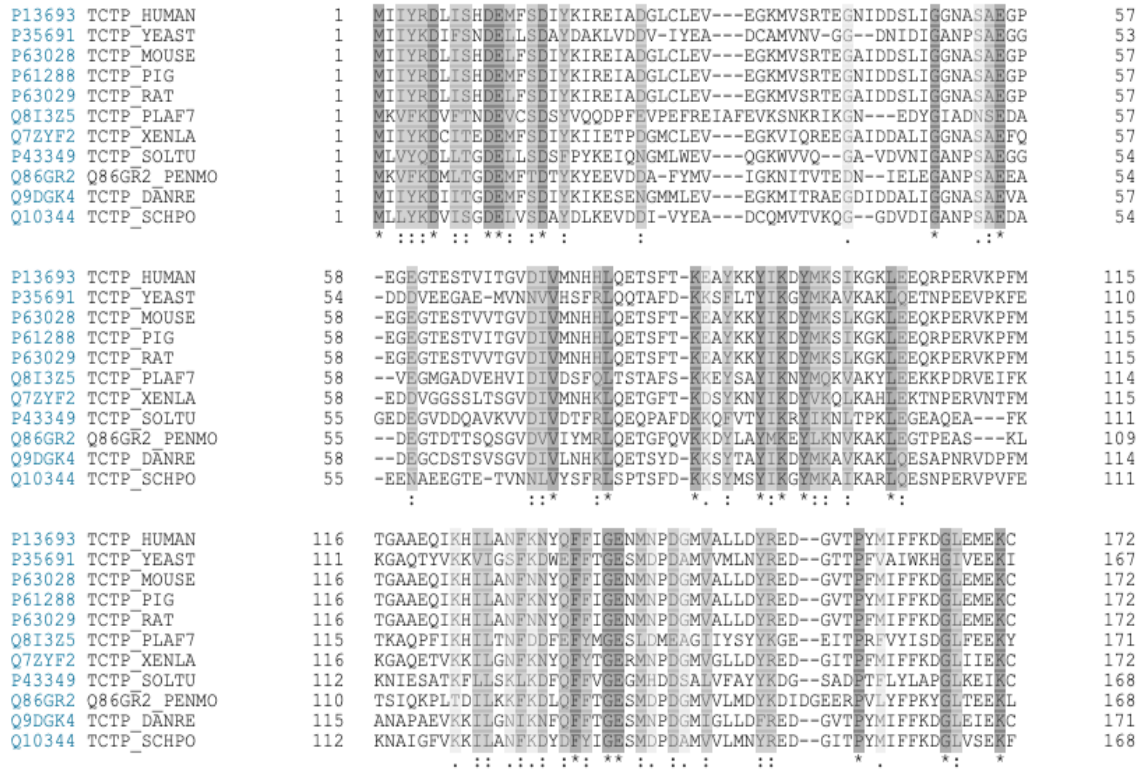

Figure 1.6. Sequence homology of fortilin. Multiple sequence alignment of fortilin protein in different species. Uniprot.org identifier is provided on the left with species name. Residues highlighted in dark grey have 100% sequence homology while residues highlighted in lighter greys have at least 50% sequence homology between species analyzed.

The first solution structure of fortilin, also known as p23, was solved using nuclear NMR spectroscopy in 2001 from the yeast strain *Schizosaccharomyces pombe*.[73] The authors of this NMR study highlighted a structural similarity between fortilin and the guanine nucleotide-free chaperone protein, mammalian suppressor of Sec4 (Mss4) in their β-barrel structure, specifically (**Figure 1.5**). The key difference between *S. pombe* TCTP and human fortilin are the length of protein and mass, 168 and 172 amino acids and 19,049 and 19,595 Da, respectively. Cys172 forms a cysteine dimer of two fortilin molecules via intermolecular disulfide bond.[76] TCTP has since been both crystallized and solution structures solved by NMR with protein data bank (PDB) structures provided in **Table 1.2.**

Table 1.2. X-ray crystal and NMR solution structures of TCTP.

PDB Entry	Method	Species	Reference
2LOY	NMR	*C. elegans*	[77]
2KWB	NMR	*C. elegans*	Not yet published
1YZ1	X-ray	*H. sapiens*	[78]
2HR9	NMR	*H. sapiens*	[79]
3EBM	X-ray	*H. sapiens*	[80]
509L/M	X-ray	*H. sapiens*	[81]
4Z9V	X-ray	*H. sapiens*	[82]
2MVM/N	NMR	*H. sapiens*	[83]
6IZB/E	X-ray	*H. sapiens*	Not yet published
509K	X-ray	*M. musculus*	[81]
6J2Y	NMR	*N. oceanica*	[84]
3P3K	X-ray	*P. falciparum*	[85]
1TXJ	X-ray	*P. knowlesi*	[86]
1H6Q/1H7Y	NMR	*S. pombe*	[73]

The solution structure of human fortilin was solved by NMR spectroscopy in 2007.[79] This study also characterized the calcium binding site of fortilin, where fortilin had been previously described to play a role in calcium scavenging in calcium-dependent apoptosis. In 2013, an X-ray crystallographic structure of TCTP from *Plasmodium falciparum* was also characterized.[87] The structure of fortilin is highly conserved across species, as depicted in **Figure 1.7**.

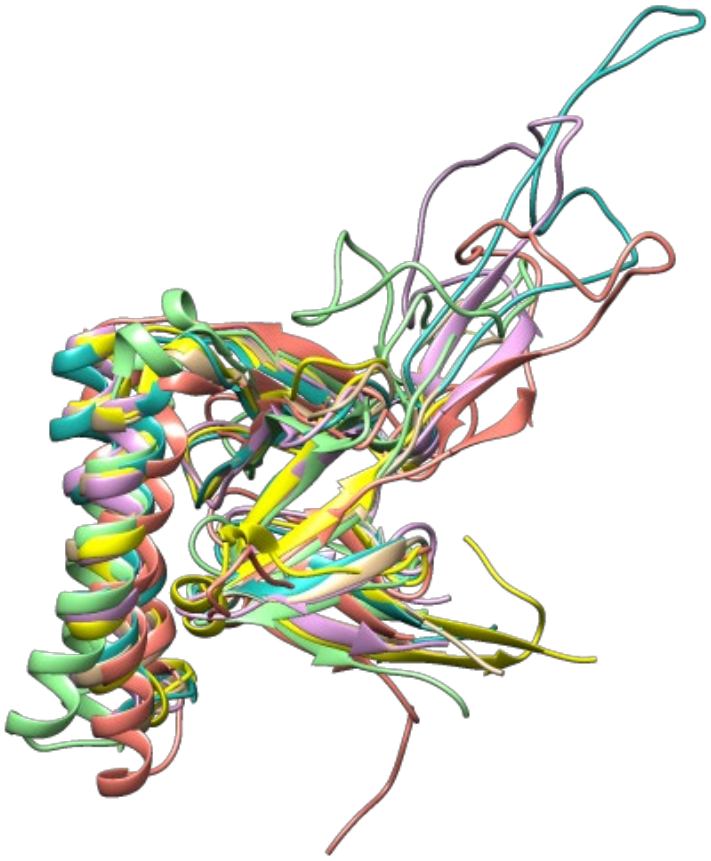

Figure 1.7. Structural homology of fortilin across species. PDB structures 2HR9 (sea green), 1H6Q (violet), 1YZ1 (tan), 2KWB (green), 3P3K (yellow) and 6J2Y (red-orange) have been structurally aligned using UCSF Chimera v1.13.1.[88]

1.2.3 Known Functions of Fortilin: Anti-Apoptotic

Fortilin has many known functions both involving anti-apoptotic and cell growth and proliferation functions (**Figure 1.8**). While much research focuses on fortilin's anti-apoptotic function, it is important to note that fortilin is also involved in many cell growth and proliferation functions as well that do not necessarily involve preventing apoptosis.

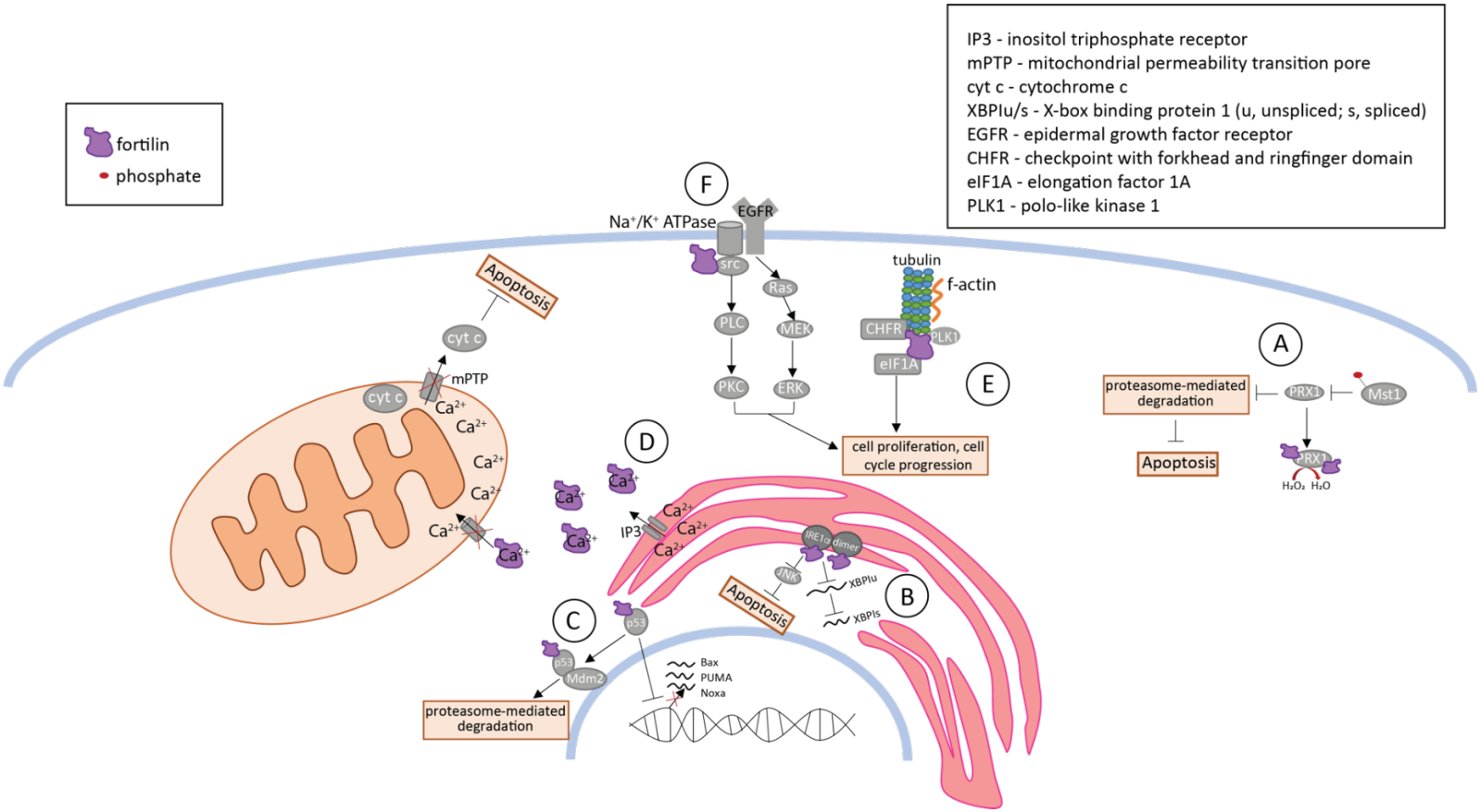

Figure 1.8. Known cellular pathways of fortilin. A) PRX-1 binding (Chattopadhyay et al. 2016) B) IRE1□ binding (Pinkaew et al. 2017) C) p53 binding (Chen et al. 2011) D) calcium scavenging (Fujise et al. 2007) E) tubulin binding (Gachet et al. 1999) F) Na+/K+ ATPAse and EFGR activity (Kim et al. 2009)

1.2.3.a PRX1 Binding and Activity

Fortilin was found to bind peroxiredoxin-1 (PRX1) *in vivo* using an assay to detect nicotinamide adenine dinucleotide phosphate (NADPH) consumption by PRX1.[89] Peroxiredoxins are a family of proteins that protect cells from oxidative damage by reactive oxygen species (ROS) and are also known as natural killer enhancing factors (NKEF) because they can enhance natural killer cell cytotoxicity when presented against tumor cells.[90] In this assay, addition of fortilin to PRX1 increased its NADPH consumption activity by 2.9 fold higher than PRX1 alone, while fortilin alone did not increase NADPH activity. These data indicate that fortilin potentiates the activity of PRX1, while not having endogenous peroxidase activity itself.

Additionally, fortilin was found to protect PRX1 from phosphorylation by mammalian sterile twenty 1 (Mst1), a serine/threonine kinase, further potentiating PRX1 activity (**Figure 1.8 A**). When phosphorylated at its T90 and T183 residues by Mst1, PRX1 becomes inactivated and is subsequently targeted for proteasomal degradation.[91] In an *in vitro* experiment, addition of Mst1 to PRX1 decreased NADPH consumption by 75.3%. When fortilin was present, PRX1 activity was rescued, such that only a 43.5% decrease in NADPH consumption was observed. While the exact mechanism for Mst1 inhibition by fortilin has not been elucidated, computational predictions suggest that T90 and T183 residues of PRX1 dimers are physically blocked by fortilin from phosphorylation by Mst1.[89]

1.2.3.b IRE1α Binding and Function

Endoplasmic reticulum (ER) stress sensors are proteins that are detached from the ER membrane in response to oxidative stress as part of the unfolded protein response

(UPR) in order to bind and sequester proteins that have been misfolded.[92] One of these proteins, inositol-requiring enzyme 1α (IRE1α), is ubiquitously expressed in mammals and has been shown to bind fortilin both *in vitro* and *in vivo* in liver-fortilin-overexpressing mice.[93] IRE1a is a multifunctional protein. On one hand, the kinase domain, upon dissociation from GRP78, auto-transphosphorylates and then its RNase domain splices X-box binding protein-1 (XBP1) mRNA to produce XBP1s, a transcription factor that then translocates to the nucleus and initiates transcription of a set of UPR-related genes.[94] On the other hand, the kinase domain of IRE1α also activates the Jun N-terminal (JNK) pro-apoptotic pathway by recruiting the scaffold protein TRAF2 and apoptosis signal-regulating kinase (ASK1), which then phosphorylates JNK and activates the pathway.[93] Fortilin was found to prevent ER stress from activating ERE1α by preventing its protein kinase and RNase activities (**Figure 1.8 B**).[93]

1.2.3.c p53 Binding and Anti-Apoptotic Activity

Fortilin has a presence in the nucleus, the reason for which was unclear, and still remains ambiguous.[71] However, in 2011 it was determined that fortilin binds and inhibits the function of the transcriptional regulator p53 and prevents transcriptional activation of the pro-apoptotic protein Bax (**Figure 1.8 C**).[95] In this study, fortilin was first found to be co-localized with p53 in the nucleus, and not the nucleoli or cytosol, of U2OS cells containing overexpressed hemagglutinin (HA)-tagged fortilin using both confocal microscopy as well as co-immunoprecipitation assays. Additionally, it was determined that both the N and C termini of fortilin were required for binding p53, as a glutathione-S-transferase (GST)-tagged fortilin was able to pull down p53 in co-immunoprecipitation experiments when compared to GST alone or deletion mutants containing amino acids

121-172. It was found that the domains containing the N terminus (amino acids 1-70) and the C terminus (amino acids 121-172) could pull down p53, while the intermittent amino acids (71-120) could not.[95] These finding narrow the p53 putative binding site to near the N and C termini of fortilin, independent of the presence of a GST affinity tag. However, ideal conditions for binding studies require a cleaved GST tag from fortilin to ensure no interference during binding. Computational docking done in the same study suggest that fortilin blocks p53 binding to DNA by binding to the single-stranded DNA binding domain (SSDBD) of p53.[95] *In vitro* studies need to be done to elucidate the true binding site of fortilin to p53.

1.2.3.d Calcium Scavenging

Calcium binding was first indicated in *Trypanosoma brucei* in 1992 and was subsequently confirmed in various species.[96–101] The mechanism by which calcium scavenging by fortilin affects the cells was determined in 2007 (**Figure 1.8 D**).[102] Fortilin was first confirmed to bind calcium by $^{45}CaCl_2$ overlay assay, wherein proteins separated by SDS-PAGE are then transferred to a PVDF membrane and treated with $^{45}CaCl_2$ and phosphor-imaged to detect $^{45}Ca^{++}$. Next, 6his-fortilin was found to change its secondary structure when in the presence of 10 mM Ca^{++} when analyzed via spectropolarimetry. Once these *in vitro* studies were obtained, *in vivo* analysis both in U2OS and MEF cell lines were performed. Utilizing thapsigargin, increased in Ca^{++} levels were induced, leading to Ca-induced apoptosis. $siRNA_{fortilin}$ transfection in U2OS cells led to significant increase in intracellular Ca^{++} levels, indicating that the presence of fortilin decreases overall Ca^{++} concentration in the cell. This experiment was repeated in $MEF_{fortilin+/-}$ cells and compared to $MEF_{fortilin+/+}$ cells ($MEF_{fortilin-/-}$ cells are not

successfully isolated due to their lethal nature).[103] In $MEF_{fortilin+/-}$ cells, the cellular concentrations of fortilin are approximately one-half of that of $MEF_{fortilin+/+}$ cells, and when challenged by thapsigargin, $MEF_{fortilin+/-}$ cells exhibit higher levels of Ca^{++}, indicating that fortilin levels directly affect intracellular Ca^{++} levels and therefore exhibits scavenging activity.

1.2.4 Known Functions of Fortilin: Cell Growth and Proliferation

1.2.4.a Tubulin Binding

GST-fortilin fusion protein has been demonstrated to bind both α and β-tubulin *in vitro* (**Figure 1.8 E**).[104] The experiments performed in this study were done against GST controls to indicate that GST does not interfere with binding itself, however no study has yet been done with fortilin with no fusion tag, which does not rule out completely the possibility that an affinity tag may contribute to binding. Through the efforts of antibody staining using a rabbit antipeptide antibody to localize fortilin and a mouse monoclonal antibody against α-tubulin for microtubule staining, fortilin was found to be associated with microtubules using confocal microscopy.[104] In this study, fortilin levels were also determined during different phases of cell cycle progression using fluorescent assisted cell sorting (FACS) and found to be associated with microtubules during G_1, S, G_2 and M phases, as well as being bound to the mitotic spindle during metaphase, leading to dispatchment during the metaphase-anaphase transition. This study was among the earliest to hint at a role for fortilin in cell cycle progression.

These findings were confirmed and expanded upon in 2009 when Bazile et al. determined that TCTP aides in cell shape regulation by its interaction with both microtubules and actin in both normal and cancer cells.[105] In *Xenopus* XL2 cells,

transfected fortilin containing a Myc tag was found to form along microtubules when visualized by binding with a primary antibody (anti-c-myc) and secondary fluorescent antibody fluorescein isothiocyanate and rhodamine-B isothiocyanate conjugated. Fortilin was also observed in this manner to be colocalized in the mitotic spindle poles during mitosis. However, microtubule dynamics were not affected by fortilin, as evident in an assembly/disassembly assay performed with wild-type 6His-tagged fortilin and truncated fortilin where a suspected binding domain sequence (amino acids 82-121), determined in the previously mentioned study, were deleted and tested.[104] The conclusion, here, is such that while fortilin contains a sequence that binds putatively to microtubules, neither its presence nor absence affects microtubule assembly or disassembly.

1.2.4.b Na/K-ATPase and EGFR

Fortilin was determined to prevent epidermal growth factor receptor (EGFR) phosphorylation in HeLa cells upon inhibition of the Na^+/K^+-ATPase protein (**Figure 1.8 F**).[106] Fortilin binds Na^+/K^+-ATPase within the third cytoplasmic domain to inhibit its activity for maintaining cellular concentrations across the cellular membrane.[107] EGFR family proteins share a common ancestral backbone and are critical in cell growth, development and homeostasis.[108] A GFP-TCTP construct was found to induce EGFR phosphorylation in HeLa cells in the same manner as EGF and Ouabain, a hypotension drug.[106] These findings, the authors claim, indicated that fortilin overexpression may induce cell migration and that this, along with fortilin's anti-apoptotic activity may influence tumorigenesis.

1.2.4.c Prevention of Alcohol-Induced Liver Damage via PRX1 Binding

There is evidence to suggest that over-expression of fortilin in certain cell types may not always lead to a detrimental effect. When alcohol is consumed, the liver metabolizes alcohol through alcohol dehydrogenase, the microsomal ethanol oxidizing system, and aldehyde oxidase to produce ROS such as hydrogen peroxide.[109] A role of PRX1 is to convert hydrogen peroxide into hydrogen and water, thus protecting liver cells from damage.[110] One study done on liver-specific overexpression of fortilin in mice found that PRX1 phosphorylation was reduced and PRX1 activity enhanced in mice containing overexpressed liver fortilin when compared to fortilin-knockdown mice. [89] This activity prevented alcohol-induced liver damage when mice were administered with 10g/kg body weight of alcohol.[89]

1.2.4.d BMP Pathway and Embryo Survival

The bone morphogenic proteins (BMPs) bind serine/threonine kinase receptors, known as BMP receptors, and are involved in signal transduction.[111] In this study, the overall goal was to develop a mouse line that was fortilin deficient (fortilin$^{+/-}$) as well as fortilin knockout (fortilin$^{-/-}$). While fortilin$^{+/-}$ mice were found to be perfectly healthy and able to reproduce, fortilin$^{-/-}$ embryos did not survive. These findings indicated the possibility of an embryonic development role for fortilin, which was supported by qRT-PCR and immunostaining on fortilin expression at the early developmental stages. RNAs isolated from embryonic mice showed a peak in fortilin transcription at 9.5 days post coitum (dpc), followed by a decrease over three days, and then back up to peak levels between 16-18 dpc. Fortilin was determined to be an inhibitor of the BMP pathway in *Xenopus* embryos, which share 68% homology with human fortilin (**Figure 1.6**). In this

study, it was determined that fortilin inhibits the BMP-4 pathway in both *Xenopus* and MEF cells by blocking BMP4 and blocks induction of Msx2, a pro-apoptotic protein, thus leading to decreased apoptosis and subsequent embryo loss.[103]

1.2.5 Current research strategies for targeting fortilin in disease

1.2.5.a Known Small Molecule Binders of Fortilin and Characterized Binding Sites

Ca^{2+}

In 2007, the calcium binding site for human fortilin was determined via NMR spectroscopy.[79] In this study, small amounts of calcium chloride were titrated in to a ^{15}N labeled sample of 6His-tagged fortilin and the binding kinetics were measured as the calcium concentration increased and peaks on the NMR spectrum, corresponding to different amide groups in the peptide backbone of the protein, shifted. Based on this study, which focused its efforts on the peak shift of Tyr132, a dissociation constant, or K_d, was estimated to be between 22 and 25 mM. The putative binding site was determined to be amongst amino acids Q133, N131, D150, L149, Y132 and Y151 with oxygen atoms on Q133, N131 and D150, all located within the β-barrel, forming the corresponding binding site and other residues shifting in response to calcium binding (**Figure 1.9)**.[79] The binding constant determined here is not in conjunction with other estimated binding constants determined by other groups, where a range from 8 to 10 mM was previously determined.[96,102] Feng et al. (2007) argue that for the 8 mM binding constant that was previously determined, deletion experiments were used to determine the K_d and thus this constant does not apply to natively folded fortilin.[79] For the 10 mM dissociation constant, a GST-tagged fortilin was used and thus we cannot rule out effects

due to GST interference even though control experiments using GST alone were performed.[102] Experiments replicated by our lab using NMR spectroscopy and both GGS-fortilin and fortilin-strep constructs have determined K_d values of 13 and 29 mM, respectively, indicating that the presence of affinity tags and extra amino acids may influence calcium binding.

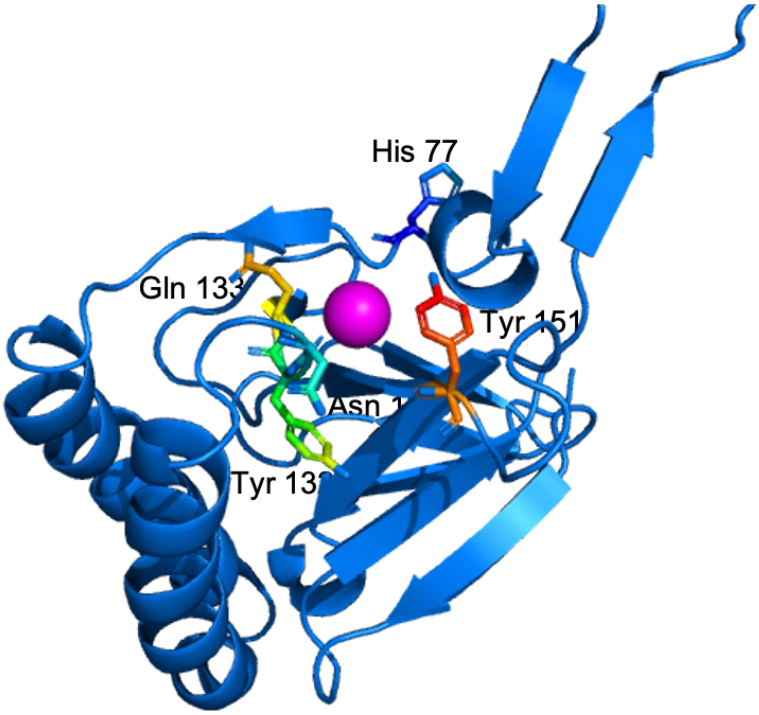

Figure 1.9. Calcium binding to fortilin. Fortilin binds calcium wedged between the β barrel and the α2 and α3 helices. Binding residues are shown as sticks and labeled.

Dihydroartemisinin and Artemisinin

Dihydroartemisinin (DHA) and artemisinin are both drugs used in the treatment of malaria (**Figure 1.10**). DHA was found to bind *Plasmodium falciparum* fortilin containing a T7 peptide affinity tag in 1998 and then discovered to bind human GST-fortilin in 2008.[112,113] While the DHA binding site has not yet been characterized, the artemisinin site has been characterized in *P. falciparum* fortilin as of 2016.[114] In this

study, bioorthogonal click chemistry was used to determine the binding site, using heme as an activator of artemisinin for binding with fortilin. The binding site for artemisinin is closer to the N and C termini, which have been indicated as required sequences for activity, and the amino acids within range include H181, Y175, E16, V7, K9, D15, T13 and N14 (**Figure 1.10**). It should be noted that the sequence for *P. falciparum* is slightly different than that of human fortilin (see **Figure 1.6**).[114] While the sequences for human *P. falciparum* are slightly different, their structures are highly conserved and computational predictions of binding done by our lab are found in the same location for DHA as artemisinin.

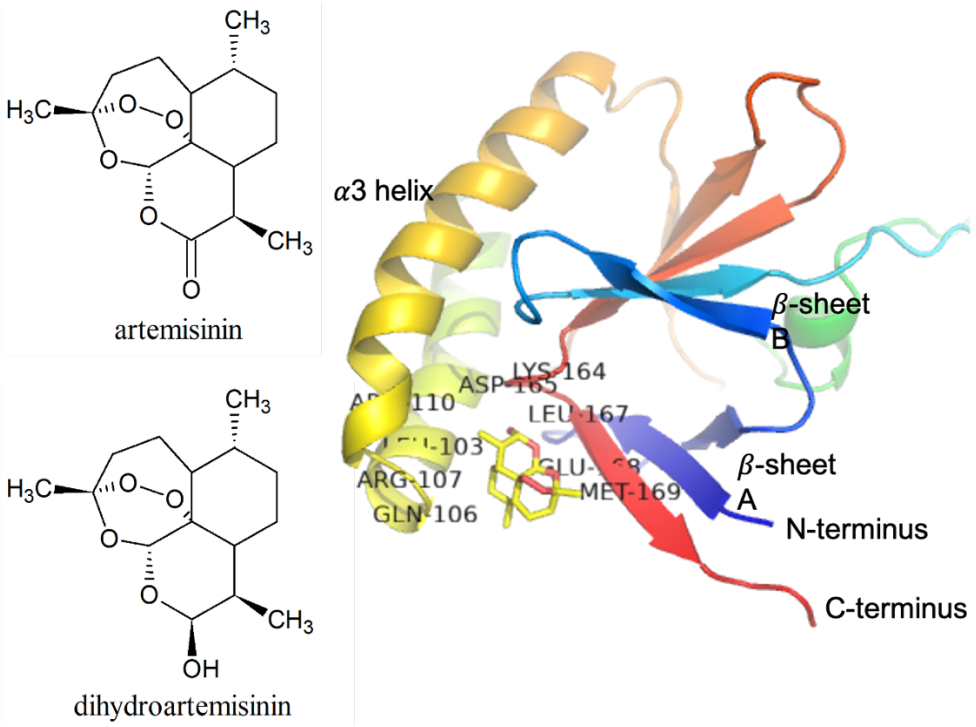

Figure 1.10. Structures of DHA and artemisinin and binding to fortilin. Left – structures of artemisinin and DHA. Right – Computationally predicted binding site of both DHA and artemisinin using DHA as the SMI here. Residues proximal to DHA within 3Å are shown. Computational prediction was done using AutoDock Vina.[22]

1.2.5.b Heart Disease: Rational Drug Design and Drug Discovery

Cardiovascular diseases (CVD) are the leading causes of death worldwide. These include coronary heart disease, heart failure, stroke and hypertension and are prevalent in approximately 48.0% of individuals aged 20 and older in the United States alone.[115] Patients presenting with heart disease are commonly prescribed statin-based medications, which are cholesterol-formation inhibiting drugs, in an effort to reduce low-density lipoprotein (LDL) levels, wherein cholesterol is found. However, in a nationwide study of lipid levels amongst patients hospitalized with CVD, approximately half of the 136,905 patients studied had LDL levels within the normal to low range.[116] These findings were further explored in 2017, when another hospital study concluded patients presenting with atherosclerosis, where no previous risk factors were determined, these patients had normal LDL-cholesterol levels. These findings highlight the need to develop novel treatments for CVD that do not directly target cholesterol formation. Efforts are currently underway to target fortilin for rational drug development in atherosclerosis.[35,117]

Fortilin was first proposed to be a viable target for drug development for atherosclerosis in 2013 when pro-atherosclerotic, fortilin deficient, mice were found to have ameliorated levels of atherosclerotic plaque and increased macrophage apoptosis.[118] The overarching hypothesis is such that when fortilin function is inhibited, macrophage apoptosis is propagated and less atherosclerotic plaques form (**Figure 1.11**).

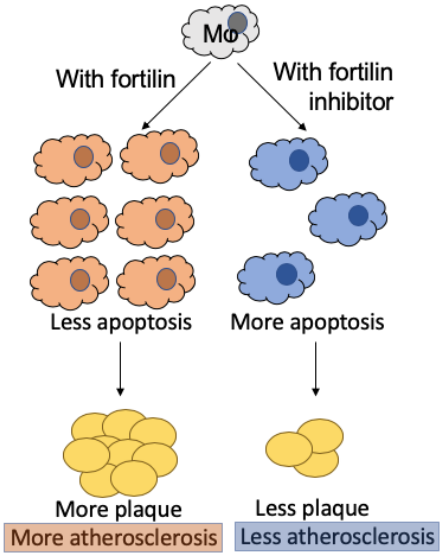

Figure 1.11. Fortilin potentiates foam cell formation. Fortilin prevents macrophage apoptosis and propagates plaque formation. When inhibited, macrophages may undergo normal apoptosis and prevent plaque formation.

1.3 NMR for Structural Characterization of Proteins and Rational Drug Design

1.3.1 Structural Determination of Proteins by NMR

In 1985, the first solution-state protein structure determined by NMR was published by Williamson et al. for the proteinase inhibitor IIA from bull seminal plasma.[119] This new technique revolutionized structural elucidation of proteins because until then, X-ray crystallography was the standard for structure determination. X-ray crystallography requires the formation of protein crystals, whose generation can prove quite trivial. Additionally, while SMI binding sites may be determined by X-ray, dynamics studies are impossible. The development of protein techniques by NMR spectroscopy allows for high resolution data that allows for dynamics studies for protein-ligand interaction as well as dynamic structure elucidation in solution. The main drawback to NMR over crystallography is such that proteins must be smaller in size, up to 40-50 kDa, before analysis gets trivial because signals from too many molecules can

be difficult to analyze. As for crystallography, if a protein can be crystallized, it can be analyzed. Indeed, fortilin has been crystallized many times (**Table 1.2**).

In order to elucidate a three-dimensional protein structure, high concentrations of isotopically labeled protein must be used, typically at a final concentration between 1-2 mM.[120] To achieve a protein concentration of 1-2 mM for a protein the side of fortilin can be fairly difficult logistically as isotopically labeled reagents such as $^{14}NH_4Cl$ and ^{13}C glucose are more expensive than their non-labeled counter parts. Isotopic labeling of protein is a requirement for NMR spectroscopy because of atomic quantized spin. Atomic nuclei containing odd mass or odd atomic number have the quantum mechanical property of spin and can therefore be detected by NMR spectrometers.[121] As proteins are composed of amino acids and contain high levels of nitrogen, carbon and hydrogen, isotopic enrichment is necessary for structure determination. For larger proteins than 50 kDa, ^{2}H labeling of proteins may be necessary in order to suppress the proton signal to elucidate structures. Reducing agents such as deuterated dithiothreitol (d-DTT) or tris(2-carboxyethyl)phosphine (TCEP) hydrochloride are used to prevent dimer formation in solution. Sodium phosphate buffers, as opposed to hydrogen phosphate buffers, are most commonly used to prevent signal interference from unwanted protons, as well as an optimized concentration of sodium chloride for protein stability. These conditions are optimized for 3D determination of NMR solution structures.

Fortilin is an ideal candidate for NMR structure studies because it is relatively small (approximately 19 kDa). For protein analysis by NMR, mg quantities of protein are achieved by recombinant protein expression and purification techniques using *E. coli* competent cell lines, or even yeast strains such as *P. pastoris* (**Figure 1.12**).[120]

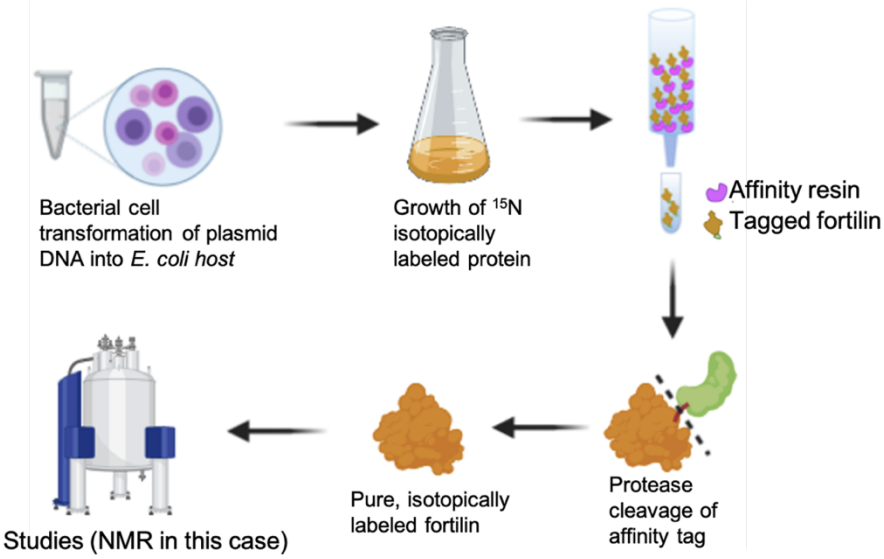

Figure 1.12. Protein preparation for NMR. Recombinant protein expression and purification techniques are used to generate mg quantities of isotopically labeled protein for analysis by NMR.

1.3.2 Binding Site Determination of SMIs to Protein by NMR

Protein-ligand interactions may be determined by NMR and is a commonly used technique in structure based drug design (SBDD) for the rational development of drugs for clinical use.[122] Using NMR, binding sites on proteins that have been determined to be potential targets are titrated with small molecules that bind specifically to the protein of interest. This is done by taking ^{15}N heteronuclear spin quantum coupling (HSQC) spectra of the native protein, followed by adding in small amounts of SMI to determine which peaks shift in response to increased amounts of small molecule. Binding isotherms are used to determine binding constants, or K_d, values and the amino acids involved in binding can be identified in this manner, called chemical shift mapping.[123] We proposed to use this technique with fortilin to known binders such as DHA and artemisinin to map out binding sites of fortilin such that progress can be made in the rational drug design of atherosclerosis drugs.

1.4 Conclusions

Drug discovery is a long process that involves approximately 8-12 years and $3 billion. Drug repurposing provides a path by which researchers can use already clinically tested and FDA approved drugs in order to find drugs that may treat a different disease from the one the drug obtained approval to treat. In the realm of CVD and atherosclerosis in particular, a critical need exists to develop novel drugs that target a mechanism other than cholesterol formation, be they already approved drugs or novel. Fortilin is a relatively novel protein that was first characterized in 2001 and is found to be involved in myriad functions including anti-apoptotic, growth and proliferation. In atherosclerosis, fortilin has been found to propagate arterial plaque formation by utilizing its anti-apoptotic function to prevent macrophage apoptosis. The size of human fortilin, approximately 19 kDa, makes it a good candidate for SBDD by NMR spectroscopy in a rational drug design workflow. In order to study fortilin using this workflow, high quantities of pure, isotopically labeled protein must be recombinantly expressed in an *E. coli* competent cell expression system. The results of the work shown in this dissertation provide the basis for expressing mg amounts of fortilin protein wherein an affinity expression tag can be cleaved, and a construct can be generated without an affinity tag at the N terminus. Studies performed via DSF and NMR spectroscopy with SMI's are also shown in this work.

CHAPTER TWO: EXPRESSION AND PURIFICATION OF A CLEAVABLE RECOMBINANT FORTILIN FROM *ESCHERICHIA COLI* FOR STRUCTURE ACTIVITY STUDIES

Under review in *Protein Expression and Purification* as of August 6, 2021

Maranda S. Cantrell[1,2], Jackson D. Wall[2], Xinzhu Pu[3], Matthew Turner[3], Luke Woodbury[3], Ken Fujise[4], Owen M. McDougal[2] and Lisa R. Warner[2]

[1]Biomolecular Sciences Ph.D. Program, Boise State University

[2]Department of Chemistry and Biochemistry, Boise State University

[3]Biomolecular Research Center, Boise State University

[4]Harborview Medical Center, University of Washington

2.1 Introduction

Atherosclerosis, or the hardening and narrowing of arterial walls, is the leading cause of death worldwide.[124] Atherosclerogenesis occurs when low density lipoproteins (LDL) in plasma diffuse into the intima of arteries and then become oxidized (oxLDL), followed by uptake into macrophages. Macrophages eventually form foam cells, which over time develop into plaques on the arteries, leading to blockages in blood flow that cause cardiac events such as infarction, stroke, hypertension, etc. Presently, medications used to treat atherosclerosis largely depend on inhibiting the formation of cholesterol *in vivo* via the use of statins, which can cause undesirable side effects. For example, 3-

hydroxy-3-methyl-glutaryl-Co-A (HMG-CoA) reductase inhibitors (statin drug class) can cause leg cramps in patients at night that lead to decreased compliance with treatment.[125] Additional side effects may include cataracts and short-term memory loss.[126] Moreover, a recent study of 136,905 people showed that nearly half of all patients brought into the emergency room with heart attacks had normal to low LDL levels in their blood.[116] This finding made evident the need to develop drugs that target other mechanisms in the pathology of atherosclerosis than the *in vivo* formation of high cholesterol.

Fortilin is a promising drug target to treat atherosclerosis.[35] Fortilin, also known as translationally controlled tumor protein (TCTP), or histamine releasing factor (HRF), is a highly conserved anti-apoptotic protein.[127] Fortilin is a protein consisting of 172 amino acids that is found throughout the human body in the cytosol, nucleus, and mitochondria of all cell types, blood and extracellular space.[71,117] Fortilin exerts its anti-apoptotic effect through multiple mechanisms; including calcium complexation and p53 inactivation, but it contributes to atherosclerosis by keeping macrophages in the M1 pro-inflammatory phenotype.[35,128] Fortilin has been implicated in the progression of atherosclerosis by reducing macrophage apoptosis by binding to and inhibiting p53, a transcription factor that regulates the transcription of BAX, a pro-apoptotic protein. This mechanism promotes foam cell formation, leading to deposits on arterial walls.[128] Fortilin also exhibits anti-apoptotic activity by scavenging free calcium in the cytoplasm of cells, thus exerting a protective effect from calcium-induced apoptosis.[102] Specifically, inhibition of the pro-survival activity of could provide an orthogonal strategy to treat atherosclerosis by shutting down the protective effects of fortilin.

Fortilin is a 19 kDa protein that has 11 beta-strands and an extended flexible loop between residues Tyr 39 and Val 66 (**Figure 2.1a**). The amino- and carboxy-termini are in proximity to one another, creating a cavity that could be interrogated for small molecule binding. The calcium binding site is coordinated by six oxygen atoms within the beta barrel among residues H77, N131, Y132, Q133, and Y151 (**Figure 2.1b)**.[79] While a direct connection between fortilin, calcium scavenging, and atherosclerosis has not yet been made, calcium-dependent apoptosis does occur during ox-LDL-induced apoptosis and it is hypothesized that fortilin could play a role through its calcium scavenging activity.[129]

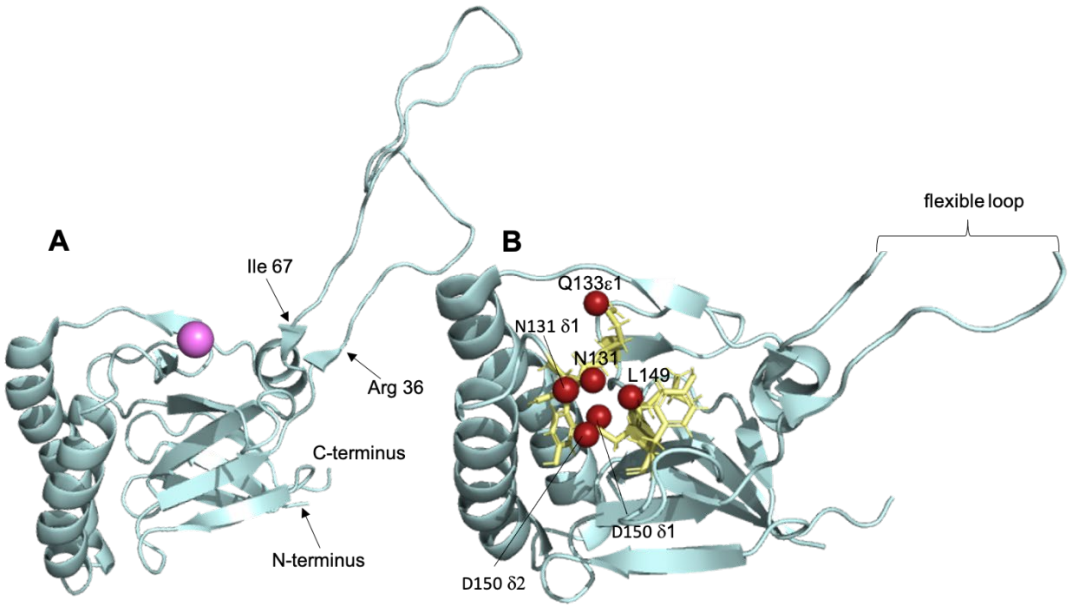

Figure 2.1. Calcium-bound fortilin. A) Side view of fortilin (blue) bound to calcium (magenta) with residues labeled for the flexible loop, the N- and C-termini, and B) downward view of fortilin bound to calcium with complexed oxygen atoms (red) shown and residues in proximity displayed as sticks. PDB structure 2HR9.

A structure-based approach to targeting fortilin will provide important information for drug screening and defining drug binding sites. Structure-based drug design (SBDD) is a technique commonly used to create small molecule therapeutics that

specifically target a given protein.[122,130] Solution nuclear magnetic resonance spectroscopy (NMR) is an excellent tool for SBDD, for example, in screening small molecule inhibitors (SMIs), mapping binding hot spots, and determining binding affinities and kinetics.[122] A solution structure of recombinant fortilin has been reported using NMR.[79] Feng et al., used a construct with a 6His affinity tag and required high salt (200 mM) conditions for high quality NMR spectra.

NMR experiments require milligram quantities of pure, isotopically enriched and bioactive protein. *E. coli* expression platforms are routinely used as they allow for straightforward, high yield and affordable isotope enrichment.[131] Ideally, an affinity tags used in protein purification should be removed by enzymatic cleavage to ensure no pseudo binding effects due to the presence of the affinity tag. The N- and C-termini of fortilin form a beta strand that forms a pocket in the native structure. Affinity tags attached at either the N- or C- terminus complicate the potential to target this site. Functional studies of fortilin with an affinity tag are inconclusive due to the presence of the affinity tag at the suspected small molecule binding site.[113,114] Here, we describe the design and assessment of several fortilin constructs for the purpose of expressing and purifying a recombinant fortilin molecule with minimal non-native residues. Inclusion of a short GGS linker between an HRV 3C protease cleavage site and the N-terminus of fortilin resulted in milligram quantity of isotopically enriched ^{15}N GGS-fortilin. Calcium binding was observed by NMR titrations, demonstrating the structure and activity of this construct were maintained. The work presented here shows that pure recombinant fortilin can be proteolytically cleaved from an affinity tag and retain biological activity by the insertion of a GGS linker sequence.

2.2 Materials and Methods

2.2.1 Expression and Purification of S219V TEV Protease from E. coli

Recombinant TEV protease was expressed and purified using plasmid #8827 from Addgene (pRK793) in BL21 (DE3) strain *E. coli* cells. From a glycerol stock, 20 mL of LB containing 100 µg/ml ampicillin, 25 µg/ml chloramphenicol was inoculated, and incubated overnight at 37 ºC with shaking at 200 rpm. This overnight culture was then used to inoculate 1L LB containing 100 µg/ml ampicillin, 25 µg/ml chloramphenicol with shaking at 37 ºC with 200 rpm. Once the OD_{600} reached between 0.5-0.7, a pre-induction sample equivalent to 1 mL of cells at OD_{600} of 0.8 was collected, and the culture flasks placed on ice and gently rotated every few minutes to cool the cultures. The incubator was then set to 30 ºC and the cultures were reintroduced at the elevated temperature and expression was induced with 1 mM IPTG, with shaking at 200 rpm. This culture was incubated overnight. On the third day, a post-induction sample equivalent to 1 mL of cells at OD_{600} of 0.8. The pre- and post-induction samples were used to analyze expression using SDS-PAGE. Lysis was halted by pouring the cultures into pre-weighed 500 mL centrifuge bottles and the cultures centrifuged at 6000 x g for 30 min at 4 ºC. After centrifugation, the supernatants were removed, and the mass of the pelleted bacteria weighed. The pellet was resuspended in 40 mL of lysis buffer consisting of 50 mM Tris-Cl pH 8.0, 300 mM NaCl, 20 mM imidazole, 10% (w/v) sorbitol, 20 mM 2-mercaptoethanol, 0.02 mg/ml lysozyme, and 1X HALT protease inhibitors (Thermofisher, USA). The suspension was sonicated on ice water at 60% power, 30 sec on/30 sec off for 4.5 min of total pulse time and a 75 µl sample collected for SDS-PAGE to check post sonication pellet and supernatant. The sonicated suspension was centrifuged

at 16,000 x g for 30 min at 4 ºC. The supernatant was collected and filtered using a 0.45 µm PES filter. To the filtered lysate, 5 mL of Ni-NTA superflow slurry (Qiagen Cat #30410/30430) was added and the mixture incubated overnight at 4 ºC with rocking. On the fourth day, the lysate/resin mix was loaded into a column and the flow through collected. Purification was carried out with a BioLogic LP System using EconoColumn 1.0 x 10 cm chromatography columns (Bio-Rad, Hercules, CA, USA). To line A, the lysis buffer described previously was attached. To line B, the same lysis buffer with the only difference being a 300 mM imidazole concentration was attached. Buffer A was run over the column at a flow rate of 1.0 mL/min until the A_{280} stabilized, all while collecting the flow through. The program for protein purification was as follows: Line A for 10 min, Line B (0%-100% B, 1.0 mL/min) for 60 min, hold Line B for 10 min, and back to 100% A for 10 min. Results were evaluated by SDS-PAGE. Fractions containing purified TEV protease were combined, and protein concentration determined by absorbance at 280 nm. Pooled fractions were diluted to a final concentration of 1 mg/ml in a 50% glycerol solution, and 0.5 mL aliquots stored at -80 ºC.

2.2.2 Expression Plasmid Constructs

The fortilin-StrepTag II construct plasmid was purchased from IBA Lifesciences in the pASG-IBA3 expression vector (Göttingen, Germany). All other plasmids were purchased from ATUM (Newark, CA) using their pD441-SR vector. These constructs consisted of glutathione S-transferase (GST), maltose binding protein (MBP), and 6-histidine (6His) affinity tags, human rhinovirus (HRV) 3C and tobacco etch virus (TEV) protease recognition sites, and glycine-glycine-serine (GGS) linkers of varying length

$(GGS)_N$ where N = 0, 1, 2 or 3 at the N-terminus of fortilin in the pD441-SR expression vector.

2.2.3 Expression of Recombinant Fusion Proteins

Plasmids were transformed into 50 µL of competent *E. coli* cells using the heat-shock method at 42 °C. Single colonies were inoculated into 5 mL of Luria-Bertoani (LB) medium containing 50 µg/mL kanamycin and grown at 37 °C overnight with shaking at 250 rpm. One mL of each overnight culture was inoculated into 100 mL LB medium containing 50 µg/mL kanamycin and grown at 37 °C with shaking at 250 rpm until the OD_{600} reached between 0.60 and 0.80. Once reached, IPTG was added to 0.1 mM to induce protein expression. Expression continued at these conditions for 6 h. Expression was halted by centrifugation at 4,000 x g for 20 min and expression analyzed by SDS-PAGE on 12% bis-acrylamide gels.

2.2.4 Expression of ^{15}N-labeled Recombinant Fusion Proteins for NMR Spectroscopy

Plasmids were transformed into 50 µL of competent *E. coli* cells using the heat-shock method at 42 °C. Single colonies were inoculated into 5 mL of LB medium containing 50 µg/mL kanamycin and grown at 37 °C and grown for approximately 8 hours. One mL of each culture was inoculated into 50 mL of M9 minimal media containing 50 µg/mL kanamycin and grown at 37 °C overnight.

2.2.5 Cell Lysis

Cell pellets (approximately 0.13 g each) from 100 mL cultures were resuspended in 2 mL lysis buffer containing 150 mM NaCl, 50 mM tris-HCl pH 7.8, 1 mM EDTA and 0.1% Triton X-100. Lysozyme was added to a final concentration of 0.25 mg/ml as well as ½ tablet of HALT protease inhibitor cocktail (Pierce, Rockford, IL). The lysate was

then subjected to sonication at 70 % power for 30 sec on/ 30 sec off for a total of two minutes. Samples were then centrifuged at 17,000 x g for 45 min at 4 °C. The resulting lysate was filtered through a 0.45 μm cellulose acetate filter and subjected to affinity purification.

2.2.6 Purification of GST-3C-$(GGS)_N$-Fortilin and GST-3C-TEV-Fortilin from BL21(DE3) Cells

GSTrap sepharose 4B 1 mL pre-packed columns were used for purification (GE Healthcare, Marlborough, MA). Separate columns were used for each linker sequence to avoid contamination of samples. Samples were loaded onto the column with a flow rate of 1.0 mL/min and washed with 1X phosphate buffered saline (PBS) with a flow rate of 1.0 mL/min for 20 mL, followed by a 10 mL elution with GSTrap elution buffer containing 50 mM Tris-HCl pH 8.0 and 10 mM reduced glutathione. Elution was followed by a 10 mL wash at 1.0 mL/min with 1X PBS (**Appendix A. Figs 1-3 and 5**). All solutions used for affinity chromatography were filtered through 0.22 μm nylon filters and degassed under vacuum with rigorous stirring for at least one hour.

2.2.7 Purification of 6His-MBP-10N-3C-TEV-Fortilin and MBP-TEV-Fortilin

Amylose resin (New England Biolabs, Ipswich, MA) was used for purification of MBP-tagged proteins. An approximately 50% slurry of affinity beads to 20% ethanol were used to pack a column by gravity until the column volume reached 3 ml. The column was equilibrated with 25 mL of column buffer containing 20 mM Tris-HCl pH 7.4, 0.2 M NaCl and 1 mM EDTA. The clarified lysate was added to the column and the flow through collected. This step was repeated once to improve protein binding. Next, the column was washed with 10 column volumes (CV) of the column buffer described above.

This was followed by elution by flowing 5 CV of column buffer containing 10 mM maltose, collected over three elution steps. A final wash step of 10 CV column buffer was performed to remove any remaining protein (**Appendix A. Figs. 4 and 6**).

2.2.8 Purification of 6His-TEV-Fortilin

Nickel agarose resin (HisPur^{TM} Ni-NTA Superflow agarose, Thermofisher, USA) was used for purification of 6His-TEV-fortilin. An approximately 50% slurry of affinity beads to 20% ethanol we used to pack a column by gravity until the column volume reached 3 ml. The column was equilibrated with 25 mL of buffer containing 50 mM Tris-Cl pH 8.0, 300 mM NaCl, 20 mM imidazole. Next, the clarified lysate was added to the column and the flow through collected. This step was repeated once to improve binding to the column. The column was then washed with 10 CV of buffer containing 50 mM Tris-Cl pH 8.0, 300 mM NaCl, 20 mM imidazole. This was followed by elution with 5 CV of buffer containing 50 mM Tris-Cl pH 8.0, 300 mM NaCl, 200 mM imidazole (**Appendix A. Fig. 5**).

2.2.9 Cleavage of Affinity Tags from Fusion Proteins and Removal of Proteases

Samples containing purified fusion protein underwent cleavage with either human rhinovirus 3C (HRV 3C) protease and/or tobacco enterovirus (TEV) protease using the Pierce HRV 3C protease solution kit (Pierce, Rockford, IL) according to manufacture protocols, as well as an in-house grown TEV protease using 2 µL protease solution for every 200 µg of protein. Protease removal was also done according to manufacture protocols by purification over glutathione agarose or sepharose beads or HisPur Ni-NTA Superflow Agarose (Thermo Scientific, Waltham, MA). The cleaved protein was separated by size exclusion chromatography using an S75 column equilibrated withinto

100 mM NH_4HCO_3 (GE Healthcare, USA). Fractions containing pure protein were combined and concentrated using 5 MWCO PES Vivaspin 20 columns (Sartorious, Stonehouse, UK) by centrifugation at 4000 x g until the volume reached approximately 10 mL. These were then aliquoted such that microcentrifuge tubes contained 2 mg protein each and lyophilized at 2 atm and -80 °C overnight using a LabConco FreeZone 2.5 Plus lyophilizer (LabConco, Kansas City, MO, USA). Samples were stored at -20 °C.

2.2.10 SDS-PAGE Analysis of Protein Expression, Purification and Cleavage

Protein expression, purification and cleavage steps were analyzed using sodium dodecyl sulfate polyacrylamide gel electrophoresis (SDS-PAGE). Samples were prepared such that equal loading was observed in each gel. Gels (12%) resolving and stacking (6%) gels were made according to standard protocol and used for protein separation. Quantification was done using GelAnalyzer 19.1.[132]

2.2.11 NMR Spectroscopy for Activity Assay via Calcium Titration of $(GGS)_N$-Fortilin

Lyophilized $(GGS)_N$-fortilin (1.76 mg) was resuspended in 500 µL of a 20 mM tris-Cl buffer, pH 8.0, containing 200 mM NaCl and 10% D_2O. An aqueous 1 M $CaCl_2$ stock solution was used for each titration. All experiments were performed at 308 K on a 600 MHz Bruker Ultrashield NMR spectrometer equipped with a cryoprobe. For each titrant, 1-2 µL stock $CaCl_2$ was added to a microcentrifuge test tube containing the NMR sample. This was then placed into a glass NMR tube, with care taken to avoid air bubbles. This was then placed in the NMR spectrometer and measurements taken. Data analysis was done using ccpNMR Analysis V3.[133,134]

2.2.12 LC-MS Based Proteomics Analysis

Proteomic analysis was performed using a method established previously with modifications.[135] Excised gel pieces were destained in 50 mM ammonium bicarbonate/50% acetonitrile, reduced in 10 mM DTT for 60 min at 56 ºC, and alkylated in 55 mM iodoacetamide for 60 min at room temperature in the dark. Gel pieces were then digested with proteomics grade trypsin (Thermo Fisher Scientific, Waltham, MA, USA) overnight at 37 ºC. Resulting peptide mixtures were chromatographically separated on a reverse-phase C_{18} column (10 cm x 75 µm, 3 µm, 120 Å) and analyzed on a Velos Pro Dual-Pressure Linear Ion Trap mass spectrometer (Thermo Fisher Scientific) as described previously.[135]

Peptide spectral matching and protein identification were achieved by database search using Sequest HT algorithms in Proteome Discoverer 2.2 (Thermo Fisher Scientific). Raw spectrum data were searched against a protein sequence database containing the anticipated sequences and UniProtKB/Swiss-Prot protein database for *E. coli* (acquired from www.uniprot.org on November 3, 2020). Main search parameters included: trypsin, maximum missed cleavage site of two, precursor mass tolerance of 1.5 Da, fragment mass tolerance of 0.8 Da, fixed modification of cysteine carbamidomethylation (+57.021 Da), and variable modification of methionine oxidation (+15.995 Da). Decoy database search was performed to calculate false discovery rate (FDR). Proteins containing one or more peptides with FDR≤0.01were considered positively identified and reported.

2.2.13 Statistical Analysis

Statistical analysis was carried out using IBM SPSS Statistics 26 for Windows (IBM Corp., Armonk, NY) Statistical significance of differences between groups was evaluating using one-way analysis of variance (ANOVA), and Bonferroni post-hoc test used to assess the significance of differences between individual groups. Values of $p < 0.05$ were considered to be statistically significant. Data are presented as ± standard deviation (SD).

2.2.14 Figure Generation

Figures were made using GraphPad Prism v. 8 (GraphPad, San Diego, CA), Inkscape v. 0.92 (Free Software Foundation, Boston, MA) as well as Adobe Illustrator v. 24.1 (Adobe Inc., San Jose, CA).

2.3 Results

2.3.1 Expression and Purification of Recombinant Human Fortilin.

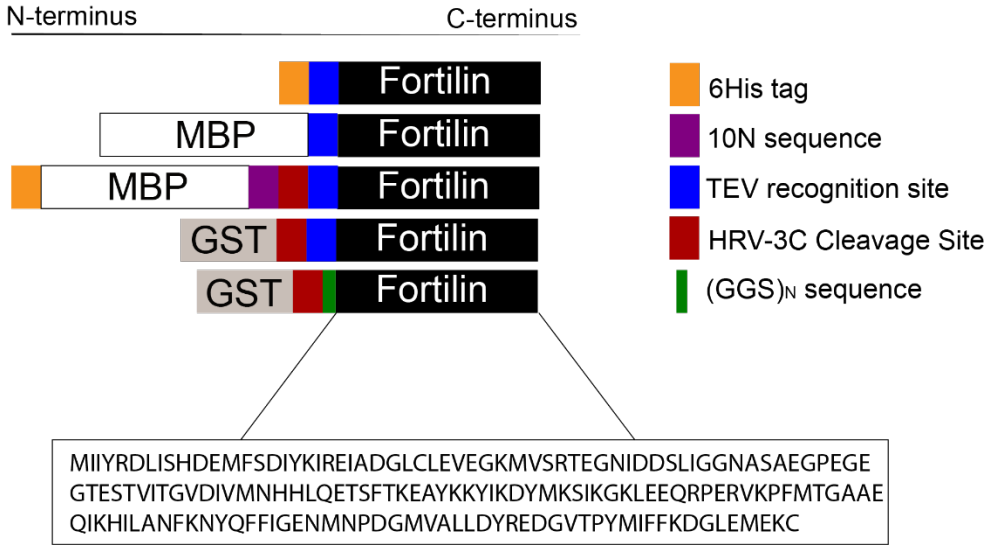

Figure 2.2. Constructs used for recombinant fortilin expression, purification, and cleavage. All constructs were made in ATUM's pD441-SR vector.

Initial efforts to produce a tag-less version of fortilin were hindered by an inability to remove affinity tags by enzymatic cleavage. TEV protease cleavage sites were designed adjacent and N-terminal to fortilin in constructs that included a 6His, a maltose binding protein (MBP), and a dual tagged 6His-MBP tag (**Figure 2.2**). The 6His-TEV-fortilin, MBP-TEV-fortilin and the 6His-MBP-10N-3C-TEV-fortilin constructs were all resistant to TEV protease after 48 hours incubation at room temperature (**Figures 2.3 and 2.4**). The activity of the TEV protease was confirmed on an in-house construct that is identical to the MBP-TEV-fortilin except that is contains the oncostatin M gene (MBP-TEV-OSM) (**Figure 2.3**; Lane 2).

It is well-documented that affinity tags can introduce steric hinderance, making the enzymatic cleavage less efficient, although this does not explain the resistance of the 6His-TEV-fortilin construct. Further, the 6His-MBP-10N-3C-TEV-fortilin construct has an additional Human 3C rhinovirus protease cleavage site N-terminal to the TEV cleavage site. Treatment of the 6His-MBP-10N-3C-TEV-fortilin with 3C protease after 24 hours at 4 ºC resulted in 72% cleaved fortilin, albeit with an additional remaining 3C (Leu-Glu-Val-Leu-Phe-Gln-Gly-Pro) and TEV (Glu-Asn-Leu-Tyr-Phe-Gln-Gly-Ser) amino acids; with no additional cleavage observed after 48 hours. These observations led us to hypothesize that for efficient cleavage, a linker was needed between the protease cleave site and the fortilin protein.

Incorporating a GGS linker between the protease cleavage site and fortilin increases enzymatic protease cleavage efficiency by increasing the space between the protein and cleavage site. Here, we chose to incorporate GGS linkers between the protease cleavage site and the N-terminus of fortilin. We chose the repeating GGS motif

because of the flexibility, experimentally determined random coil behavior, and charge neutrality.[136,137] GGS linker units were either not included in the construct $(GGS)_0$ or included in increasing repeats of GGS from $(GGS)_1$ to $(GGS)_3$. Addition of just one GGS linker to the N-terminus of fortilin was sufficient to produce a successfully cleaved construct, with approximately 86.5% recovered GGS-fortilin after cleavage with 3C protease (**Table 2.1**). Addition of two GGS linker sequences provided 81.5% recovery of $(GGS)_2$-fortilin, and addition of three GGS linkers provided for 85% recovery. Confirmation of cleavage reactions was analyzed by SDS-PAGE (**Figure 2.5**) and compared to a positive control of GST-3C-Syk protein (included in the Pierce Protease kit) to ensure protease efficacy. All samples were also compared against negative controls wherein no protease was added. While addition of extra $(GGS)_N$ linkers provided equivalent recovery of $(GGS)_N$-fortilin, we decided that just one GGS linker would be sufficient for NMR studies as well as reduce the effects of potential steric hindrance from more than one GGS linker sequence at the N terminus. Addition of one GGS linker sequence at the N-terminus of fortilin provides sufficient access for a protease to cleave an affinity tag from fortilin for biological studies.

All constructs produced soluble and good quantities of fortilin; recovery yields are available in **Table 2.1**. Yields were quantified in comparison to the respective non-cleaved construct on the same SDS gel.

Table 2.1. Percent yield of tag free fortilin after one day to cleave constructs. Yields quantified using SDS PAGE image analysis using GelAnalyzer.

Construct	Cleaved construct	Percent (%) recovery of cleaved fortilin
6His-TEV-fortilin	fortilin	0
6His-MBP-10N-3C-TEV-fortilin	TEV-fortilin	72
GST-3C-TEV-fortilin	TEV-fortilin	28
GST-3C-$(GGS)_0$-fortilin	fortilin	< 1
GST-3C-$(GGS)_1$-fortilin	GGS-fortilin	87
GST-3C-$(GGS)_2$-fortilin	$(GGS)_2$-fortilin	82
GST-3C-$(GGS)_3$-fortilin	$(GGS)_3$-fortilin	85

2.3.2 Cleavage MBP Constructs Provided Insight for How to Successfully Cleave an Affinity Tag from Fortilin.

MBP-TEV-fortilin was cleaved by TEV protease after 48 hours incubation at room temperature. Uncleaved MBP-TEV-fortilin can be seen to appear at approximately 62 kDa on an SDS-PAGE gel (**Figure 2.3**). A dark band at 42 kDa indicates the MBP affinity tag, which was expressed in conjunction with the MBP-TEV-fortilin construct. For the 6His-MBP-10N-3C-TEV-fortilin construct, cleavage was observed upon addition of HRV 3C protease after one day, with no additional cleavage after two days. No cleavage was observed for this construct upon addition of TEV protease. In **Figure 2.3**, arrows indicate cleaved TEV-fortilin after one and two days, respectively. No additional cleavage was observed after two days of cleavage reaction, indicating that just one day is required for cleavage to be successful. Both constructs were run against a house-made positive control of MBP-TEV-OSM, or Oncostatin M, a construct known to cleave successfully upon addition of TEV protease.[138] A positive control for HRV 3C protease is shown in **Figure 2.5**, where the GST-Syk protein has been successfully cleaved, demonstrating that both proteases were active at the time of use.

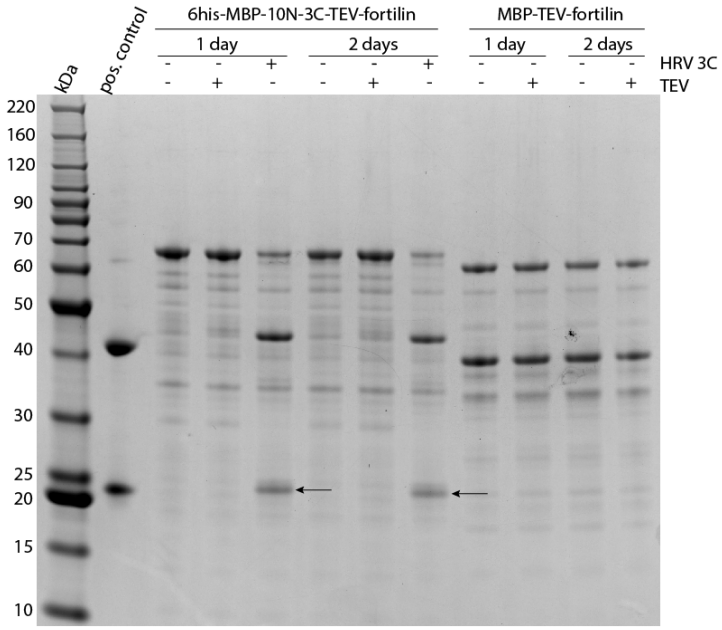

Figure 2.3. MBP construct cleavage reactions. SDS-PAGE gel of TEV and 3C protease cleavage reactions. Cleavage reactions of MBP constructs against a positive control lane of MBP-TEV-OSM. Uncleaved MBP-TEV-fortilin can be seen to appear at approximately 62 kDa on an SDS-PAGE gel. A band at 42 kDa indicates the MBP affinity tag, presumably due to abortive translations for the MBP-TEV-fortilin construct. Arrows indicate successfully cleaved TEV-fortilin.

2.3.3 GST Affinity Tags Were Cleaved With 3C Protease While 6His-TEV Cleavage Was Unsuccessful.

The GST-3C-TEV-fortilin construct showed no cleavage after two days of incubation with TEV protease (day 2 data not shown). However, upon incubation with HRV 3C protease, cleavage was observed after just one day. TEV-fortilin is indicated by an arrow in **Figure 2.4**. As for the 6His-TEV-fortilin construct, no cleavage was observed upon addition of TEV protease after two days of incubation at room temperature. The 6His-TEV-fortilin band was confirmed by mass spectrometry, demonstrating that cleavage had not occurred. The positive control band in **Figure 2.4** is MBP-TEV-OSM, which showed that the TEV protease was active. The positive control for HRV 3C indicates that the 3C protease is active when used against the GST-3C-Syk (**Figure 2.5**).

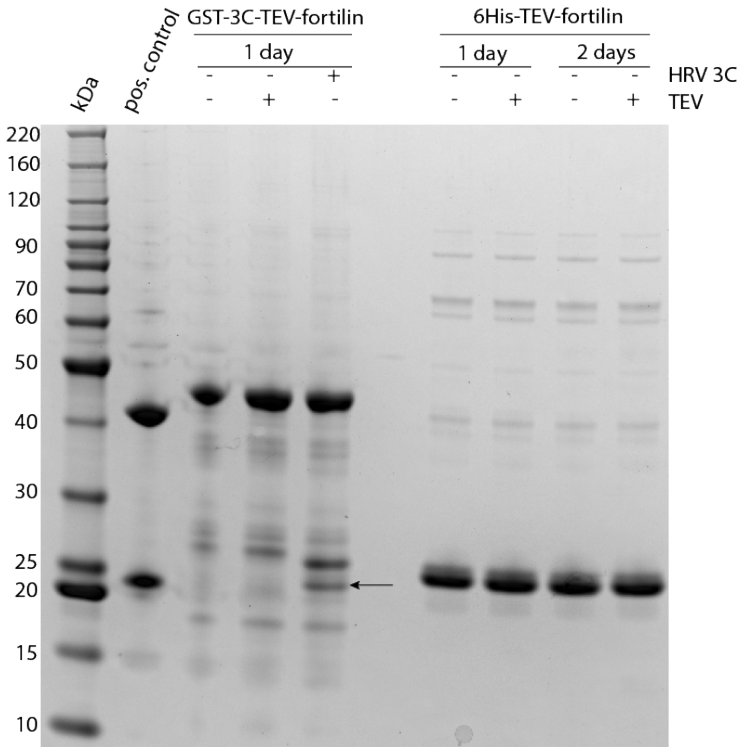

Figure 2.4. Protease cleavage sites located proximal to the N-terminus are resistant to cleavage. Cleavage reactions of GST and 6His constructs against a positive control lane of MBP-TEV-OSM. Protein ladder is shown in the first lane to indicate molecular weight markers on a 12% bis-acrylamide gradient SDS gel. The arrow indicates successfully cleaved TEV-fortilin, where the 3C cleavage site is N-terminal to the TEV protease cleavage site.

2.3.4 Insertion of $(GGS)_N$ Linkers Allow for Affinity Tag Cleavage.

Because the previous constructs containing TEV sequences between the 3C sequence and the fortilin sequence showed successful cleavage, we investigated whether a glycine-glycine-serine (GGS) linker repetition sequence would also result in successful cleavage at the N-terminus and yield intact protein. We used $(GGS)_N$ linker sequences where N = 0, 1, 2 or 3 (see **Figure 2.5**). The positive control lane consists of GST-3C-Syk, which was used to show protease activity. We found that the inclusion of just one GGS linker sequence $(GGS)_1$ led to cleaved fortilin with the sequence GGS-fortilin; this result was verified against a negative control of $(GGS)_0$, as well as no addition of HRV 3C protease. While additional linker sequences proved successful, we moved forward

with $(GGS)_1$-fortilin for NMR analysis to minimize N-terminal binding interference by tag amino acids.

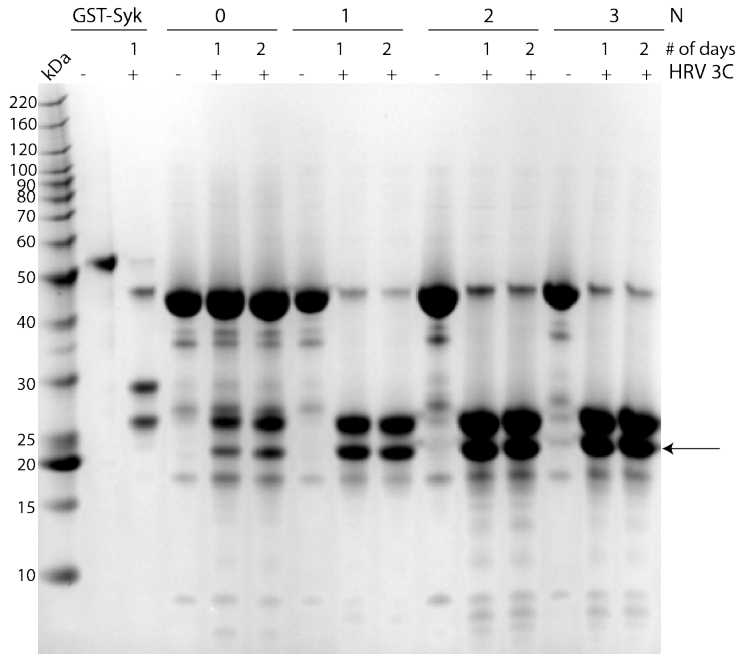

Figure 2.5. Cleavage reactions of (GGS)N constructs. N = 0, 1, 2 or 3 against a positive control lane of cleaved GST-3C-Syk. Protein ladder is shown in the first lane to indicate molecular weight markers on a 12% polyacrylamide SDS gel. Arrows indicate successfully cleaved (GGS)N-fortilin that was confirmed by mass spectrometry.

2.3.5 Biological Activity of Fortilin.

2.4.5.a Calcium Titration of $(GGS)_1$-Fortilin.

a 1 M aqueous solution of calcium chloride ($CaCl_2$) was titrated into a solution of 176 mM $(GGS)_1$-fortilin. Aliquots of 1 µL $CaCl_2$ were used for each titration point for a total of 6 points. Notable peak shifts in the titration can be seen in **Figure 2.6** where arrows indicate increasing concentrations of $CaCl_2$. The combined chemical shifts were calculated for peaks with large shifts (list them here) were used to calculate K_d values

using the binding isotherm: $\frac{Kd+L+R-\sqrt{(Kd+L+R)^2-4RL}}{2R} * Bmax$. We determined a binding K_d of 14.2 ± 3.7 mM.

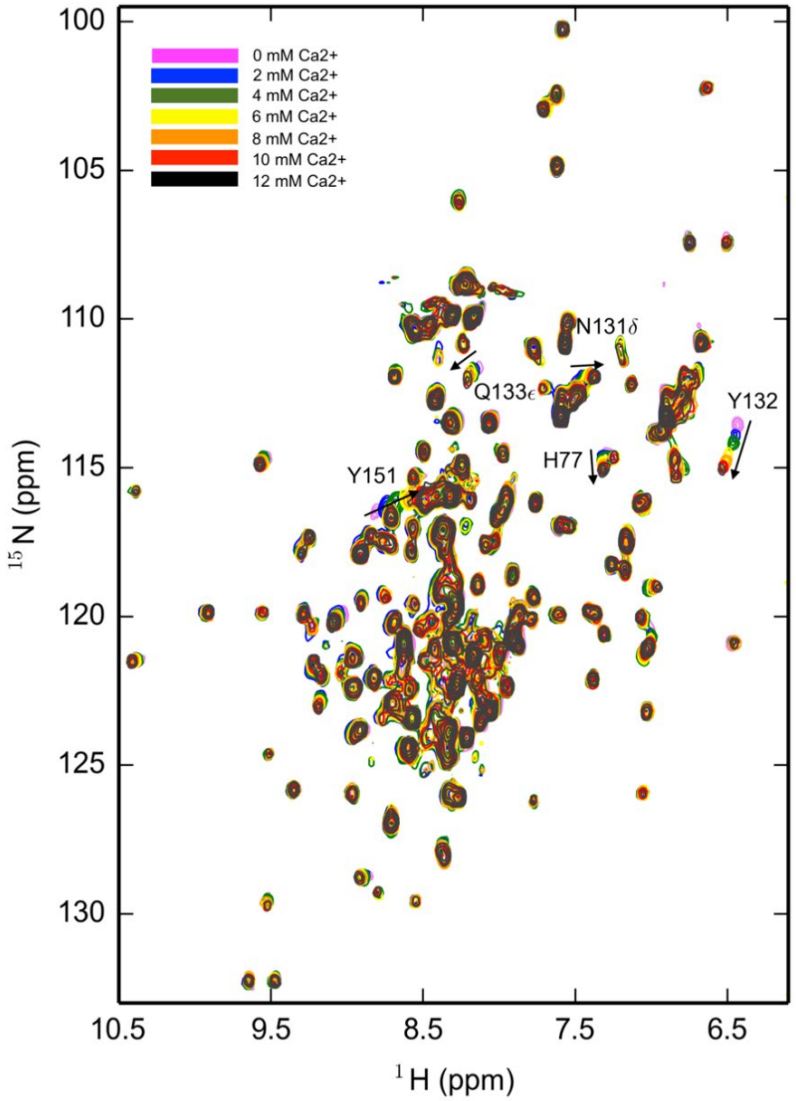

Figure 2.6. 1H,15N HSQC spectral overlay of GGS-fortilin titrated with calcium. Y132, Y151, N131, Q133, and H77 are labeled with arrows indicating increasing concentrations of calcium.

2.4 Discussion

The successful cleavage of the 6His-MBP-10N-3C-TEV-fortilin and GST-3C-TEV-fortilin constructs led us to the hypothesis that, at the N-terminus, space is required

for a protease searching for a cleavage recognition sequence to gain access to the cleavage site. Insertion of just one GGS linker sequence, at the N-terminus and before the cleavage site, provided 78% recovery of GGS-fortilin (**Figure 2.5**). Further characterization of this activity needs to be done to determine the mechanism by which native fortilin hinders protease activity at the N-terminus. According to computational ligand docking studies performed by our lab that were consistent with a previous study, the N-terminus is a predicted location for small molecule binders and is required for activity.[93,139] Additionally, the N-terminus has been shown to be highly conserved among various species and is required for fortilin's anti-apoptotic activity both *in vivo* and *in vitro* when binding to Bcl-xL, a protein that is required in cell survival maintenance.[139] This is experimentally backed by previous work published using *Plasmodium falciparum*, where the artemisinin binding site was characterized, and the binding site was near the N-terminus.[114] Indeed, previous computational work published by our lab has shown that fortilin binds peroxiredoxin-1 (PRX-1), a protein implicated in reactive oxygen species (ROS)-mediated apoptosis, near the N-terminus.[89] It should be noted, however, that to date the binding site for artemisinin to human fortilin has not been characterized in human fortilin, while evidence suggests that dihydroartemisinin (DHA) does bind human fortilin.[113,114]

It is well established that fortilin binds to calcium and the binding site has been characterized (see **Figure 2.1)**.[79,98,101] For the present study, we reproduced $CaCl_2$ titration analysis with the ^{15}N-labeled $(GGS)_1$-fortilin protein using NMR spectroscopy and obtained a K_d value of 14.2 μM, which is within reason to previously reported K_d's for Ca^{2+}.[79] Multiple literature reports provide the K_d values for calcium binding to fortilin

at 7.58 μM, 17.5 μM, 22 mM and 25 mM.[79,96,102] The present study shows that recombinant fortilin, in the absence of an affinity tag, still binds calcium. Biologically, fortilin binds calcium to mediate histamine release from basophils, which play a critical role in immune system function.[127]

2.5 Conclusions

The present study has shown that recombinant, pure, isotopically labeled fortilin can be produced with a cleavable affinity tag when just one GGS linker is added to the N-terminus. This indicates that the N-terminus is partially hidden from protease in the absence of the linker sequence. More studies need to be performed to not only determine the mechanism by which addition of a GGS sequence facilitates cleavage, but to also characterize the interaction of small molecules at the N-terminus, such as artemisinin and DHA, which bind but have not been characterized in human recombinant fortilin.[113,114] Additionally, NMR studies need to be performed on fortilin in other expression systems, such as yeast, to explore the possibility of post-translational modifications (PTMs), and to determine the differences in binding between recombinant fortilin products in *E. coli*, *P. pastoris*, and human cell lines.

CHAPTER THREE: STRUCTURE AND TITRATION STUDIES OF NOVEL FORTILIN CONSTRUCTS WITH AFFINITY TAGS WITHIN THE FLEXIBLE LOOP

Manuscript in preparation

Maranda S. Cantrell[1], Aaron D. Ajeti[1], Ken Fujise[2], Owen M. McDougal[1], Lisa R. Warner[1]

[1]Department of Chemistry and Biochemistry, Boise State University

[2]Department of Cardiology, University of Washington

3.1 Introduction

Cardiovascular diseases (CVDs) such as atherosclerosis are a significant global health issue.[115] According to the Center of Disease Control, cardiovascular disease ranks number one for mortality rates in the United States with an average morbidity rate of 659,041 deaths per year.[140] CVDs also account for an average of 110 billion dollars in expenditures for diagnoses and treatments with the average cost per year trending upward.[141] Other projections for CVD include 45.1% of the US population having some form of CVD by the year 2035.[142] The combined need to lower mortality rates, disease prevalence, and health expenditures requires a drastic acceleration of our efforts to combat CVDs, especially atherosclerosis.

The current treatments for atherosclerosis work to lower cholesterol production and levels in the blood.[115] Unfortunately, these treatments are insufficient as atherosclerosis is dependent on the formation of foam cells that form from circulating macrophages, as opposed to high levels of cholesterol.[115,143,144] The formation of foam

cells is initiated when circulating monocytes take up oxidized low density lipoproteins (oxLDL) and differentiate into macrophages.[143] Typically oxLDLs will trigger cellular apoptosis, but if that mechanism is inhibited, the macrophages will continue to phagocytize oxLDLs and form foam cells.[143] These foam cells are then allowed to deposit on the walls of arteries and form plaques, promoting atherosclerosis. Over time, blockages may form and lead to cardiac events such as heart attack and stroke.

In 2013, mouse studies were performed to determine whether the protein fortilin promoted the progression of atherosclerosis.[118] In this study, the gene to express LDL receptor (LDLR) was knocked down ($LDLR^{-/-}$) in order to form a mouse model of atherosclerosis formation.[118] These mice were then crossbred with mice that had one copy of the fortilin gene knocked down ($fortilin^{+/-}$). This cross breeding generated mice that were $fortilin^{+/-}$ $LDLR^{-/-}$ and $fortilin^{+/+}$ $LDLR^{-/-}$.[118] It was discovered that mice with the heterozygous expression of fortilin upregulates the mechanism of apoptosis of macrophages and hinders the development of plaques.[118] These mouse models provided strong evidence that fortilin was a potential target for drugs to treat atherosclerosis.

Fortilin is a 172 amino acid, 19 kDa polypeptide comprised of two α-helices, a nine strand β-barrel, and a large flexible loop (**Figure 3.1**).[145] A point of interest for rational drug design of inhibitors of fortilin is the close proximity of the amine (N) terminus and the carboxylic (C) terminus that may function as the ligand binding domain.[145] In order to determine drug candidates that will target and inhibit the indigenous function of fortilin, a structure-based approach has been initiated.

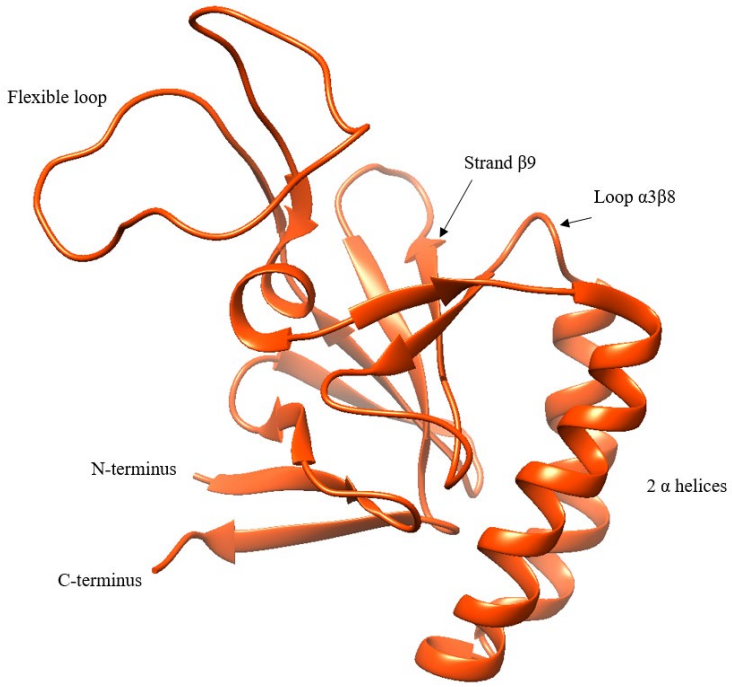

Figure 3.1. Structural characteristics of fortilin. The secondary structures contained within fortilin include two α-helices, one nine-strand β-barrel, and one flexible loop. Another structural quality of interest is the neighboring N- and C-termini. Strand β9 and Loop Lα3β8 contain the coordination sites for Ca2+ binding.

Nuclear magnetic resonance (NMR) spectroscopy is a common method to elucidate the structure of macromolecules and potential binding sites with other molecules.[146–149] Heteronuclear single quantum coherence spectroscopy (HSQC), provides a "fingerprint" spectrum of proteins where each peak correlate to either an amide in the backbone or a side chain amine in the protein. Although NMR has proven to be a powerful tool to advance drug discovery, it is important to note that there are limitations to NMR.[148] NMR is a relatively insensitive technique that requires milligram quantities of isotopically enriched protein to perform a structural or dynamic study.[148] The *Escherichia coli* (*E. coli*) expression system has previously been successful in expressing the necessary amounts of recombinant fortilin.[150] High purity fortilin has been successfully attained using a nickel affinity column and 6-histidine (6His) affinity tail fused to fortilin at the N terminus.[79] NMR structure models have been reported for

fortilin, as well as Ca^{2+} affinity evidenced by side chain proton chemical shifts correlated to Ca^{2+} titration, observed by $^{1}H/^{13}C$ HSQC NMR studies.[79] However, to date, recombinant fortilin protein has not been purified in the absence of an affinity tag attached at either the N- or C-terminus.

Affinity chromatography is a widely used technique in protein purification to simplify the overall purification process.[151] The affinity tag is placed on a protein for it to bind to an affinity column, permitting all of the other water-soluble proteins to be washed away. The affinity tagged protein can then be eluted from the column by addition of a competitive binder of the column solid support, resulting in the displacement of the protein of interest. In the primary sequence of a protein, the affinity tag, typically located at the N-terminus, is followed by a protease cleavage sequence i.e., tobacco etch virus (TEV) protease (ENLYFQ) or human rhinovirus 3C (HRV 3C) protease (LEVLFQ), before the protein sequence begins. The protease cleavage sequence allows for proteolytic cleavage of the affinity tag such that no amino acids are left behind at the N-terminus. Previous work done by our lab showed that addition of a GGS amino acid linker sequence at the N-terminus of fortilin could be successfully cleaved and Ca^{2+} affinity conserved.[150] However, we were unable to remove the GGS tag from the N-terminus which provides uncertainty regarding the ability of inhibitors bind at the computationally predicted, N-terminus, ligand binding site.[89,93]

There is a growing precedent for placing affinity tags within non-structured locations of proteins for purification purposes as well as activity studies, specifically with FLAG and myc antibody affinity tags.[152,153] However, for NMR studies, milligram quantities are required, whereas antibody chromatography is typically performed in

smaller amounts due to the increased cost. To address this, we designed three different constructs (NSer46, CSer46 and CGly56) of fortilin, with the strep-tag affinity sequence (WSHPQFEK) inserted inside of the flexible loop at different locations (**Figure 3.2)**. The loop constructs were designed to eliminate the need for protease cleavage and removed non-native residues at the N and C termini of fortilin. We performed CD and NMR analysis to determine whether the overall structure of fortilin was greatly altered by the introduction of mutants and performed Ca^{2+} titrations using NMR spectroscopy to determine if Ca^{2+} binding affinity was conserved.

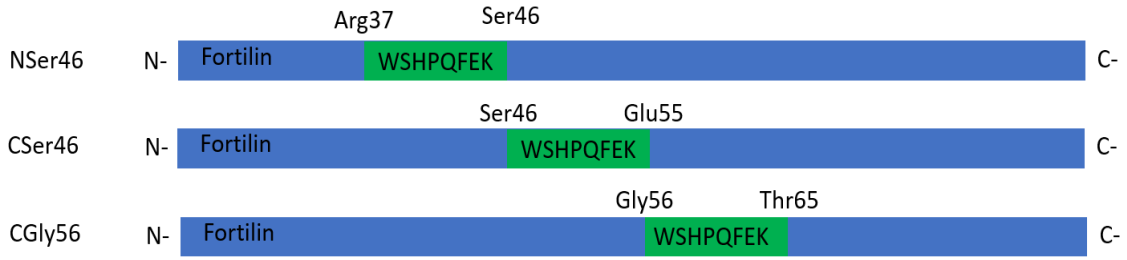

Figure 3.2. A block diagram showing the locations of the eight-residue strep affinity tag (green) within the flexible loop (blue). Top: shows a location of the affinity tag on amide end of Ser46. Middle: shows a location of the affinity tag on the carboxy end of Ser46. Bottom: shows the location of the affinity tag on the carboxy end of Gly56. The integrity of the structures of the mutant constructs were determined by NMR studies and compared to that of wild type fortilin (PDB 2HR9). Ca^{2+} titrations were then performed to assess retention of Ca^{2+} affinity.

3.2 Materials and Methods

3.2.1 Plasmids

All plasmids used in this study for the loop constructs were purchased from ATUM (Newark, CA, USA) using their pD441-SR expression vector. The wild-type fortilin-strep construct was purchased from IBA Lifesciences (Göttingen, Germany) using their pASG-IBA3 expression vector.

3.2.2 Bacterial Cell Transformation and Cell Stock Preparation

For transformation, 1-5 μL of plasmid DNA was added to 50 μL of competent BL21(DE3) *E. coli* cells and incubated on ice for 20 min. Cells were then heat shocked by incubating at 42 °C for 45 seconds, followed by incubation on ice for 2 min. To this, 500 μL of LB broth was added and the solution incubated with shaking at 225 rpm at 37 °C for 45 min. Two LB agar plates containing 25 mg/ml kanamycin were used for plating, with 50 μL spread on one plate and 450 μL spread on the second plate using a turn table and L-shaped spreader. These plates were incubated upside down at 37 °C overnight. For cell stocks, a swipe of colonies was added to 5 mL of LB containing either 25 μg/ml kanamycin (for loops constructs) or 50 μg/ml ampicillin (for fortilin-strep) and incubated at 37 °C for 6-8 hours with shaking at 225 rpm. A sterile 50% aqueous glycerol solution was used to add 500 μL of glycerol to 500 μL of the cell culture. This mixture was flash frozen in liquid nitrogen and stored at -80 °C.

3.2.3 Protein Expression.

Expression was generated from plated cells on LB agar containing either 25 μg/ml kanamycin (for loop constructs) or 50 μg/ml ampicillin (for fortilin-strep) either from 50% glycerol cell stocks or from bacterial cell transformation of plasmids. Multiple colonies from a LB agar plate were inoculated into 5 mL of LB containing either kanamycin or ampicillin and incubated at 37 °C with shaking at 225 rpm for 6-8 hours. The culture was then centrifuged at 4000 x g for 10 min at 30 °C and the media discarded. The pellet was resuspended in 50 ml of pre-warmed M9 minimal media containing appropriate antibiotic in a 250 mL Erlenmeyer flask and incubated overnight at 37 °C. The next morning, this culture was transferred to a 50 mL conical tube and

centrifuged at 30 °C for 10 min, and the media discarded. The pellet was resuspended in 1 L of pre-warmed M9 minimal media containing antibiotic and ^{15}N-NH_4Cl as the sole nitrogen source and 0.5 g/L ^{15}N isogro (Thermofisher, USA). This culture was incubated at 37 °C with shaking at 225 rpm until the OD_{600} reached 0.5-0.7 (about 2 hours) and either IPTG (for the loop constructs) added to a final concentration of 1 mM or anhydrotetracycline (for the fortilin-strep construct) to a final concentration of 0.2 μg/ml to induce protein expression, and the temperature lowered to either 30 °C for 6-hour expression, or to 18 °C for overnight expression. Expression was halted by centrifugation at 4000 x g for 20 min at 4 °C. Pellets from 1 L cultures were resuspended in 40 mL lysis buffer containing 100 mM Tris-Cl pH 8.0, 150 mM NaCl, 1 mM EDTA as well as 0.1 mg/ml chicken egg white lysozyme (FisherSci, USA), 1 crushed tablet of Pierce protease inhibitor cocktail (Thermofisher, USA) and 1 μL of DNase (Thermofisher, USA). This solution was stored at -20 °C until purification for up to 2 weeks.

3.2.4 Cell Lysis.

Lysis solutions were thawed in a room temperature water bath until no ice remained (approximately 30 min). Lysis was obtained by sonication at 70% amp for 3 minutes of total sonication (6 cycles of 30 sec on, 30 sec off). During sonication, samples were kept on ice containing NaCl to keep the samples as cold as possible during this process. After sonication, samples were centrifuged at 20,000 x g for 45 min at 4 °C. The supernatant was collected and filtered through at 0.45 μM PES syringe filter (Fisher, USA) and the precipitate discarded. The clarified lysate was immediately used for affinity chromatography to purify protein. Lysis steps were checked via SDS-PAGE.

3.2.5 Protein Purification

The clarified lysate was kept on ice during all purification steps and all buffers were sterile filtered with 0.22 μM PES and vacuum degassed. For purification, the Strep-Tactin XT- 4Flow high capacity (IBA Lifesciences, Germany) pre-packed 5 mL cartridge was connected to a BioLogic LP (Bio-Rad, USA) system with lysis buffer (described above) as "buffer A" and elution buffer containing lysis buffer plus 50 mM biotin as "buffer B." All flow rates were 2.5 ml/min. The column was equilibrated with 2 column volumes (CV) buffer A before loading the lysate onto the column. After the lysate was loaded, the column was washed with buffer A until the A_{280} consistently read 0.0 (approximately 5 CV). The protein was eluted with buffer B for 3 CV followed by immediate regeneration of the column with 15 CV of a 3M $MgCl_2$ solution. The $MgCl_2$ was removed by washing the column with 15 CV of buffer A. For this process, 1.0 mL fractions were collected for each step and purification checked by SDS-PAGE. Purified protein was buffer exchanged into 100 mM ammonium bicarbonate by concentrating the protein eluate in a 7 MWCO spin concentrator (Fisher, USA). Once the volume reached approximately 0.5 mL, 100 mM ammonium bicarbonate was added to the 20 mL fill line and the sample centrifuged at 4000 x g at 4 °C. This process was repeated for a total of 4 centrifugations to ensure that no elution buffer remained in the sample. This sample was then concentrated to make ~1.0 mL aliquots containing ~10.0 mg protein and lyophilized on a LabConco lyophilizer overnight. Lyophilized samples were stored at -20 °C. Concentrations were estimated using both BCA assay kit (Thermofisher, USA) and by A_{280} readings using Beer's Law.

3.2.6 Circular Dichroism of Wild-Type and Mutant Constructs.

Purified lyophilized samples were reconstituted into 50 mM sodium phosphate buffer, pH 7.5, containing 100 mM NaF, and 1 mM TCEP. CD spectra were collected using a Jasco J-810 spectropolarimeter. Wild-type fortilin was measured at 0.1117 mg/mL, fortilin CGly56 was measured at 0.0980 mg/mL, and fortilin NSer46 was measured at 0.1050 mg/mL. Samples were analyzed in a 0.1 cm cuvette at 20 °C. Three spectra were collected for each sample at 1 nm intervals from 275 nm to 170 nm. Three baseline spectra were collected using the same instrument parameters. The sample and baseline spectra were averaged, and the baseline spectra were subtracted from the sample spectra. The resulting spectra were converted from theta machine units (θ) to delta epsilon units (Δε) using the following equation:

$$\Delta\varepsilon = \theta \times \frac{0.1 \times MRW}{P \times CONC \times 3298}$$

where θ = machine unit, mean residue weight (MRW) = protein weight (Da)/number of residues – 1, path length (P) = cuvette path length (cm), protein concentration (CONC) = protein concentration in mg/mL. The resulting spectra were analyzed with the DichroWeb server, using the CDSSTR analysis program and reference set 4.[154–156]

3.2.7 3D NMR Resonance Sample Preparation and Conditions

Lyophilized, $^{15}N/^{13}C$-labeled mutant protein was prepared in ~10 mg aliquots. CGly56 mutant protein was prepared in 500 µL of a 50 mM sodium phosphate pH 7.5, 200 mM NaCl, 1 mM TCEP with 0.1 mM TSP in D_2O added as a reference standard. CSer46 mutant protein was prepared in 500 µL of a 50 mM sodium phosphate pH 7.5, 50 mM NaCl, 1 mM TCEP with 0.1 mM TSP in D_2O added as a reference standard.

3.2.8 $^{1}H/^{15}N$-HQSC NMR Sample Preparation and Conditions.

For SMI titrations, approximately 2 mg ^{15}N-labeled lyophilized protein was resuspended in 500 μL of NMR buffer containing 50 mM sodium phosphate, pH 7.8, 50 mM NaCl, 0.1 mM TSP, 10% D_2O and 1 mM d-DTT. 1-2 μL of a 10 mM SMI stock was added for each titration point. For calcium titrations, 2 mg ^{15}N-labeled lyophilized protein was resuspended in 500 μL of buffer containing 20 mM Tris-Cl pH 7.4, 200 mM NaCl, 10% D_2O and 1 mM d-DTT. 1-2 mL of a 1 M $CaCl_2$ stock solution was added for each titration point, up to a total of 20 μL calcium.

3.3 Results and Discussion

3.3.1 Expression and Purification of Mutant Constructs

Expression and purification yielded high quantities of recombinant fortilin mutant protein (**Table 3.1**). These amounts are ideal for NMR analysis because high quantities are required, as NMR is a relatively insensitive technique.[148] Purification was checked by SDS-PAGE and can be found in Appendix B, **Figures B1-B5**. Protein concentrations were estimated via A_{280} measurement or by bicinchoninic acid (BCA) assay using a standard calibration curve with bovine serum albumin (BSA). In brief, BCA assay is performed by making a diluted standard curve of BSA and chelating with Cu^{2+} to form Cu^{1+} in an alkaline environment followed by reaction with BCA for colorimetric detection and measurement at λ = 562 nm. Replicate samples with protein are treated with copper and then BCA in the same manner as BSA. Comparison is made to the standard curve to approximate the concentration in mg/ml with a detection limit of 2.0 mg/ml.

Table 3.1. Yield in mg of fortilin construct after final purification steps. *Lyophilized aliquots are in 2 mg amounts for ^{15}N labeled, and 10 mg aliquots for $^{15}N/^{13}C$ labeled protein.

Construct	Label type	Yield (mg)	# of lyophilized aliquots*
CGly56	^{15}N	8.15	4
NGly56	^{15}N	15.66	7
NSer46	^{15}N	6.34	3

3.3.2 Structural Analysis of Mutant Constructs

3.3.2.a Circular Dichroism of Secondary Structures of CGly56 and NSer46 Versus WT Fortilin

The structure of the fortilin mutant constructs appears to be conserved when the affinity tag is placed within the flexible loop when analyzed by both circular dichroism and NMR spectroscopy. Changes to the α-helical, β-strand, turn and unordered structures determined by CD can be found in **Table 3.2**. According to the secondary structure analysis, the NSer46 construct appears to be the closest in secondary structure to the wild-type construct (**Figure 3.3**). These results indicate that the introduction of eight consecutive amino acid mutations within the flexible loop region of fortilin does not considerably change the secondary structure of fortilin. This is a promising result for future analysis with SMIs to perform titrations wherein binding is predicted at the N and C termini of fortilin.

Table 3.2 Calculated secondary structure percentages for WT fortilin and two of the loop mutants.

Sample	Total α-helical	Total β-strand	Turns	Unordered	NRMSD
WT	9	33	23	35	0.040
CGly56	9	36	22	33	0.016
NSer46	9	34	24	33	0.033

The overall α-helical structure remains exactly the same for each construct, indicating that no changes to the α-helical content are made when introducing mutations within the flexible loop. The overall β-strand content has changed, but only slightly, for each construct, remaining relatively unchanged along with the total turns and unordered structure of the protein. These findings are consistent with previous findings of the rigidity of the majority of the structure of fortilin.[79] While both constructs are similar in secondary structure to the native protein, the NSer46 constructs is slightly closer overall. The normalized root mean standard deviation (NRMSD) value is an indication of the goodness of fit for the data to the reference set used, with NRMSD < 0.05 being considered a good fit. For the data collected, all spectra have relatively low NRMSD values ranging from 0.016 to 0.040 (**Table 3.2**).

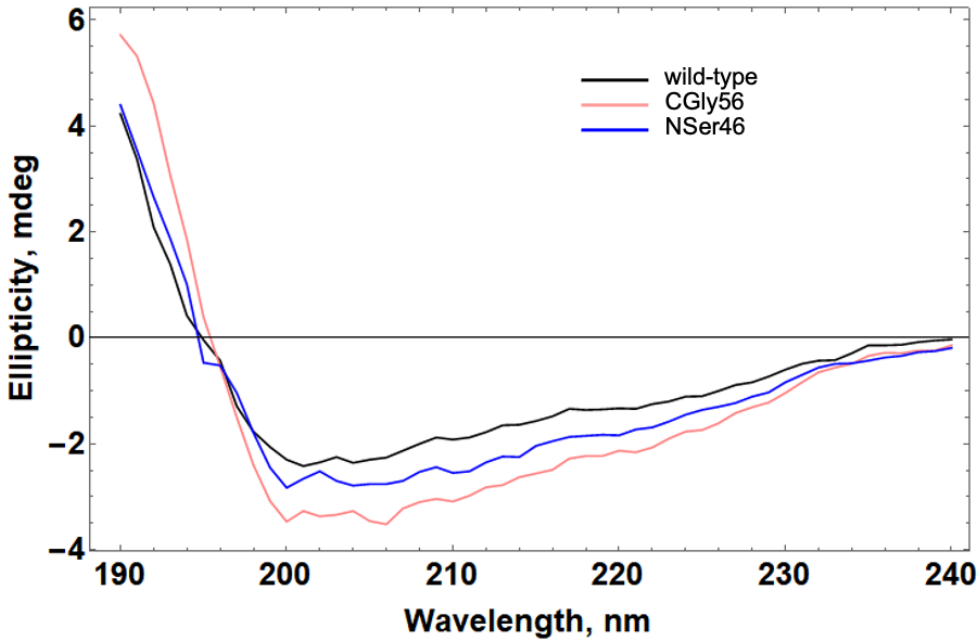

Figure 3.3 Structural integrity of fortilin is conserved in mutant constructs. CD spectra showing the secondary structure analysis of wild-type (black) versus CGly56 (pink) and NSer46 (blue).

3.3.3 NSer46 (007)

3.3.3.a $^{1}H/^{15}N$-HSQC Comparisons to Wild Type Fortilin

The NSer46 mutant construct was analyzed by NMR spectroscopy and the $^{1}H^{15}N$ HSQC spectra compared to wild-type fortilin-strep protein. The spectrum of the fingerprint region of mutant fortilin appears to be relatively conserved when compared to the same chemical shift region as WT (**Figure 3.4**). The greatest changes to the spectra appear at the dimensions indicated by boxes and arrows where peaks have either shifted from the wild-type (in red) peak or appeared as new peaks in the spectrum. The amino acid Q121, which contains two amino groups (one in the backbone and one in the side chain) has shifted in the spectrum slightly, which may indicate a slight change in the overall structure near that residue. There are two new peaks at ppm values of {10.5, 115} and {6.01, 115}, which may be amino acids from the affinity tag, though sequential backbone assignments are required to confirm this.

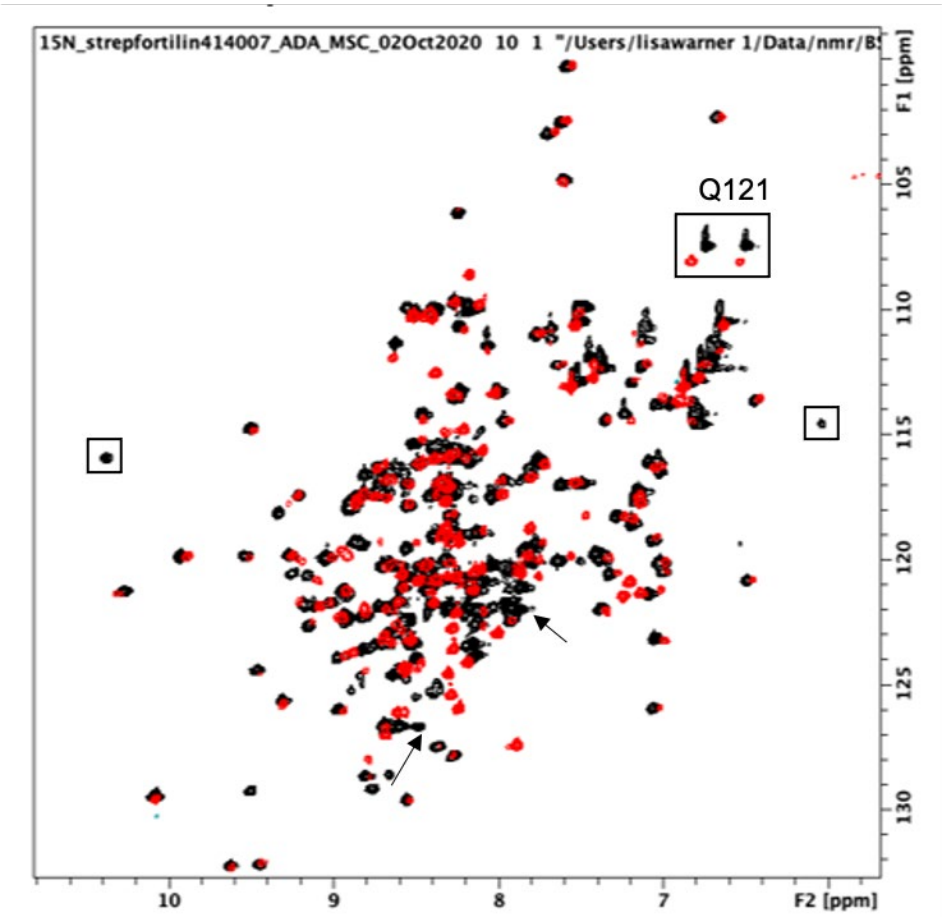

Figure 3.4. A comparison of wild type fortilin and the NSer46 mutant construct as shown by 1H/15N-HSQC NMR spectroscopy. The wild type fortilin spectrum (red) is overlayed with the mutant construct spectrum (black) to observe differences in peak signals. When overlayed most signals remained the same, with the few differing signals likely accounting for the strep tag mutation.

3.3.3.b NMR Titration with Calcium

To confirm whether *in vitro* biological activity was conserved after the introduction of mutations within the flexible loop, we performed calcium titrations with NSer46. As increasing amounts of $CaCl_2$ are added, peaks are observed to shift (**Figure 3.5**). The peak for amino acid Y132 was chosen as a representative peak for calcium binding, because it has been used previously to determine K_d values, and it appears to shift the most dramatically over the course of Ca^{2+} titration.[79,150] These results are consistent with previously published data.[79]

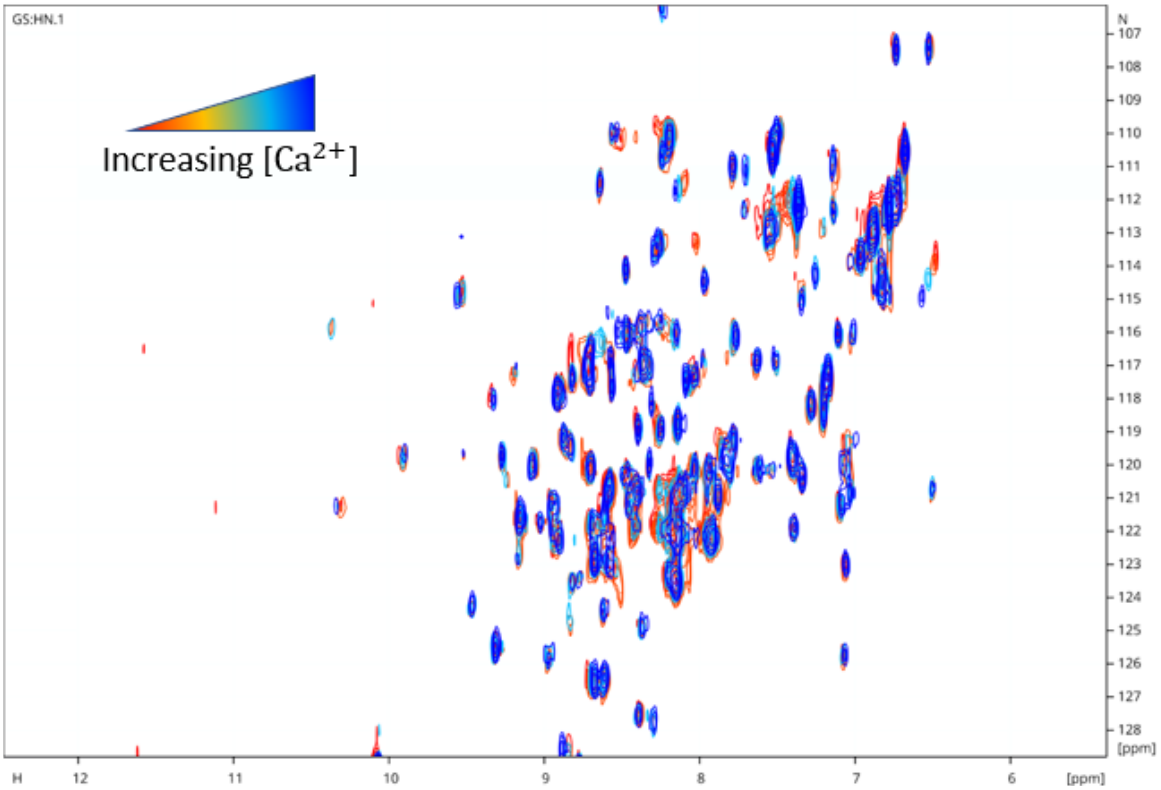

Figure 3.5. An overlay of 1H/15N-HSQC spectra during a Ca2+ titration experiment with NSer46. The residue peaks shift hot (red) to cold (blue) colors with the addition of CaCl2. Y132 (indicated with a black arrow) showed a prominent downfield shift during the titration with Ca2+, consistent with literature reports for WT fortilin (shift is indicated by an arrow).

The calcium titration data were analyzed using the Langmuir binding isotherm: $\frac{Kd+L+R-\sqrt{(Kd+L+R)^2-4RL}}{2R} * Bmax$ where L = ligand and R = receptor concentrations. The peak for Y132 was followed and the changes in ^{1}H and ^{15}N chemical shifts recorded as calcium concentration increased. Using this binding fit for the data, a dissociation constant of 27.8 ± 4.63 mM was calculated for NSer46 to calcium (**Figure 3.6**).

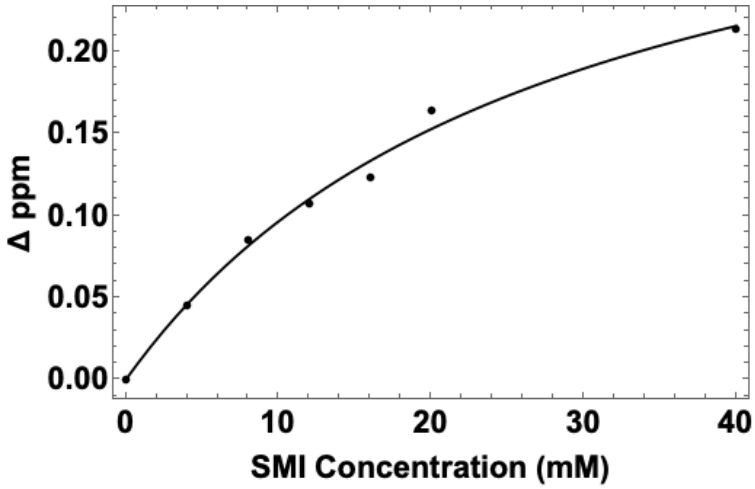

Figure 3.6. Calcium binds NSer46 mutant fortilin with an estimated dissociation constant of 27.8 ± 4.63 mM.

3.3.4 CGly56 (004)

3.3.4.a $^{1}H/^{15}N$-HSQC of CGly56

The fortilin mutant construct fingerprint $^{1}H/^{15}N$-HSQC spectrum appears to be of a similar nature to the wild type and NSer46 constructs, indicating a conserved structure (**Figure 3.7**). Differences is spectral quality in **Figure 3.7** are attributed to the spectra being recorded on different resolution spectrometers. The CGly56 construct HSQC was recorded on an 800 MHz spectrometer, which being a higher field strength, provides higher resolution spectra. There are some changes in appearance between the fingerprint spectra of WT versus NSer46 and CGly56 indicated in **Figure 3.7**. Sequential backbone assignments and 3D structural data must be complete to obtain full structural information on these constructs.

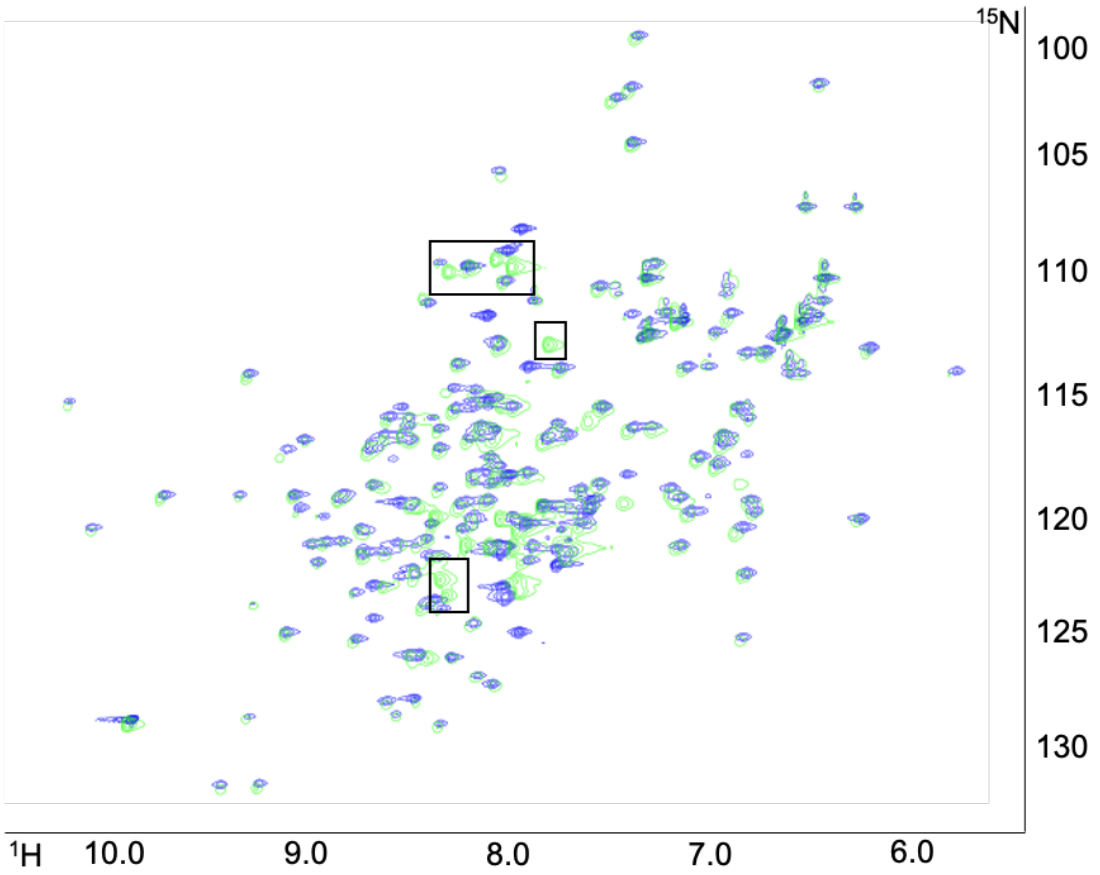

Figure 3.7. A comparison of CGly56 mutant fortilin (blue) 1H/15N-HSQC NMR spectrum overlaid on the spectrum of NSer46 mutant construct (green). The spectral overlay shows high structure homology, with differing signals most likely attributable to the strep tag location. Major differences in peak signal are boxed.

3.4 Conclusions & Future Directions

Loop mutant constructs were generated with the purpose of removing the possibility of residual amino acids at the N and C termini of fortilin, such that activity studies may be performed were binding at the N or C termini may be performed. The mutant constructs appear to have good conservation of secondary and tertiary protein structure as compared to WT fortilin when analyzed by both CD and NMR spectroscopy. The NSer46 mutant has conserved Ca^{2+} binding affinity and is relatively similar to the K_d estimated with native fortilin of between 22 and 25 mM that was also determined by NMR spectroscopy following Y132.[79] The next step for this project is to complete

calcium titrations for all mutant constructs as well as to solve the solution structures by NMR spectroscopy to confirm the CD and HSQC results. While the data presented here provide evidence to the structural integrity of fortilin mutants, solving the solution structures will aid in confirming that the overall structure of fortilin has not been changed significantly by the introduction of loop mutants. This is done by first collecting 3D spectra to coordinate the fingerprint $^{1}H/^{15}N$-HSQC to the 3D spectra to make sequential peptide backbone assignments followed by molecular minimizations with nuclear Overhauser effect spectroscopy (NOESY) data to determine through-space couplings between atoms. This will be done to confirm the structural integrity of the mutant proteins.

CHAPTER FOUR: PRELIMINARY STRUCTURE ACTIVITY STUDIES OF FORTILIN

Maranda S. Cantrell (unpublished)

4.1 Introduction

The determination of binding sites on protein targets is crucial to the rational drug design process. By determining different positions on a protein where a drug target may bind, changes can be made to the drug target to allow for more binding specificity and drug efficacy. There are three popular methods used today to structurally characterize protein binding sites and these are cryo-electron microscopy (cryo-EM), X-ray crystallography and NMR. Cryo-EM is an emerging technique that has gained popularity in recent years for its simple sample preparation methods and ease of use. However, it is a relatively expensive technique and cryo-EM equipment is not yet widely available. X-ray crystallography requires the formation of crystals, which can be nontrivial to make and can take many months or even years to form, let alone crystallizing a protein-target complex, which involves yet more method development. NMR, in comparison, is a more rapid technique, although the amount of protein required for NMR studies are quite high, in the mg range, and solubility can be a limiting factor. Another drawback of NMR is that proteins ideally must range in size between 1 and 50 kDa for optimal analysis. As the size of the protein analyzed gets larger, too many signals complicate the spectra and subsequent analysis. Fortilin is a 19 kDa protein that can now be expressed in mg quantities, making it a suitable candidate for analysis by NMR spectroscopy.

Molecular dynamics (MD) is a powerful tool used to provide a basis level of understanding the lowest energy conformation of many molecules and proteins. MD is often used for predicting where and how a ligand may interact with a target in the absence of experimental data. Additionally, many MD programs, such as GROMACS, are free to use and widely available to researchers.[157] MD in conjunction with a docking program like Autodock Vina can be used to perform high throughput screening (HTS) methods, like the computational prediction for large quantities of molecules contained in electronic databases. Computational HTS is an ideal tool to use prior to experimental screening of SMIs to proteins, because it is incredibly cost effective, rapid and provides valuable structure-function insights.

Before using an expensive experimental technique such as NMR, X-ray and cryo-EM, assays should be performed to determine the best conditions for stability of the protein, as well as small molecule binding assays to determine which drugs analyzed will bind the protein target. Drug candidates that show promise in early assays may be taken on to NMR analysis to determine their binding site on the protein and can then move forward in the drug design process. Fortilin was analyzed by computational screens as well as differential scanning fluorimetry (DSF) to determine the optimal buffer conditions to keep the protein stable in solution, at the concentration needed for NMR experiments, as well as perform a small molecule screen to see identify which candidates may be used in NMR determination of binding site location.

DSF, also known as “thermal shift assay,” is a technique that was first developed in 1991 by Semisotnov et al., and improved for its use with quantitative polymerase chain reaction (qPCR) equipment by Pantoliano et al., in 1997.[158,159] The general workflow for

this technique is that the protein is denatured over a temperature gradient and the melting temperature of the protein is recorded as a fluorescent reporter signal. Fluorescent reporters may be intrinsic to the protein, such as a green fluorescent protein (GFP) tag or via the use of a tryptophan residue(s), or they may be extrinsic, such as SYBR orange or other commercially available dyes. As your protein denatures with the increase in temperature, the dye binds to hydrophobic residues in the protein and the fluorescent signal increases with rising temperature. For TCTP, the use of an extrinsic dye is necessary, because TCTP does not contain tryptophan residues. Stability assays of the protein are first performed with a buffer screen to determine the average melting temperature of the protein as well as determine the optimal buffer conditions. Next, a SMI screen may be performed. Addition of small molecule drugs to the sample can either increase (stabilize) or decrease (destabilize) protein stability and provide a yes/no answer as to whether a SMI should be considered for NMR titration experiment. The results presented here are from DSF screening for buffer stability as well as SMI binding to determine the candidates that could go on for study by NMR spectroscopy. We used SMI candidates to perform NMR titrations with different TCTP recombinant protein constructs to determine potential binding site residues on TCTP.

4.2 Materials and Methods

4.2.1 Computational Docking using Autodock Vina

The solution NMR structure of fortilin has been determined.[79] The PDB file for this structure, 2HR9 was used for all experiments. Drug candidate structures were provided by our collaborator Dr. Brian Blagg at Notre Dame University and docking performed on structures with K_d values below 10 nM (determined experimentally using

SPR by Dr. Blagg's group and can be found in **Table 4.1**. GROMACS software was used to perform molecular dynamics on fortilin to find the lowest energy structure using the AMBER03 force field and TIP3P water model.[157,160] The AMBER03 force field was chosen because it is most applicable to MD simulations with proteins, as each amino acid within the protein is allowed its main charge, if need be and is designed for solution phase simulations.[161] The TIP3P water model was chosen because its rigid water molecule model is ideal for HTS and it has a relatively low computational cost.[162] The protein was solvated in a cubic box and ions added to make the protein neutral in charge. Energy minimizations at constant pressure (NVT) and constant temperature (NPT) were performed before minimizing the final structure.

Once minimized, Autodock Vina software v.1.1.2 was used to perform molecular docking of the drug candidates in **Table 4.1** to predict their binding sites.[22] Simulations were run such that fortilin was made to be a rigid structure, which is not ideal for a real-world situation, but is necessary for higher throughput screening of drug candidates to obtain information in a time-sensitive manner.

Table 4.1. Structures used for computational docking experiments to estimate K_d values for binding to WT fortilin. The K_d values displayed in this table were experimentally determined using SPR.

Urea Compound

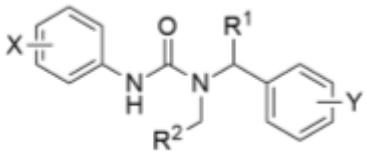

Compound Name	X	Y	R^1	R^2	K_d (nM)
AZU_3	m-Cl, p-Cl	p-OH	CH_3	Ph-CH_2	0.46
AZU_6	m-Cl, p-Cl	o-OH	CH_3	CH_3CH_2	1.6
AZU_8	m-Cl	o-OH	CH_3	Ph-CH_2	0.81
AZU_9	o-Cl	o-OH	CH_3	Ph-CH_2	1.74
AZU_13	m-CH_3	o-OH	CH_3	Ph-CH_2	1.26
AZU_20	m-Cl, p-Cl	p-F	CH_3	Ph-CH_2	1.55
AZU_22	m-Cl, p-Cl	p-NO_2	CH_3	Ph-CH_2	0.01
AZU_23	m-Cl, p-Cl	p-CH_3	CH_3	Ph-CH_2	4.90

Thiourea Compound

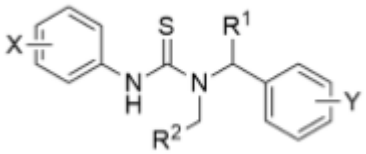

AZTU_5	m-Cl, p-Cl	o-OH	H	Ph-CH_2	9.54
AZTU_6	m-Cl, p-Cl	o-OH	CH_3	CH_3CH_2	0.03
AZTU_7	p-Cl	o-OH	CH_3	Ph-CH_2	1.29
AZTU_8	m-Cl	o-OH	CH_3	Ph-CH_2	1.89

Thiourea hydroazide compound

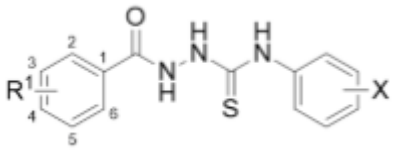

AZTH_1	H	--	o-Cl	--	2.66
AZTH_7	3-OMe, 4-OMe	--	o-Cl	--	4.53
AZTH_12	3-OMe, 4-OMe, 5-OMe	--	o-Cl, m-Cl	--	2.46

4.2.2 Differential Scanning Fluorimetry of Fortilin-Strep

4.2.2.a Buffer Screen to Determine Optimal Conditions for Fortilin Protein

Recombinant fortilin-strep (preparation described in section 3.2) was resuspend in a dilution buffer containing 10 mM sodium phosphate (NaPi), pH 7.5 and 10 mM NaCl to a final concentration of 100 μM. To this solution, either 10 or 20 μL (done to determine an optimal dye concentration) of a 5000 X stock of SYPRO Orange fluorescent dye in DMSO (Thermofisher, USA) was added. Stocks (5X) of the buffers described in **Table 4.2** were prepared. To each well in a 0.2 mL 96-well plate, 40 μL of protein solution was added with 10 μL of the corresponding 5X buffer solution. The samples were run on a Quant Studio 3 Real Time PCR System (Thermofisher, USA). The temperature gradient was as follows: 25 ºC hold for 1 min, 1 ºC/s to 95 ºC, hold 95 ºC for 2 min, return to 25 ºC.

Table 4.2 Buffer screen conditions for fortilin-strep. A total of 30 unique buffer conditions were used for this analysis.

Buffer	[NaCl], mM	pH
50 mM NaPi	50 mM	6.5, 7.0, 7.5
	150 mM	6.5, 7.0, 7.5
	250 mM	6.5, 7.0, 7.5
50 mM HEPES	50 mM	7.0, 7.5, 8.0
	150 mM	7.0, 7.5, 8.0
	250 mM	7.0, 7.5, 8.0
50 mM Tris	50 mM	7.0, 7.5, 8.0, 8.5
	150 mM	7.0, 7.5, 8.0, 8.5
	250 mM	7.0, 7.5, 8.0, 8.5
1X PBS	none	

4.2.2.b SMI Screen for Potential Hits

Fortilin-strep at 100 μM in a 1X PBS solution was prepared containing 20X SYPRO orange dye. To each well, 48 μL of fortilin solution was added along with 2 μL

of a SMI stock solution of 10 μM. The SMI molecules used, in duplicates, for this study were artemisinin, dihydroartemisinin (DHA), ampicillin, kanamycin, biotin, 10B4, 10B5, 10B6, 10B7, 26A3, 26A4, 10.3, 10.4 and 10.5. Structures with shortened names are SMIs derived from the OSM project with Dr. Jorcyk's lab and are protected intellectual property. These samples were run with the same temperature gradient as described in 4.2.2.a.

4.2.3 NMR Titration Analysis with Small Molecules

Lyophilized protein (2 mg) of either wild-type, NSer46 or CGly56 was reconstituted in 500 μL of NMR buffer (50 mM NaPi, pH 7.5, 50 mM NaCl, 10% D_2O, 0.1 mM TSP, 16 μM reducing agent [DTT or TCEP]). $^{1}H/^{15}N$-HSQC spectra were collected on a Bruker 600 MHz NMR spectrometer fitted with a cryoprobe. SMIs tested against these constructs included 26A3 (10 mM stock in DMSO), 11CO9 (50 mg/ml stock in DMSO) or artemisinin (10 mg/ml stock in DMSO). For each titration, 1-2 μL of SMI was added into the NMR sample and spectra recorded at 37 ºC. SMI was added and titration samples run until either the SMI stock crashed in solution or sample was depleted. Filenames and parameters may be found in Appendix D.

4.3 Results and Discussion

4.3.1 Computational Docking Results

The root-mean-square deviation (RMSD) structure of the last 50 ps of the minimization for the backbone of the protein relative to the equilibrated structure can be seen in **Figure 4.1**. The structure determined from the minimization versus the NMR solution structure have little difference in value. The MD results are expected to be

similar to the experimental RMSD for the structure, as NMR structures are typically rendered as the lowest energy structure.

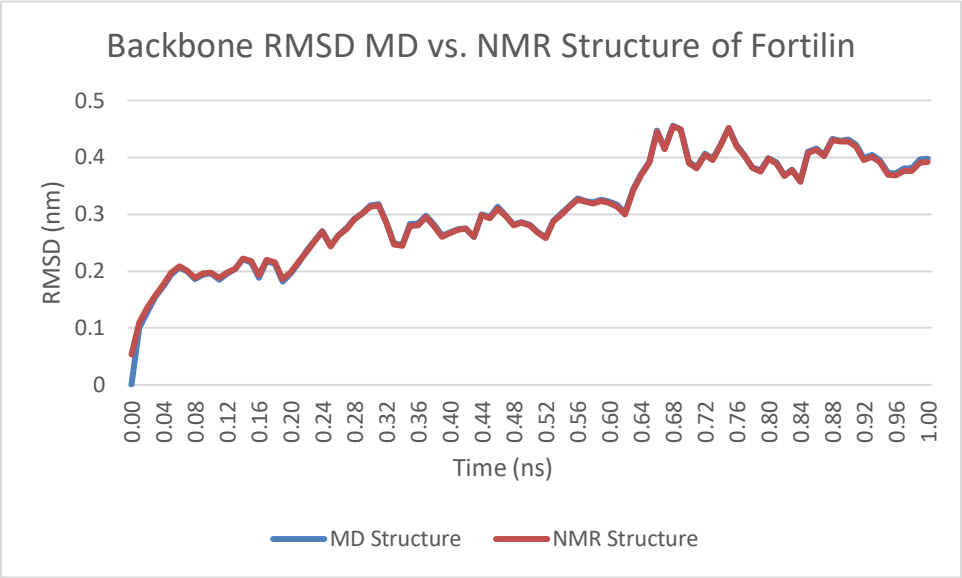

Figure 4.1. RMSD structure derived from the MD simulation vs. the solution derived NMR structure.

For the purpose of simplicity, the docked structure that will be discussed in some detail is AZU_22, which has the lowest experimental K_d value (001 nm). Docking experiments performed determined the lowest energy conformation of AZU_22 to fortilin seen in **Figure 4.2**. A binding affinity of -5.6 kcal/mol was predicted for the best fit conformation. In comparison with the experimentally determined binding affinity (assuming T=298 K) of -14.9 kcal/mol, this leaves an error of 62.4 %.

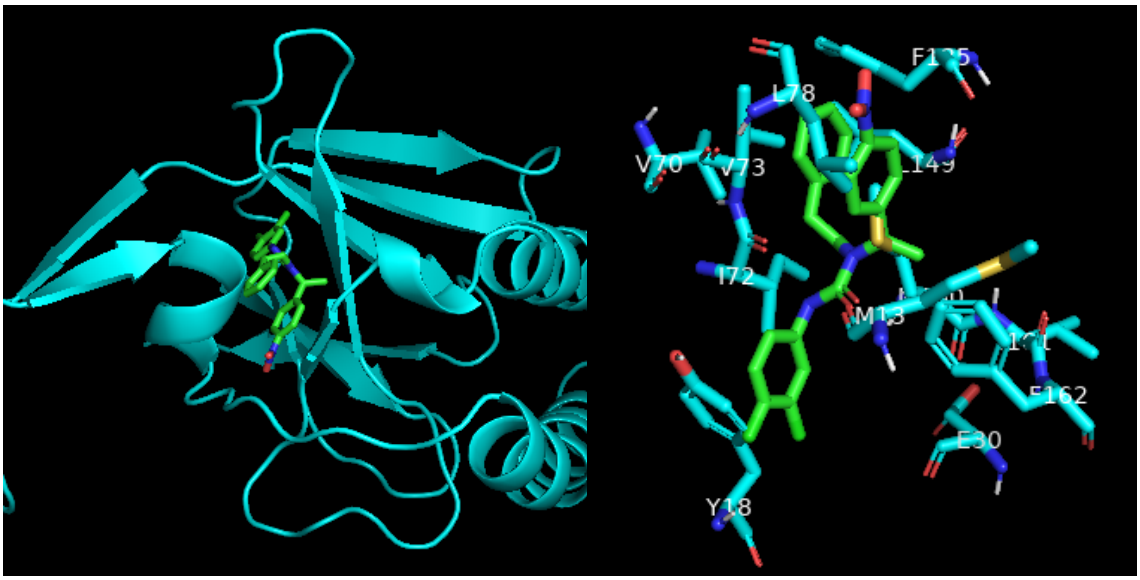

Figure 4.2 Left) Molecule AZU_22 docked onto fortilin with flexible loop cut off for ease of visualization. Right) Residues labeled within 1 Å of AZU_22.

The binding affinities and theoretical error are listed in **Table 4.3**. The percent error is fairly high across the SMIs with an average error of 55.6 ± 4.0 %. One possible explanation for this result is that making the structure completely inflexible and using a rigid water molecule model was not ideal for this experiment. What could be done is allowing for some flexible side chains within the box of allowed binding for small molecule inhibitors since this was not a true HTS computational experiment and the computational cost decreases with the lowered amount of SMIs for screening.

Table 4.3 Experimental and predicted binding affinity values from SPR versus computational docking experiments with Autodock Vina.

Compound Name	Experimental Binding Affinity (kcal/mol)	Predicted Binding Affinity (kcal/mol)	Percent Error (%)
AZU_3	-12.7	-5.8	54.3
AZU_6	-11.9	-5.2	56.3
AZU_8	-12.4	-5.6	54.8
AZU_9	-11.9	-5.3	55.5
AZU_13	-12.1	-5.6	53.7
AZU_20	-12.0	-5.5	54.2
AZU_22	-14.9	-5.6	62.4
AZU_23	-11.3	-5.7	49.6
AZTU_5	-10.9	-5.5	49.5
AZTU_6	-14.3	-5.4	62.2
AZTU_7	-12.1	-5.1	57.9
AZTU_8	-11.9	-4.6	61.3
AZTH_1	-11.7	-5.1	56.4
AZTH_7	-11.3	-5.3	53.1
AZTH_12	-11.7	-5.5	53.0

The docking experiments performed may not be entirely representative of the binding interactions that will be determined by NMR spectroscopy. This is because the structure utilized by Autodock Vina was entirely rigid, with no flexibility allowed. Future docking experiments should be performed to allow for flexible side chains such that more realistic binding information can be predicted. However, without NMR data to determine fortilin binding sites for small molecule inhibitors, no reliable docking information can be obtained. Knowledge of where a small molecule binds experimentally is required to make accurate predictions for future docking studies. The NMR titrations were performed to determine the binding sites with the first round of drug candidates. The ultimate goal of this research is to develop more drugs for atherosclerosis, so that we will be one step closer once binding information to small molecule inhibitors is obtained.

4.3.2 DSF Buffer Screen Results

Fortilin was determined to be stable in a wide variety of buffers across a wide range of pH values. The most stable pH range was 7.0 to 8.0. There appeared to be no major differences in buffer selection as long as the pH was within the optimal range (**Figure 4.3**). The average melting temperature (T_m) was calculated to be 65.08 ºC in 1X PBS for this experiment. To my knowledge, this is the only recorded T_m for recombinant fortilin protein available. Additionally, this screen was performed using two different concentrations of SYPRO Orange dye (10X or 20X). While the majority of the conditions appear to show little difference in T_m based on dye concentration, a few of the conditions had some clear differences in signal. These include 50 mM HEPES, 250 mM NaCl, pH 8.0; 50 mM Tris, 150 mM NaCl, pH 8.0; and one of the 1X PBS samples. Further studies need to be performed to optimize SYPRO Orange dye concentrations in the sample along with careful attention to pipetting error, as these may have contributed to the differing results.

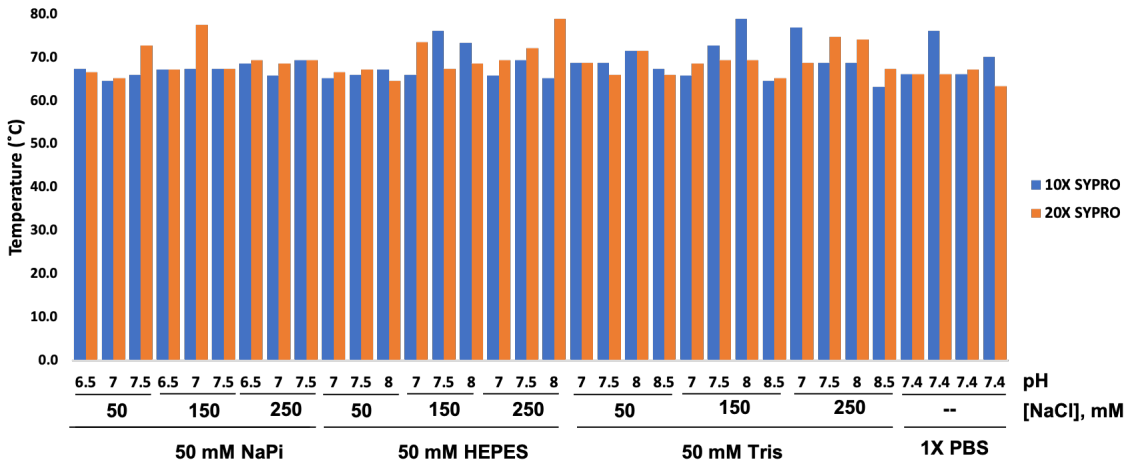

Figure 4.3 Fortilin is stable in a pH range of 6.5 to 8.0 and in a wide variety of buffers at two different SYPRO Orange concentrations. Fortilin has a melting temperature of 65.08 ºC.

4.3.3 DSF SMI Screen Results

For SMI screens using DSF, an indication that a protein binds a given target is indicated by a change in T_m of the protein. This can be either a stabilizing compound, wherein the T_m for the protein increases, or this can be a destabilizing compound, wherein the T_m for the protein decreases. As a general rule, a change of T_m by approximately 2 ºC can be considered a "hit" for binding. Unfortunately, no real significant hit was obtained for fortilin based on this requirement. The SMIs tested against fortilin and the change in T_m is shown for molecules that changed the T_m by anything over 1 ºC (**Figure 4.4**). Calcium, well established as a binder to fortilin, changed the T_m significantly to 68.418 ºC. A few candidates were chosen from this data and used to evaluate binding via NMR spectroscopy, namely 11C09 and 26A3.

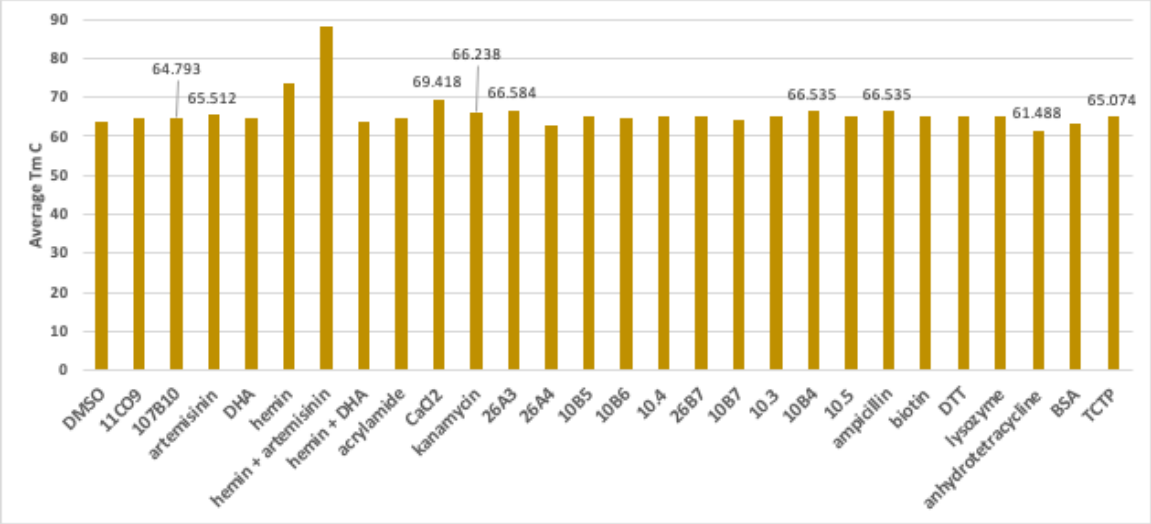

Figure 4.4 SMI screen of fortilin-strep using DSF.

At first glance, hemin as well as hemin + artemisinin appeared to alter the T_m of fortilin greatly. However, by looking at the actual melting curve itself, we see that the data is inconclusive for both samples, as represented in **Figure 4.5**. The left side of

Figure 4.5 shows an ideal derivatized melting curve plot for DSF SMI screening, while the plot for the hemin addition to the sample is shown on the right.

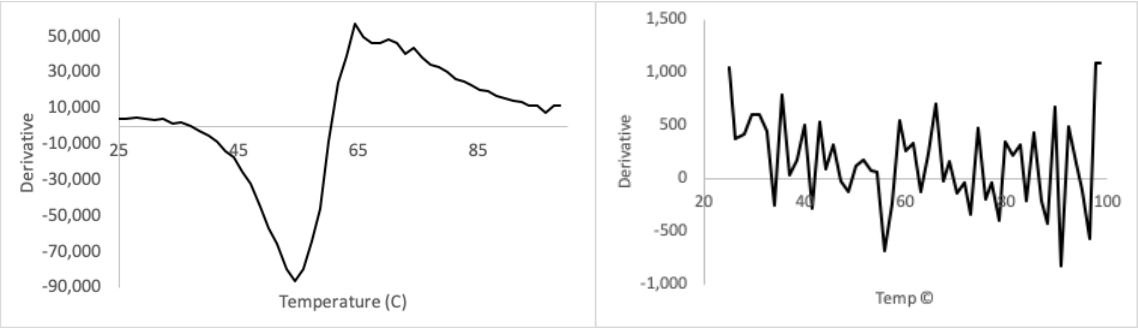

Figure 4.5 DSF melting curve derivative plot of hemin with fortilin strep (right) with a representative melting curve with no SMI bound (left).

While the addition of hemin and hemin + artemisinin appeared at first to have altered the melting temperature of fortilin-strep, a further look at the graphical representation of the melting curve showed no observed binding and an incomplete spectrum (**Figure 4.5**). This is likely due to hemin's colorful hue, as it is a black powder. Indeed, hemin absorbs in an overlapping wavelength range as SYPRO Orange (400-430 nm and 450-550 nm, respectively.[163] This being a fluorometric assay, the color of hemin may interfere with the signal received by the PCR machine and as a result DSF may not be the best method to determine a "hit" for binding of hemin to fortilin.

4.3.4 NMR Titration Results

4.3.4.a Fortilin-Strep with 11CO9

The SMI 11CO9 is a molecule that was sent by our collaborator and has shown promise as a candidate for a novel atherosclerosis drug in *in vivo* animal studies. The structure is currently undergoing patenting and therefore cannot be shared here. This titration led to no observed binding during NMR experiments (**Figure 4.6**). For

simplicity, only the first and last spectrum are shown. This was after 20 µL of titrant had been added to the solution and no binding observed.

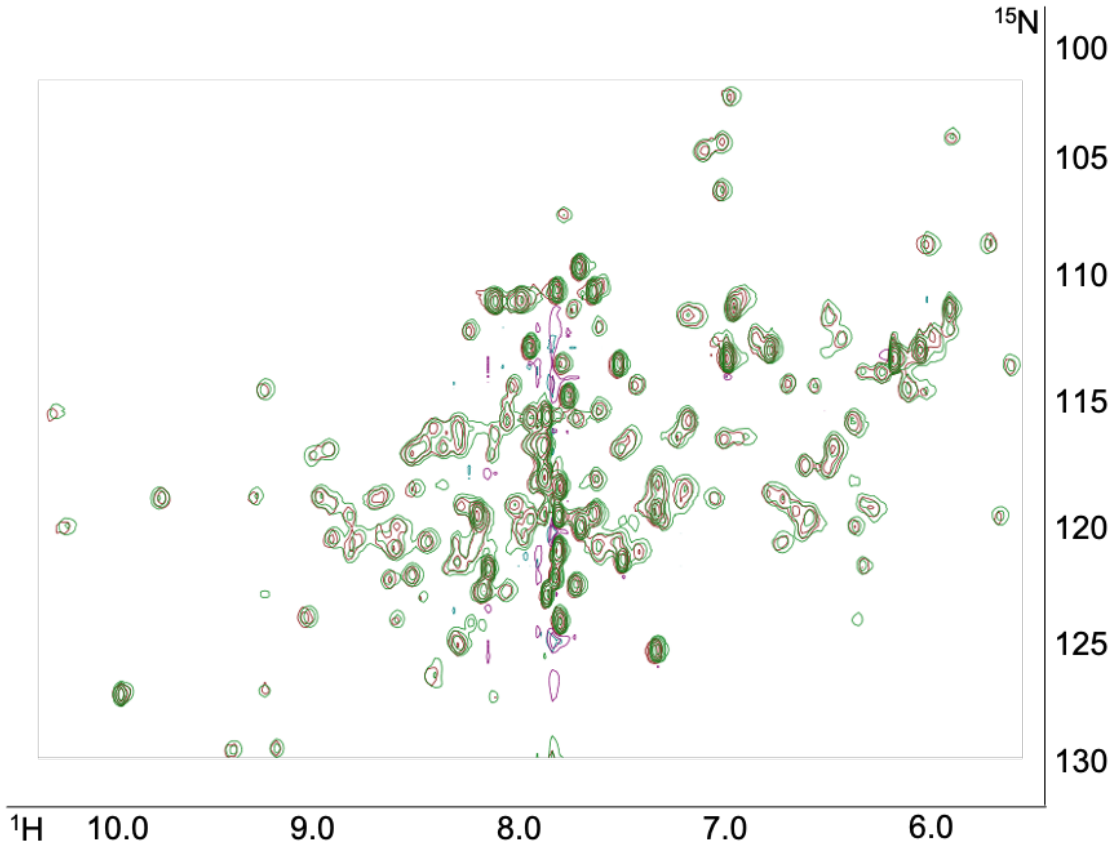

Figure 4.6. Titration of fortilin-strep with SMI 11CO9. Increasing amounts of 11CO9 appear from the first spectrum (1 µL stock, purple) to the last spectrum (20 µL stock, green). Binding was not observed using NMR spectroscopy.

4.3.4.b CGly56

Artemisinin is an anti-malarial drug and has been shown experimentally to bind the *P. falciparum* fortilin protein, whose protein sequence can be found in **Figure 1.6**.[114] Because the structural homology of different species of fortilin is so highly conserved, we hypothesized that artemisinin would bind in a similar location on the protein and with similar affinity. However, titration analysis with CGly56 indicated no binding with

artemisinin (**Figure 4.7**). This analysis was repeated with similar results on NSer46 (data not shown).

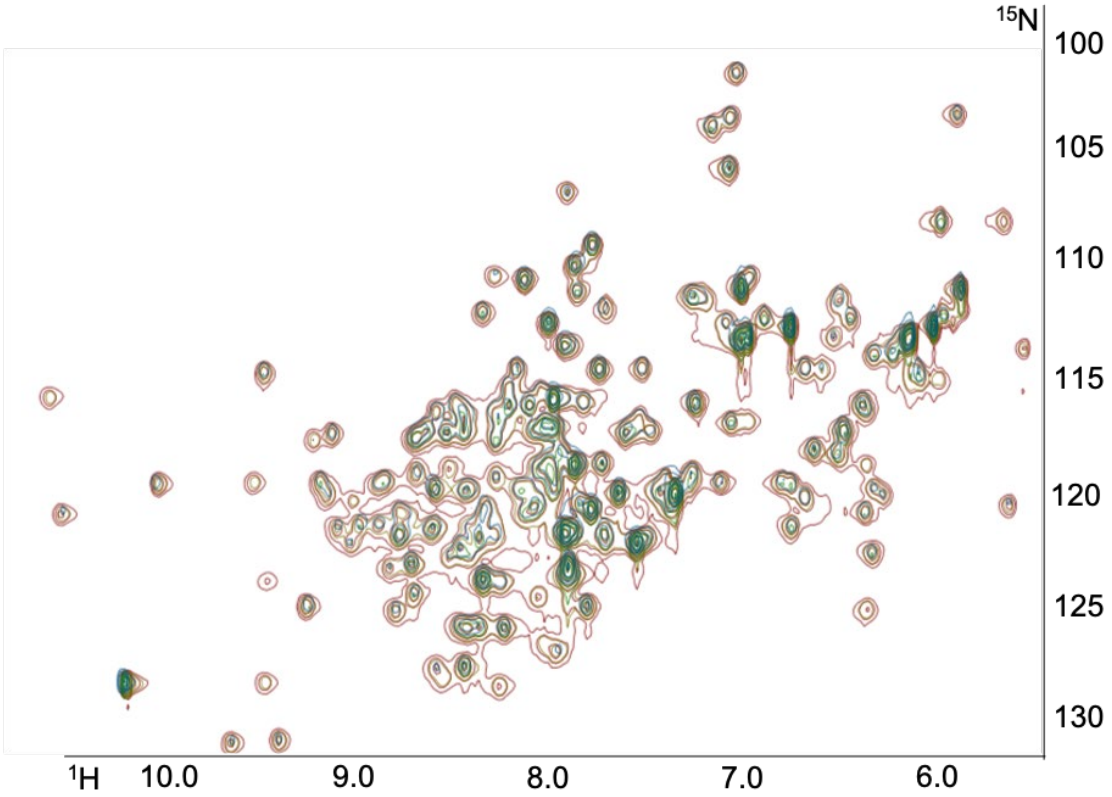

Figure 4.7 Binding is not observed with mutant construct CGly56 and anti-malarial drug artemisinin.

4.3.4.c NSer46

The SMI 26A3 is a synthesized molecule made by researchers in Dr. Don Warner's lab at Boise State University. This molecule did not appear to have binding with NSer46, however the sample was depleted before the ideal stopping point of titration, so further analysis with this SMI is required to determine whether 26A3 really does not bind fortilin (**Figure 4.8**). We have preliminary binding curve data extrapolated from the shifts in the

HSQC to obtain preliminary K_d values for each shifting residue.

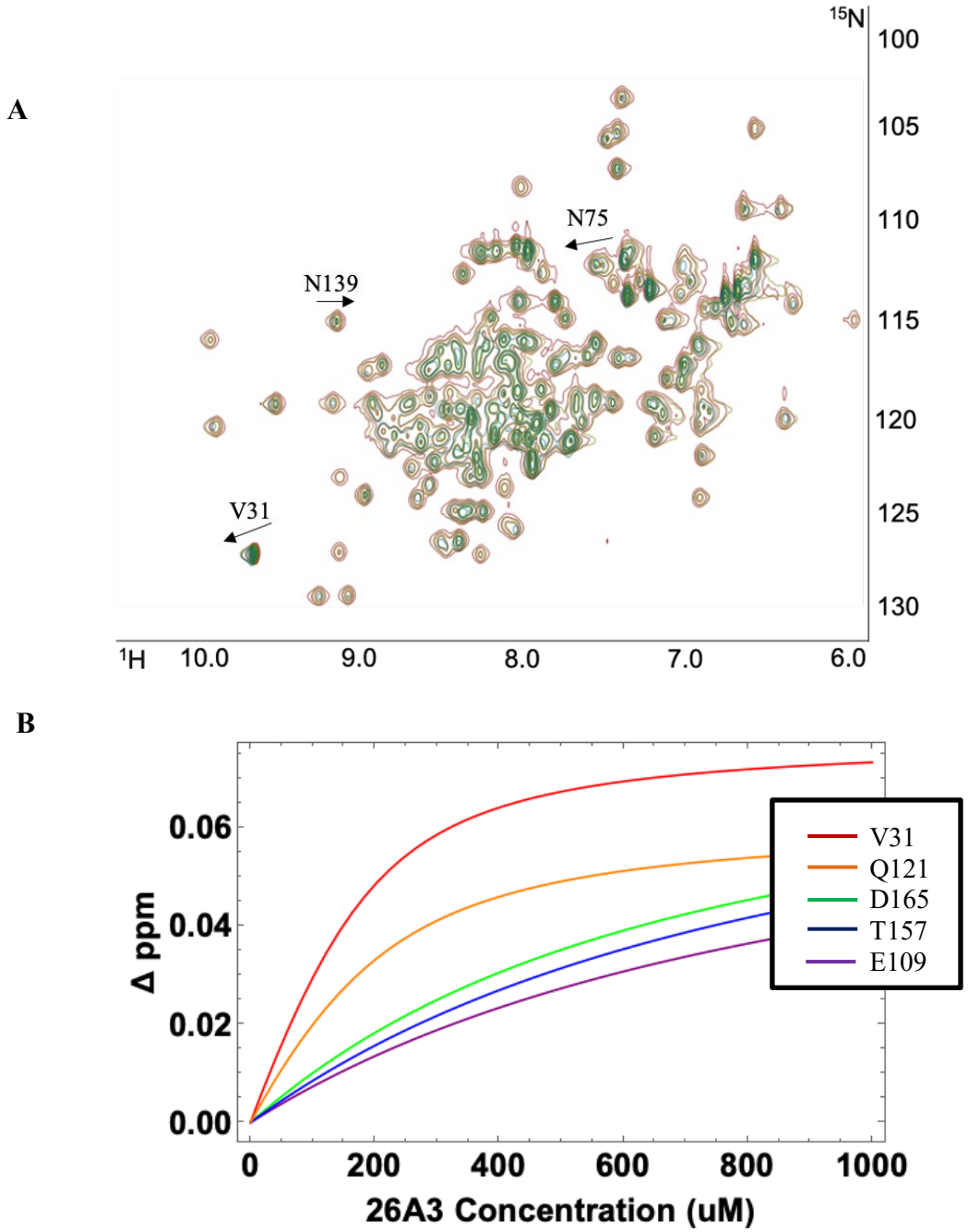

Figure 4.8. Mutant fortilin NSer46 potentially binds SMI 26A3. A) observed peak shifts are questionable with the current data. Arrows indicate the direction of the potential peak shift and corresponding amino acids are labeled. B) Binding curves extrapolated from the data for a given peak shift.

4.4 Conclusions & Future Directions for This Dissertation

The results presented in this body of work portend to the preliminary research conducted in order to perform structural activity relationships with recombinant fortilin protein. In Chapter 2, a recombinant fortilin construct was developed such that the first ever cleaved construct with no affinity tag could be produced. In Chapter 3, loop mutant constructs were generated such that potential binding for ligands at the N- and C-termini could be explored. In Chapter 4, the preliminary SMI binding studies were performed to rule out SMIs that did not bind fortilin or the mutant constructs. There is much to be explored for fortilin using NMR spectroscopy. Previous mass spectrometry data collected by our lab indicate that there may be some PTMs on fortilin, indicated by the presence of an 11 kDa difference in mass, that are not being accounted for in the recombinant *E. coli* construct (**Figure 4.9)**. When expressed in the human embryonic kidney (HEK) 293 cell line, fortilin presents with a molecular weight of approximately 32 kDa. When expressed in *E. coli*, fortilin presents with a molecular weight of 21 kDa. These differences may be due to the presence of PTMs, though there is very little research done to support this. Only three PTMs, acetylation, phosphorylation and ubiquination, have been confirmed for fortilin.[164–167]

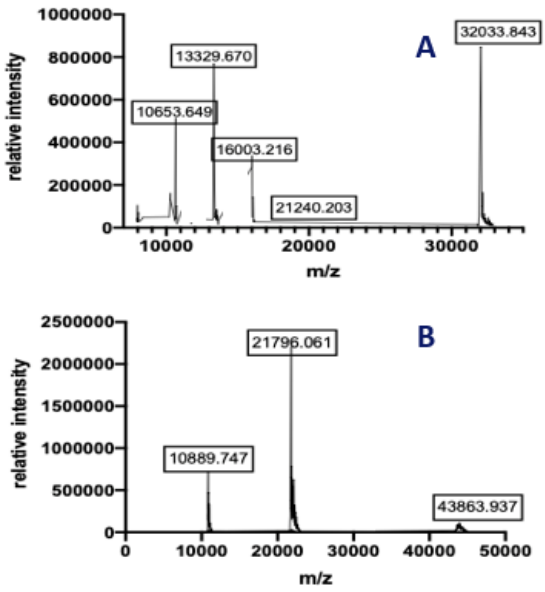

Figure 4.9 Recombinant human fortilin expressed in HEK293 cells has a significantly greater mass than fortilin expressed in *E. coli*. Mass spectrometry data of A) HEK293-expressed fortilin (mw 32 kDa) and B) *E. coli*-expressed 6His-fortilin (mw 21 kDa).

Future plans are to change to a yeast expression system in *Pichia pastoris* such that potential glycosylation PTMs may be analyzed by NMR spectroscopy as well as determine whether SMIs can bind. Isotopically labeling protein becomes more difficult with a more complex cell system, but yeast expression for NMR is quite common.[148] Additionally, the *E. coli* versus *P. pastoris* versus human cell line (HEK293, for example) recombinantly expressed fortilin should be analyzed by mass spectrometry to determine what PTMs may be present. In the past, most preliminary studies have been performed with a recombinant GST-tagged fortilin that has not been cleaved. This construct was used to determine that DHA bound fortilin, and artemisinin binding studies have been performed with non-human fortilin constructs. These are indications that the recombinant fortilin expressed in *E. coli* possesses significant differences to human fortilin. A future student would be encouraged to explore the realm of PTM via the use of isotopically labeled yeast-expressed fortilin as well as using mass spectrometry to

determine the identification of potential PTMs present. There is much to do in the realm of structural characterization and SMI binding determination of fortilin.

REFERENCES

(1) Scannell, J. W.; Blanckley, A.; Boldon, H.; Warrington, B. Diagnosing the Decline in Pharmaceutical R&D Efficiency. *Nat. Rev. Drug Discov.* **2012**, *11* (3), 191–200. https://doi.org/10.1038/nrd3681.

(2) GNS, H. S.; GR, S.; Murahari, M.; Krishnamurthy, M. An Update on Drug Repurposing: Re-Written Saga of the Drug's Fate. *Biomed. Pharmacother.* **2019**, *110* (October 2018), 700–716. https://doi.org/10.1016/j.biopha.2018.11.127.

(3) Ashburn, T. T.; Thor, K. B. Drug Repositioning: Identifying and Developing New Uses for Existing Drugs. *Nat. Rev. Drug Discov.* **2004**, *3* (8), 673–683. https://doi.org/10.1038/nrd1468.

(4) Hubsher, G.; Haider, M.; Okun, M. S. Amantadine: The Journey from Fighting Flu to Treating Parkinson Disease. *Neurology* **2012**, *78* (14), 1096–1099. https://doi.org/10.1212/WNL.0b013e31824e8f0d.

(5) Li, X.; Rousseau, J. F.; Ding, Y.; Song, M.; Lu, W. Understanding Drug Repurposing From the Perspective of Biomedical Entities and Their Evolution: Bibliographic Research Using Aspirin. *JMIR Med. Informatics* **2020**, *8* (6), e16739. https://doi.org/10.2196/16739.

(6) Colombo, D.; Ammirati, E. Cyclosporine in Transplantation - a History of Converging Timelines. *J. Biol. Regul. Homeost. Agents 25* (4), 493–504.

(7) Varothai, S.; Bergfeld, W. F. Androgenetic Alopecia: An Evidence-Based Treatment Update. *Am. J. Clin. Dermatol.* **2014**, *15* (3), 217–230. https://doi.org/10.1007/s40257-014-0077-5.

(8) Ross, D. M.; Hughes, T. P. Cancer Treatment with Kinase Inhibitors: What Have We Learnt from Imatinib? *Br. J. Cancer* **2004**, *90* (1), 12–19. https://doi.org/10.1038/sj.bjc.6601507.

(9) Cao, C.; Moult, J. GWAS and Drug Targets. *BMC Genomics* **2014**, *15* (Suppl 4), 1–14. https://doi.org/10.1186/1471-2164-15-S4-S5.

(10) Rudrapal, M.; J. Khairnar, S.; G. Jadhav, A. Drug Repurposing (DR): An Emerging Approach in Drug Discovery. In *Drug Repurposing - Hypothesis, Molecular Aspects and Therapeutic Applications*; IntechOpen, 2020; p 13. https://doi.org/10.5772/intechopen.93193.

(11) King, M. D.; Long, T.; Pfalmer, D. L.; Andersen, T. L.; McDougal, O. M. SPIDR: Small-Molecule Peptide-Influenced Drug Repurposing. *BMC Bioinformatics* **2018**, *19* (1), 138. https://doi.org/10.1186/s12859-018-2153-y.

(12) Campillos, M.; Kuhn, M.; Gavin, A. C.; Jensen, L. J.; Bork, P. Drug Target Identification Using Side-Effect Similarity. *Science (80-.).* **2008**, *321* (5886), 263–266. https://doi.org/10.1126/science.1158140.

(13) Tam, V.; Patel, N.; Turcotte, M.; Bossé, Y.; Paré, G.; Meyre, D. Benefits and Limitations of Genome-Wide Association Studies. *Nat. Rev. Genet.* **2019**, *20* (8), 467–484. https://doi.org/10.1038/s41576-019-0127-1.

(14) Nabirotchkin, S.; Peluffo, A. E.; Rinaudo, P.; Yu, J.; Hajj, R.; Cohen, D. Next-Generation Drug Repurposing Using Human Genetics and Network Biology. *Curr. Opin. Pharmacol.* **2020**, *51*, 78–92. https://doi.org/10.1016/j.coph.2019.12.004.

(15) Miller, I. N.; Cronin-Golomb, A. Gender Differences in Parkinson's Disease: Clinical Characteristics and Cognition. *Mov. Disord.* **2010**, *25* (16), 2695–2703. https://doi.org/10.1002/mds.23388.

(16) Sawada, H.; Ibi, M.; Kihara, T.; Honda, K.; Nakamizo, T.; Kanki, R.; Nakanishi, M.; Sakka, N.; Akaike, A.; Shimohama, S. Estradiol Protects Dopaminergic Neurons in a MPP+Parkinson's Disease Model. *Neuropharmacology* **2002**, *42* (8), 1056–1064. https://doi.org/10.1016/S0028-3908(02)00049-7.

(17) Yue, Z.; Arora, I.; Zhang, E. Y.; Laufer, V.; Bridges, S. L.; Chen, J. Y. Repositioning Drugs by Targeting Network Modules: A Parkinson's Disease Case Study. *BMC Bioinformatics* **2017**, *18* (Suppl 14), 17–30. https://doi.org/10.1186/s12859-017-1889-0.

(18) Reilly, M. P.; Li, M.; He, J.; Ferguson, J. F.; Stylianou, I. M.; Mehta, N. N.; Burnett, M. S.; Devaney, J. M.; Knouff, C. W.; Thompson, J. R.; et al. Identification of ADAMTS7 as a Novel Locus for Coronary Atherosclerosis and Association of ABO with Myocardial Infarction in the Presence of Coronary Atherosclerosis: Two Genome-Wide Association Studies. *Lancet* **2011**, *377* (9763), 383–392. https://doi.org/10.1016/S0140-6736(10)61996-4.

(19) Shu, L.; Blencowe, M.; Yang, X. Translating GWAS Findings to Novel Therapeutic Targets for Coronary Artery Disease. *Front. Cardiovasc. Med.* **2018**, *5* (May), 1–9. https://doi.org/10.3389/fcvm.2018.00056.

(20) Bullock, C.; Cornia, N.; Jacob, R.; Remm, A.; Peavey, T.; Weekes, K.; Mallory, C.; Oxford, J. T.; McDougal, O. M.; Andersen, T. L. DockoMatic 2.0: High Throughput Inverse Virtual Screening and Homology Modeling. *J. Chem. Inf. Model.* **2013**, *53* (8), 2161–2170. https://doi.org/10.1021/ci400047w.

(21) Marquart, L. A.; Turner, M. W.; McDougal, O. M. Qualitative Assay to Detect Dopamine Release by Ligand Action on Nicotinic Acetylcholine Receptors. *Toxins (Basel).* **2019**, *11* (12), 1–14. https://doi.org/10.3390/toxins11120682.

(22) Trott, O.; Olson, A. Autodock Vina: Improving the Speed and Accuracy of Docking. *J. Comput. Chem.* **2010**, *31* (2), 455–461. https://doi.org/10.1002/jcc.21334.AutoDock.

(23) Jaghoori, M. M.; Bleijlevens, B.; Olabarriaga, S. D. 1001 Ways to Run AutoDock Vina for Virtual Screening. *J. Comput. Aided. Mol. Des.* **2016**, *30* (3), 237–249. https://doi.org/10.1007/s10822-016-9900-9.

(24) Koes, D. R.; Camacho, C. J. ZINCPharmer: Pharmacophore Search of the ZINC Database. *Nucleic Acids Res.* **2012**, *40* (W1), 409–414. https://doi.org/10.1093/nar/gks378.

(25) Athauda, D.; Foltynie, T. Drug Repurposing in Parkinson's Disease. *CNS Drugs* **2018**, *32* (8), 747–761. https://doi.org/10.1007/s40263-018-0548-y.

(26) Zhang, X.; Che, C. Drug Repurposing for Parkinson's Disease by Integrating Knowledge Graph Completion Model and Knowledge Fusion of Medical Literature. *Futur. Internet* **2021**, *13* (1), 1–13. https://doi.org/10.3390/fi13010014.

(27) Gelosa, P.; Castiglioni, L.; Camera, M.; Sironi, L. Repurposing of Drugs Approved for Cardiovascular Diseases: Opportunity or Mirage? *Biochem. Pharmacol.* **2020**, *177* (January), 113895. https://doi.org/10.1016/j.bcp.2020.113895.

(28) Mao, X.-Y. Drug Repurposing in Neurological Diseases: Opportunities and Challenges. In *Drug Repurposing - Hypothesis, Molecular Aspects and Therapeutic Applications*; IntechOpen, 2020; Vol. 32, pp 137–144. https://doi.org/10.5772/intechopen.93093.

(29) Chen, X.; Gumina, G.; Virga, K. G. Recent Advances in Drug Repurposing for Parkinson's Disease. *Curr. Med. Chem.* **2019**, *26* (28), 5340–5362. https://doi.org/10.2174/0929867325666180719144850.

(30) Ballard, C.; Aarsland, D.; Cummings, J.; O'Brien, J.; Mills, R.; Molinuevo, J. L.; Fladby, T.; Williams, G.; Doherty, P.; Corbett, A.; et al. Drug Repositioning and Repurposing for Alzheimer Disease. *Nat. Rev. Neurol.* **2020**, *16* (12), 661–673. https://doi.org/10.1038/s41582-020-0397-4.

(31) Shakkour, Z.; Issa, H.; Ismail, H.; Ashekyan, O.; Habashy, K. J.; Nasrallah, L.; Jourdi, H.; Hamade, E.; Mondello, S.; Sabra, M.; et al. Drug Repurposing: Promises of Edaravone Target Drug in Traumatic Brain Injury. *Curr. Med. Chem.* **2021**, *28* (12), 2369–2391. https://doi.org/10.2174/0929867327666200812221022.

(32) Ion, G. N. D.; Mihai, D. P.; Lupascu, G.; Nitulescu, G. M. Application of Molecular Framework-Based Data-Mining Method in the Search for Beta-Secretase 1 Inhibitors through Drug Repurposing. *J. Biomol. Struct. Dyn.* **2019**, *37* (14), 3674–3685. https://doi.org/10.1080/07391102.2018.1526115.

(33) Pessetto, Z. Y.; Ma, Y.; Hirst, J. J.; Von Mehren, M.; Weir, S. J.; Godwin, A. K. Drug Repurposing Identifies a Synergistic Combination Therapy with Imatinib Mesylate for Gastrointestinal Stromal Tumor. *Mol. Cancer Ther.* **2014**, *13* (10), 2276–2287. https://doi.org/10.1158/1535-7163.MCT-14-0043.

(34) Murphy, S. L.; Xu, J.; Kochanek, K. D.; Arias, E.; Ph, D. *Mortality in the United States , 2017*; 2018.

(35) Pinkaew, D.; Fujise, K. Fortilin: A Potential Target for the Prevention and Treatment of Human Diseases. *Adv. Clin. Chem.* **2017**, *82*, 265–300. https://doi.org/10.1016/bs.acc.2017.06.006.

(36) Feletou, M. *The Endothelium: Part 1: Multiple Functions Ofthe Endothelial Cells--Focus on Endothelium-Derived Vasoactive Mediators*; Morgan & Claypool Life Sciences: San Rafael, 2011.

(37) Sakurada, M.; Yoshioka, N.; Kuse, A.; Nakagawa, K.; Morichika, M.; Takahashi, M.; Kondo, T.; Asano, M.; Ueno, Y. Rapid Identification of Gloriosa Superba and Colchicum Autumnale by Melting Curve Analysis: Application to a Suicide Case Involving Massive Ingestion of G. Superba. *Int. J. Legal Med.* **2019**, *133* (4), 1065–1073. https://doi.org/10.1007/s00414-019-02060-x.

(38) Ross, R. Atherosclerosis -- an Inflammatory Disease. *N. Engl. J. Med.* **1999**, *340* (2), 115–126.

(39) Libby, P.; Hansson, G. K. Inflammation and Immunity in Diseases of the Arterial Tree: Players and Layers. *Circ. Res.* **2015**, *116* (2), 307–311. https://doi.org/10.1161/CIRCRESAHA.116.301313.

(40) Davies, M. J. Stability and Instability: Two Faces of Coronary Atherosclerosis: The Paul Dudley White Lecture 1995. *Circulation* **1996**, *94* (8), 2013–2020. https://doi.org/10.1161/01.CIR.94.8.2013.

(41) Verma, S.; Szmitko, P. E.; Ridker, P. M. C-Reactive Protein Comes of Age. *Nat. Clin. Pract. Cardiovasc. Med.* **2005**, *2* (1), 29–36. https://doi.org/10.1038/ncpcardio0074.

(42) Nidorf, S. M.; Thompson, P. L. Why Colchicine Should Be Considered for Secondary Prevention of Atherosclerosis: An Overview. *Clin. Ther.* **2019**, *41* (1), 41–48. https://doi.org/10.1016/j.clinthera.2018.11.016.

(43) Fiolet, A. T. L.; Nidorf, S. M.; Mosterd, A.; Cornel, J. H. Colchicine in Stable Coronary Artery Disease. *Clin. Ther.* **2019**, *41* (1), 30–40. https://doi.org/10.1016/j.clinthera.2018.09.011.

(44) Leung, Y. Y.; Yao Hui, L. L.; Kraus, V. B. Colchicine-Update on Mechanisms of Action and Therapeutic Uses. *Semin. Arthritis Rheum.* **2015**, *45* (3), 341–350. https://doi.org/10.1016/j.semarthrit.2015.06.013.

(45) Redelinghuys, P.; Brown, G. D. Inhibitory C-Type Lectin Receptors in Myeloid Cells. *Immunol. Lett.* **2011**, *136* (1), 1–12. https://doi.org/10.1016/j.imlet.2010.10.005.

(46) Brennan, K.; Zheng, J. Interleukin 8. In *xPharm: The Comprehensive Pharmacology Reference*; Elsevier, 2007; pp 1–4. https://doi.org/10.1016/B978-008055232-3.61916-6.

(47) Weinblatt, M. E. Methotrexate in Rheumatoid Arthritis: A Quarter Century of Development. *Trans. Am. Clin. Climatol. Assoc.* **2013**, *124*, 16–25.

(48) Mangoni, A. A.; Tommasi, S.; Zinellu, A.; Sotgia, S.; Carru, C.; Piga, M.; Erre, G. L. Repurposing Existing Drugs for Cardiovascular Risk Management: A Focus on Methotrexate. *Drugs Context* **2018**, *7*, 1–12. https://doi.org/10.7573/dic.212557.

(49) Kinder, A. J.; Hassell, A. B.; Brand, J.; Brownfield, A.; Grove, M.; Shadforth, M. F. The Treatment of Inflammatory Arthritis with Methotrexate in Clinical Practice: Treatment Duration and Incidence of Adverse Drug Reactions. *Rheumatology* **2005**, *44* (1), 61–66. https://doi.org/10.1093/rheumatology/keh512.

(50) Cronstein, B. N.; Aune, T. M. Methotrexate and Its Mechanisms of Action in Inflammatory Arthritis. *Nat. Rev. Rheumatol.* **2020**, *16* (3), 145–154. https://doi.org/10.1038/s41584-020-0373-9.

(51) Sankrityayan, H.; Majumdar, A. S. Curcumin and Folic Acid Abrogated Methotrexate Induced Vascular Endothelial Dysfunction. *Can. J. Physiol. Pharmacol.* **2015**, *94* (1), 89–96. https://doi.org/10.1139/cjpp-2015-0156.

(52) Panja, S.; Khatua, D. K.; Halder, M. Simultaneous Binding of Folic Acid and Methotrexate to Human Serum Albumin: Insights into the Structural Changes of Protein and the Location and Competitive Displacement of Drugs. *ACS Omega* **2018**, *3* (1), 246–253. https://doi.org/10.1021/acsomega.7b01437.

(53) Crabtree, M. J.; Hale, A. B.; Channon, K. M. Dihydrofolate Reductase Protects Endothelial Nitric Oxide Synthase from Uncoupling in Tetrahydrobiopterin Deficiency. *Free Radic. Biol. Med.* **2011**, *50* (11), 1639–1646. https://doi.org/10.1016/j.freeradbiomed.2011.03.010.

(54) Zeng, L.; Yan, Z.; Ding, S.; Xu, K.; Wang, L. Endothelial Injury, an Intriguing Effect of Methotrexate and Cyclophosphamide During Hematopoietic Stem Cell Transplantation in Mice. *Transplant. Proc.* **2008**, *40* (8), 2670–2673. https://doi.org/10.1016/j.transproceed.2008.06.038.

(55) Matei, V.; Rodríguez-Vilarrupla, A.; Deulofeu, R.; Colomer, D.; Fernández, M.; Bosch, J.; Garcia-Pagán, J. C. The ENOS Cofactor Tetrahydrobiopterin Improves Endothelial Dysfunction in Livers of Rats with CCl4 Cirrhosis. *Hepatology* **2006**, *44* (1), 44–52. https://doi.org/10.1002/hep.21228.

(56) Gualtierotti, R.; Ingegnoli, F.; Boscolo, M.; Griffini, S.; Grovetti, E.; Cugno, M. Tocilizumab Effects on Coagulation Factor XIII in Patients with Rheumatoid Arthritis. *Adv. Ther.* **2019**. https://doi.org/10.1007/s12325-019-01118-x.

(57) Ruiz-Limón, P.; Ortega, R.; Arias de la Rosa, I.; Abalos-Aguilera, M. del C.; Perez- Sanchez, C.; Jimenez- Gomez, Y.; Peralbo-Santaella, E.; Font, P.; Ruiz-Vilches, D.; Ferrin, G.; et al. Tocilizumab Improves the Proatherothrombotic Profile of Rheumatoid Arthritis Patients Modulating Endothelial Dysfunction, NETosis, and Inflammation. *Transl. Res.* **2017**, *183*, 87–103. https://doi.org/10.1016/j.trsl.2016.12.003.

(58) Del Rincón, I.; Williams, K.; Stern, M. P.; Freeman, G. L.; Escalante, A. High Incidence of Cardiovascular Events in a Rheumatoid Arthritis Cohort Not Explained by Traditional Cardiac Risk Factors. *Arthritis Rheum.* **2001**, *44* (12), 2737–2745. https://doi.org/10.1002/1529-0131(200112)44:12<2737::aid-art460>3.0.co;2-%23.

(59) Hoeper, M. M.; Gibbs, J. S. R. The Changing Landscape of Pulmonary Arterial Hypertension and Implications for Patient Care. *Eur. Respir. Rev.* **2014**, *23* (134), 450–457. https://doi.org/10.1183/09059180.00007814.

(60) Gaine, S. P.; Rubin, L. J. Primary Pulmonary Hypertension. *Lancet* **1998**, *352*, 719–725.

(61) Sitbon, O.; Vonk Noordegraaf, A. Epoprostenol and Pulmonary Arterial Hypertension: 20 Years of Clinical Experience. *Eur. Respir. Rev.* **2017**, *26* (143). https://doi.org/10.1183/16000617.0055-2016.

(62) Leeper, B.; Powell, B. Pulmonary Arterial Hypertension. *Nurs. Crit. Care* **2019**, *14* (3), 14–22. https://doi.org/10.1097/01.CCN.0000554829.05209.ca.

(63) Grinnan, D.; Trankle, C.; Andruska, A.; Bloom, B.; Spiekerkoetter, E. Drug Repositioning in Pulmonary Arterial Hypertension: Challenges and Opportunities. *Pulm. Circ.* **2019**, *9* (1). https://doi.org/10.1177/2045894019832226.

(64) Trankle, C. R.; Canada, J. M.; Kadariya, D.; Markley, R.; De Chazal, H. M.; Pinson, J.; Fox, A.; Van Tassell, B. W.; Abbate, A.; Grinnan, D. IL-1 Blockade Reduces Inflammation in Pulmonary Arterial Hypertension and Right Ventricular Failure: A Single-Arm, Open-Label, Phase Ib/II Pilot Study. *Am. J. Respir. Crit. Care Med.* **2019**, *199* (3), 381–384. https://doi.org/10.1164/rccm.201809-1631LE.

(65) Parpaleix, A.; Amsellem, V.; Houssaini, A.; Abid, S.; Breau, M.; Marcos, E.; Sawaki, D.; Delcroix, M.; Quarck, R.; Maillard, A.; et al. Role of Interleukin-1 Receptor 1/MyD88 Signalling in the Development and Progression of Pulmonary Hypertension. *Eur. Respir. J.* **2016**, *48* (2), 470–483. https://doi.org/10.1183/13993003.01448-2015.

(66) Fisher, A. FDA Approves Adcirca (tadalafil) Tablets for the Treatment of Pulmonary Arterial Hypertension https://www.drugs.com/newdrugs/fda-approves-adcirca-tadalafil-pulmonary-arterial-hypertension-1366.html (accessed Nov 12, 2019).

(67) Daugan, A.; Grondin, P.; Ruault, C.; Le Monnier de Gouville, A. C.; Coste, H.; Linget, J. M.; Kirilovsky, J.; Hyafil, F.; Labaudinièret, R. The Discovery of Tadalafil: A Novel and Highly Selective PDE5 Inhibitor. 2: 2,3,6,7,12,12a-Hexahydropyrazino[1′,2′:1,6]Pyrido[3,4-b]Indole-1,4-Dione Analogues. *J. Med. Chem.* **2003**, *46* (21), 4533–4542. https://doi.org/10.1021/jm0300577.

(68) Kotera, J.; Fujishige, K.; Omori, K. Immunohistochemical Localization of CGMP-Binding CGMP-Specific Phosphodiesterase (PDE5) in Rat Tissues. *J. Histochem. Cytochem.* **2000**, *48* (5), 685–693. https://doi.org/10.1177/002215540004800512.

(69) Galiè, N.; Brundage, B. H.; Ghofrani, H. A.; Oudiz, R. J.; Simonneau, G.; Safdar, Z.; Shapiro, S.; White, R. J.; Chan, M.; Beardsworth, A.; et al. Tadalafil Therapy for Pulmonary Arterial Hypertension. *Circulation* **2009**, *119* (22), 2894–2903. https://doi.org/10.1161/CIRCULATIONAHA.108.839274.

(70) Kass, D. A.; Champion, H. C.; Beavo, J. A. Phosphodiesterase Type 5: Expanding Roles in Cardiovascular Regulation. *Circ. Res.* **2007**, *101* (11), 1084–1095. https://doi.org/10.1161/CIRCRESAHA.107.162511.

(71) Li, F.; Zhang, D.; Fujise, K. Characterization of Fortilin, a Novel Antiapoptotic Protein. *J. Biol. Chem.* **2001**, *276* (50), 47542–47549. https://doi.org/10.1074/jbc.M108954200.

(72) Acunzo, J.; Baylot, V.; So, A.; Rocchi, P. TCTP as Therapeutic Target in Cancers. *Cancer Treat. Rev.* **2014**, *40* (6), 760–769. https://doi.org/10.1016/j.ctrv.2014.02.007.

(73) Thaw, P.; Baxter, N. J.; Hounslow, A. M.; Price, C.; Waltho, J. P.; Craven, C. J. Structure of TCTP Reveals Unexpected Relationship with Guanine Nucleotide-Free Chaperones. *Nat. Struct. Biol.* **2001**, *8* (8), 701–704. https://doi.org/10.1038/90415.

(74) Bommer, U. A.; Thiele, B. J. The Translationally Controlled Tumour Protein (TCTP). *Int. J. Biochem. Cell Biol.* **2004**, *36* (3), 379–385. https://doi.org/10.1016/S1357-2725(03)00213-9.

(75) Huang, X.; Miller, W. A Time-Efficient, Linear-Space Local Similarity Algorithm. *Adv. Appl. Math.* **1991**, *12* (3), 337–357.

(76) Dong, X.; Yang, B.; Li, Y.; Zhong, C.; Ding, J. Molecular Basis of the Acceleration of the GDP-GTP Exchange of Human Ras Homolog Enriched in Brain by Human Translationally Controlled Tumor Protein. *J. Biol. Chem.* **2009**, *284* (35), 23754–23764. https://doi.org/10.1074/jbc.M109.012823.

(77) Lange, O. F.; Rossi, P.; Sgourakis, N. G.; Song, Y.; Lee, H. W.; Aramini, J. M.; Ertekin, A.; Xiao, R.; Acton, T. B.; Montelione, G. T.; et al. Determination of Solution Structures of Proteins up to 40 KDa Using CS-Rosetta with Sparse NMR Data from Deuterated Samples. *Proc. Natl. Acad. Sci. U. S. A.* **2012**, *109* (27), 10873–10878. https://doi.org/10.1073/pnas.1203013109.

(78) Susini, L.; Besse, S.; Duflaut, D.; Lespagnol, A.; Beekman, C.; Fiucci, G.; Atkinson, A. R.; Busso, D.; Poussin, P.; Marine, J. C.; et al. TCTP Protects from Apoptotic Cell Death by Antagonizing Bax Function. *Cell Death Differ.* **2008**, *15* (8), 1211–1220. https://doi.org/10.1038/cdd.2008.18.

(79) Feng, Y.; Liu, D.; Yao, H.; Wang, J. Solution Structure and Mapping of a Very Weak Calcium-Binding Site of Human Translationally Controlled Tumor Protein by NMR. *Arch. Biochem. Biophys.* **2007**, *467* (1), 48–57. https://doi.org/10.1016/j.abb.2007.08.021.

(80) Dong, S.-H.; Frane, N. D.; Christensen, Q. H.; Greenberg, E. P.; Nagarajan, R.; Nair, S. K. Molecular Basis for the Substrate Specificity of Quorum Signal Synthases. *Proc. Natl. Acad. Sci.* **2017**. https://doi.org/10.1073/pnas.1705400114.

(81) Doré, K. A.; Kashiwakura, J. ichi; McDonnell, J. M.; Gould, H. J.; Kawakami, T.; Sutton, B. J.; Davies, A. M. Crystal Structures of Murine and Human Histamine-Releasing Factor (HRF/TCTP) and a Model for HRF Dimerisation in Mast Cell Activation. *Mol. Immunol.* **2018**, *93* (June 2017), 216–222. https://doi.org/10.1016/j.molimm.2017.11.022.

(82) Thebault, S.; Agez, M.; Chi, X.; Stojko, J.; Cura, V.; Telerman, S. B.; Maillet, L.; Gautier, F.; Billas-Massobrio, I.; Birck, C.; et al. TCTP Contains a BH3-like Domain, Which Instead of Inhibiting, Activates Bcl-XL. *Sci. Rep.* **2016**, *6*, 1–11. https://doi.org/10.1038/srep19725.

(83) Wu, H.; Gong, W.; Yao, X.; Wang, J.; Perrett, S.; Feng, Y. Evolutionarily Conserved Binding of Translationally Controlled Tumor Protein to Eukaryotic Elongation Factor 1B. *J. Biol. Chem.* **2015**, *290* (14), 8694–8710. https://doi.org/10.1074/jbc.M114.628594.

(84) Yao, X.; Liu, Y. J.; Cui, Q.; Feng, Y. Solution Structure of a Unicellular Microalgae-Derived Translationally Controlled Tumor Protein Revealed Both Conserved Features and Structural Diversity. *Arch. Biochem. Biophys.* **2019**, *665* (February), 23–29. https://doi.org/10.1016/j.abb.2019.02.012.

(85) Eichhorn, T.; Winter, D.; Büchele, B.; Dirdjaja, N.; Frank, M.; Lehmann, W. D.; Mertens, R.; Krauth-Siegel, R. L.; Simmet, T.; Granzin, J.; et al. Molecular Interaction of Artemisinin with Translationally Controlled Tumor Protein (TCTP) of Plasmodium Falciparum. *Biochem. Pharmacol.* **2013**, *85* (1), 38–45. https://doi.org/10.1016/j.bcp.2012.10.006.

(86) Vedadi, M.; Lew, J.; Artz, J.; Amani, M.; Zhao, Y.; Dong, A.; Wasney, G. A.; Gao, M.; Hills, T.; Brokx, S.; et al. Genome-Scale Protein Expression and Structural Biology of Plasmodium Falciparum and Related Apicomplexan Organisms. *Mol. Biochem. Parasitol.* **2007**, *151* (1), 100–110. https://doi.org/10.1016/j.molbiopara.2006.10.011.

(87) Calderón-Pérez, B.; Xoconostle-Cázares, B.; Lira-Carmona, R.; Hernández-Rivas, R.; Ortega-López, J.; Ruiz-Medrano, R. The Plasmodium Falciparum Translationally Controlled Tumor Protein (TCTP) Is Incorporated More Efficiently into B Cells than Its Human Homologue. *PLoS One* **2014**, *9* (1), 1–6. https://doi.org/10.1371/journal.pone.0085514.

(88) Pettersen, E. F.; Goddard, T. D.; Huang, C. C.; Couch, G. S.; Greenblatt, D. M.; Meng, E. C.; Ferrin, T. E. UCSF Chimera-A Visualization System for Exploratory Research and Analysis. *J. Comput. Chem.* **2004**, *25* (13), 1605–1612. https://doi.org/10.1002/jcc.20084.

(89) Chattopadhyay, A.; Pinkaew, D.; Doan, H. Q.; Jacob, R. B.; Verma, S. K.; Friedman, H.; Peterson, A. C.; Kuyumcu-Martinez, M. N.; McDougal, O. M.; Fujise, K. Fortilin Potentiates the Peroxidase Activity of Peroxiredoxin-1 and Protects against Alcohol-Induced Liver Damage in Mice. *Sci. Rep.* **2016**, *6* (November 2015), 1–16. https://doi.org/10.1038/srep18701.

(90) Mullen, L.; Hanschmann, E. M.; Lillig, C. H.; Herzenberg, L. A.; Ghezzi, P. Cysteine Oxidation Targets Peroxiredoxins 1 and 2 for Exosomal Release through a Novel Mechanism of Redox-Dependent Secretion. *Mol. Med.* **2015**, *21* (10), 98–108. https://doi.org/10.2119/molmed.2015.00033.

(91) Rawat, S. J.; Creasy, C. L.; Peterson, J. R.; Chernoff, J. The Tumor Suppressor Mst1 Promotes Changes in the Cellular Redox State by Phosphorylation and Inactivation of Peroxiredoxin-1 Protein. *J. Biol. Chem.* **2013**, *288* (12), 8762–8771. https://doi.org/10.1074/jbc.M112.414524.

(92) Hetz, C. The Unfolded Protein Response: Controlling Cell Fate Decisions under ER Stress and Beyond. *Nat. Rev. Mol. Cell Biol.* **2012**, *13* (2), 89–102. https://doi.org/10.1038/nrm3270.

(93) Pinkaew, D.; Chattopadhyay, A.; King, M. D.; Chunhacha, P.; Liu, Z.; Stevenson, H. L.; Chen, Y.; Sinthujaroen, P.; McDougal, O. M.; Fujise, K. Fortilin Binds IRE1α and Prevents ER Stress from Signaling Apoptotic Cell Death. *Nat. Commun.* **2017**, *8* (1), 1–15. https://doi.org/10.1038/s41467-017-00029-1.

(94) Wu, R.; Zhang, Q. H.; Lu, Y. J.; Ren, K.; Yi, G. H. Involvement of the IRE1α-XBP1 Pathway and XBP1s-Dependent Transcriptional Reprogramming in Metabolic Diseases. *DNA Cell Biol.* **2015**, *34* (1), 6–18. https://doi.org/10.1089/dna.2014.2552.

(95) Chen, Y.; Fujita, T.; Zhang, D.; Doan, H.; Pinkaew, D.; Liu, Z.; Wu, J.; Koide, Y.; Chiu, A.; Lin, C. C. J.; et al. Physical and Functional Antagonism between Tumor Suppressor Protein P53 and Fortilin, an Anti-Apoptotic Protein. *J. Biol. Chem.* **2011**, *286* (37), 32575–32585. https://doi.org/10.1074/jbc.M110.217836.

(96) Haghighat, N. G.; Ruben, L. Purification of Novel Calcium Binding Proteins from Trypanosoma Brucei: Properties of 22-,24- and 38-Kilodaltion Proteins. *Mol. Biochem. Parasitol.* **1992**, *51*, 99–110.

(97) Xu, A.; Bellamy, A. R.; Taylor, J. A. Expression of Translationally Controlled Tumour Protein Is Regulated by Calcium at Both the Transcriptional and Post-Transcriptional Level. *Biochem. J.* **1999**, *342* (3), 683–689. https://doi.org/10.1042/0264-6021:3420683.

(98) Kim, M.; Jung, Y.; Lee, K.; Kim, C. Identification of the Calcium Binding Sites in Translationally Controlled Tumor Protein. *Arch. Pharm. Res.* **2000**, *23* (6), 633–636. https://doi.org/10.1007/BF02975253.

(99) Rao, K. V. N.; Chen, L.; Gnanasekar, M.; Ramaswamy, K. Cloning and Characterization of a Calcium-Binding, Histamine-Releasing Protein from Schistosoma Mansoni. *J. Biol. Chem.* **2002**, *277* (34), 31207–31213. https://doi.org/10.1074/jbc.M204114200.

(100) Gnanasekar, M.; Rao, K. V. N.; Chen, L.; Narayanan, R. B.; Geetha, M.; Scott, A. L.; Ramaswamy, K.; Kaliraj, P. Molecular Characterization of a Calcium Binding Translationally Controlled Tumor Protein Homologue from the Filarial Parasites Brugia Malayi and Wuchereria Bancrofti. *Mol. Biochem. Parasitol.* **2002**, *121* (1), 107–118. https://doi.org/10.1016/S0166-6851(02)00027-0.

(101) Bhisutthibhan, J.; Philbert, M. A.; Fujioka, H.; Aikawa, M.; Meshnick, S. R. The Plasmodium Falciparum Translationally Controlled Tumor Protein: Subcellular Localization and Calcium Binding. *Eur. J. Cell Biol.* **1999**, *78* (9), 665–670. https://doi.org/10.1016/S0171-9335(99)80052-1.

(102) Fujise, K.; Graidist, P.; Nakatomi, A.; Yazawa, M.; Phongdara, A.; Chang, J.; Lin, C. C.-J.; Tonganunt, M. Fortilin Binds Ca 2+ and Blocks Ca 2+ -Dependent Apoptosis in Vivo. *Biochem. J.* **2007**, *408* (2), 181–191. https://doi.org/10.1042/bj20070679.

(103) Koide, Y.; Kiyota, T.; Tonganunt, M.; Pinkaew, D.; Liu, Z.; Kato, Y.; Hutadilok-Towatana, N.; Phongdara, A.; Fujise, K. Embryonic Lethality of Fortilin-Null Mutant Mice by BMP-Pathway Overactivation. *Biochim. Biophys. Acta - Gen. Subj.* **2009**, *1790* (5), 326–338. https://doi.org/10.1016/j.bbagen.2009.01.012.

(104) Gachet, Y.; Tournier, S.; Lee, M.; Lazaris-Karatzas, A.; Poulton, T.; Bommer, U. A. The Growth-Related, Translationally Controlled Protein P23 Has Properties of a Tubulin Binding Protein and Associates Transiently with Microtubules during the Cell Cycle. *J. Cell Sci.* **1999**, *112* (8), 1257–1271.

(105) Bazile, F.; Pascal, A.; Arnal, I.; Le Clainche, C.; Chesne, F.; Kubiak, J. Z. Complex Relationship between TCTP, Microtubules and Actin Microfilaments Regulates Cell Shape in Normal and Cancer Cells. *Carcinogenesis* **2009**, *30* (4), 555–565. https://doi.org/10.1093/carcin/bgp022.

(106) Kim, M.; Jung, J.; Lee, K. Roles of ERK, PI3 Kinase, and PLC-γ Pathways Induced by Overexpression of Translationally Controlled Tumor Protein in HeLa Cells. *Arch. Biochem. Biophys.* **2009**, *485* (1), 82–87. https://doi.org/10.1016/j.abb.2009.02.002.

(107) Jung, J.; Kim, M.; Kim, M. J.; Kim, J.; Moon, J.; Lim, J. S.; Kim, M.; Lee, K. Translationally Controlled Tumor Protein Interacts with the Third Cytoplasmic Domain of Na,K-ATPase α Subunit and Inhibits the Pump Activity in HeLa Cells. *J. Biol. Chem.* **2004**, *279* (48), 49868–49875. https://doi.org/10.1074/jbc.M400895200.

(108) Wieduwilt M. J.; Moasser M. M. The Epidermal Growth Factor Receptor Family: Biology Driving Targeted Therapeutics. *Cell Mol Life Sci* **2011**, *65* (10), 1566–1584. https://doi.org/10.1007/s00018-008-7440-8.The.

(109) Zhou, Z.; Wang, L.; Song, Z.; Lambert, J. C.; McClain, C. J.; Kang, Y. J. A Critical Involvement of Oxidative Stress in Acute Alcohol-Induced Hepatic TNF-α Production. *Am. J. Pathol.* **2003**, *163* (3), 1137–1146. https://doi.org/10.1016/S0002-9440(10)63473-6.

(110) Wood, Z. A.; Schröder, E.; Harris, J. R.; Poole, L. B. Structure, Mechanism and Regulation of Peroxiredoxins. *Trends Biochem. Sci.* **2003**, *28* (1), 32–40. https://doi.org/10.1016/S0968-0004(02)00003-8.

(111) Miyazono, K.; Maeda, S.; Imamura, T. BMP Receptor Signaling: Transcriptional Targets, Regulation of Signals, and Signaling Cross-Talk. *Cytokine Growth Factor Rev.* **2005**, *16* (3 SPEC. ISS.), 251–263. https://doi.org/10.1016/j.cytogfr.2005.01.009.

(112) Bhisutthibhan, J.; Pan, X. Q.; Hossler, P. A.; Walker, D. J.; Yowell, C. A.; Carlton, J.; Dame, J. B.; Meshnick, S. R. The Plasmodium Falciparum Translationally Controlled Tumor Protein Homolog and Its Reaction with the Antimalarial Drug Artemisinin. *J. Biol. Chem.* **1998**, *273* (26), 16192–16198. https://doi.org/10.1074/jbc.273.26.16192.

(113) Fujita, T.; Felix, K.; Pinkaew, D.; Hutadilok-Towatana, N.; Liu, Z.; Fujise, K. Human Fortilin Is a Molecular Target of Dihydroartemisinin. *FEBS Lett.* **2008**, *582* (7), 1055–1060. https://doi.org/10.1016/j.febslet.2008.02.055.

(114) Li, W.; Zhou, Y.; Tang, G.; Xiao, Y. Characterization of the Artemisinin Binding Site for Translationally Controlled Tumor Protein (TCTP) by Bioorthogonal Click Chemistry. *Bioconjug. Chem.* **2016**, *27* (12), 2828–2833. https://doi.org/10.1021/acs.bioconjchem.6b00556.

(115) Benjamin, E. J.; Muntner, P.; Alonso, A.; Bittencourt, M. S.; Callaway, C. W.; Carson, A. P.; Chamberlain, A. M.; Chang, A. R.; Cheng, S.; Das, S. R.; et al. Heart Disease and Stroke Statistics—2019 Update: A Report From the American Heart Association. *Circulation* **2019**, *139*, e1–e473. https://doi.org/10.1161/CIR.0000000000000659.

(116) Sachdeva, A.; Cannon, C. P.; Deedwania, P. C.; LaBresh, K. A.; Smith, S. C.; Dai, D.; Hernandez, A.; Fonarow, G. C. Lipid Levels in Patients Hospitalized with Coronary Artery Disease: An Analysis of 136,905 Hospitalizations in Get With The Guidelines. *Am. Heart J.* **2009**, *157* (1). https://doi.org/10.1016/j.ahj.2008.08.010.

(117) Bommer, U. A.; Telerman, A. Dysregulation of TCTP in Biological Processes and Diseases. *Cells* **2020**, *9* (7), 1–19. https://doi.org/10.3390/cells9071632.

(118) Fujise, K.; Pinkaew, D.; Eltorky, M.; Le, R. J.; Chen, Y.; Teng, B. Fortilin Reduces Apoptosis in Macrophages and Promotes Atherosclerosis. *Am. J. Physiol. Circ. Physiol.* **2013**, *305* (10), H1519–H1529. https://doi.org/10.1152/ajpheart.00570.2013.

(119) Williamson, M. P.; Wuthrich, K. Solution Conformation of Proteinase Inhibitor IIA from Bull Seminal Plasma by 1H Nuclear Magnetic Resonance and Distance Geometry. *J. Mol. Biol.* **1985**, *182*, 295–315.

(120) *Protein NMR Techniques*, 3rd ed.; Shekhtman, A., Burz, D. S., Eds.; Methods in Molecular Biology; Humana Press: Totowa, NJ, 2012; Vol. 831. https://doi.org/10.1007/978-1-61779-480-3.

(121) *Introduction to Spectroscopy*, 4th ed.; Pavia, D. L., Lampman, G. M., Kriz, G. S., Vyvyan, J. R., Eds.; Brooks/Cole Cengage Learning: Belmont, CA, 2001.

(122) Anderson, A. C. The Process of Structure-Based Drug Design. *Chem. Biol.* **2003**, *10* (9), 787–797. https://doi.org/10.1016/j.chembiol.2003.09.002.

(123) Ziarek, J. J.; Peterson, F. C.; Lytle, B. L.; Volkman, B. F. Binding Site Identification and Structure Determination of ProteinLigand Complexes by NMR: A Semiautomated Approach. *Methods Enzymol.* **2011**, *493*, 241–275. https://doi.org/10.1016/B978-0-12-381274-2.00010-8.

(124) Benjamin, E. J.; Muntner, P.; Alonso, A.; Bittencourt, M. S.; Callaway, C. W.; Carson, A. P.; Chamberlain, A. M.; Chang, A. R.; Cheng, S.; Das, S. R.; et al. Heart Disease and Stroke Statistics—2019 Update: A Report From the American Heart Association. *Circulation* **2019**, *139*, e1–e473. https://doi.org/10.1161/CIR.0000000000000659.

(125) Pergolizzi, J. V.; Coluzzi, F.; Colucci, R. D.; Olsson, H.; LeQuang, J. A.; Al-Saadi, J.; Magnusson, P. Statins and Muscle Pain. *Expert Rev. Clin. Pharmacol.* **2020**, *13* (3), 299–310. https://doi.org/10.1080/17512433.2020.1734451.

(126) Alsehli, A. M.; Olivo, G.; Clemensson, L. E.; Williams, M. J.; Schiöth, H. B. The Cognitive Effects of Statins Are Modified by Age. *Sci. Rep.* **2020**, *10* (1), 1–14. https://doi.org/10.1038/s41598-020-63035-2.

(127) MacDonald, S. M. Potential Role of Histamine Releasing Factor (HRF) as a Therapeutic Target for Treating Asthma and Allergy. *Journal of Asthma and Allergy*. 2012, pp 51–59. https://doi.org/10.2147/JAA.S28868.

(128) Fujise, K.; Pinkaew, D.; Eltorky, M.; Le, R. J.; Chen, Y.; Teng, B. Fortilin Reduces Apoptosis in Macrophages and Promotes Atherosclerosis. *Am. J. Physiol. Circ. Physiol.* **2013**, *305* (10), H1519–H1529. https://doi.org/10.1152/ajpheart.00570.2013.

(129) Vindis, C.; Elbaz, M.; Escargueil-Blanc, I.; Auge, N.; Heniquez, A.; Thiers, J. C.; Nègre-Salvayre, A.; Salvayre, R. Two Distinct Calcium-Dependent Mitochondrial Pathways Are Involved in Oxidized LDL-Induced Apoptosis. *Arterioscler. Thromb. Vasc. Biol.* **2005**, *25* (3), 639–645. https://doi.org/10.1161/01.ATV.0000154359.60886.33.

(130) Hughes, J. P.; Rees, S. S.; Kalindjian, S. B.; Philpott, K. L. Principles of Early Drug Discovery. *Br. J. Pharmacol.* **2011**, *162* (6), 1239–1249. https://doi.org/10.1111/j.1476-5381.2010.01127.x.

(131) Rosano, G. L.; Ceccarelli, E. A. Recombinant Protein Expression in Escherichia Coli: Advances and Challenges. *Front. Microbiol.* **2014**, *5* (APR), 1–17. https://doi.org/10.3389/fmicb.2014.00172.

(132) Lazar Jr., I.; Lazar Sr., I. GelAnalyzer 19.1.

(133) Skinner, S.; Fogh, R.; Boucher, W.; Ragan, T.; Mureddu, L.; Vioster, G. J. CcpNmr AnalysisAssign: A Flexible Platform for Integrated NMR Analysis. *Biomol. NMR* **2016**, *66* (2), 111–124.

(134) Murredu, L.; Vuister, G. Simple High-Resolution NMR Spectroscopy as a Tool in Molecular Biology. *FEBS J.* **2019**, *286* (11), 2035–2042.

(135) Pu, X.; Oxford, J. T. Proteomic Analysis of Engineered Cartilage. In *Methods in Molecular Biology*; Clifton, NJ, 2015; pp 263–278. https://doi.org/10.1007/978-1-4939-2938-2_19.

(136) Evers, T. H.; Van Dongen, E. M. W. M.; Faesen, A. C.; Meijer, E. W.; Merkx, M. Quantitative Understanding of the Energy Transfer between Fluorescent Proteins Connected via Flexible Peptide Linkers. *Biochemistry* **2006**, *45* (44), 13183–13192. https://doi.org/10.1021/bi061288t.

(137) Miller, W. G. Random Coil Configurations of Polypeptide Copolymers. *J. Mol. Biol.* **1967**, *23* (1), 67.

(138) Nguyen, M. T.; Prima, M. J.; Song, J. A.; Kim, J.; Do, B. H.; Yoo, J.; Park, S.; Jang, J.; Lee, S.; Lee, E.; et al. Prokaryotic Soluble Overexpression and Purification of Oncostatin M Using a Fusion Approach and Genetically Engineered E. Coli Strains. *Sci. Rep.* **2019**, *9* (1), 1–13. https://doi.org/10.1038/s41598-019-50110-6.

(139) Yang, Y.; Yang, F.; Xiong, Z.; Yan, Y.; Wang, X.; Nishino, M.; Mirkovic, D.; Nguyen, J.; Wang, H.; Yang, X. F. An N-Terminal Region of Translationally Controlled Tumor Protein Is Required for Its Antiapoptotic Activity. *Oncogene* **2005**, *24* (30), 4778–4788. https://doi.org/10.1038/sj.onc.1208666.

(140) Underlying Cause of Death 1999-2019.

(141) Medical Expenditure Panel Survey: household component summary tables. Total expenditures in millions by condition, United States, 2014-2015.

(142) Khavjou, O.; Phelps, D.; Leib, A. Projections of Cardiovascular Disease Prevalence and Costs: 2015-2035. *RTI Int.* **2016**, No. 0214680, 1–54.

(143) Rader, D. J.; Puré, E. Lipoproteins, Macrophage Function, and Atherosclerosis: Beyond the Foam Cell? *Cell Metabolism*. 2005, pp 223–230. https://doi.org/10.1016/j.cmet.2005.03.005.

(144) Fernández-Friera, L.; Fuster, V.; López-Melgar, B.; Oliva, B.; García-Ruiz, J. M.; Mendiguren, J.; Bueno, H.; Pocock, S.; Ibáñez, B.; Fernández-Ortiz, A.; et al. Normal LDL-Cholesterol Levels Are Associated With Subclinical Atherosclerosis in the Absence of Risk Factors. *J. Am. Coll. Cardiol.* **2017**, *70* (24), 2979–2991. https://doi.org/10.1016/j.jacc.2017.10.024.

(145) Panrat, T.; Sinthujaroen, P.; Nupan, B.; Wanna, W.; Tammi, M. T.; Phongdara, A. Characterization of a Novel Binding Protein for Fortilin/TCTP - Component of a Defense Mechanism against Viral Infection in Penaeus Monodon. *PLoS One* **2012**, *7* (3). https://doi.org/10.1371/journal.pone.0033291.

(146) Hajduk, P. J.; Greer, J. A Decade of Fragment-Based Drug Design: Strategic Advances and Lessons Learned. *Nature Reviews Drug Discovery*. 2007, pp 211–219. https://doi.org/10.1038/nrd2220.

(147) Cole, C. A.; Daigham, N. S.; Liu, G.; Montelione, G. T.; Valafar, H. REDCRAFT: A Computational Platform Using Residual Dipolar Coupling NMR Data for Determining Structures of Perdeuterated Proteins in Solution. *PLoS Comput. Biol.* **2021**, *17* (2), 1–23. https://doi.org/10.1371/JOURNAL.PCBI.1008060.

(148) Rule, G. S.; Hitchens, T. K. Protein NMR Spectroscopy. *Mod. Protein Chem. Pract. Asp.* **2001**, 37–70. https://doi.org/10.1016/s0960-9822(98)70214-3.

(149) Graidist, P.; Yazawa, M.; Tonganunt, M.; Nakatomi, A.; Lin, C. C. J.; Chang, J. Y.; Phongdara, A.; Fujise, K. Fortilin Binds Ca2+ and Blocks Ca2+-Dependent Apoptosis in Vivo. *Biochem. J.* **2007**, *408* (2), 181–191. https://doi.org/10.1042/BJ20070679.

(150) Cantrell, M. S.; Wall, J. D.; Pu, S.; Turner, M.; Woodbury, L.; King, M.; Fujise, K.; McDougal, O. M.; Warner, L. R. Generation of Cleavable Recombinant Fortilin Fusion Protein in BL21(DE3) E. Coli Cells. **2021**, *manuscript*.

(151) Leong, L. E. C. The Use of Recombinant Fusion Proteases in the Affinity Purification of Recombinant Proteins. *Appl. Biochem. Biotechnol. - Part B Mol. Biotechnol.* **1999**, *12* (3), 269–274. https://doi.org/10.1385/MB:12:3:269.

(152) Einhauer, A.; Jungbauer, A. The FLAG™ Peptide, a Versatile Fusion Tag for the Purification of Recombinant Proteins. *J. Biochem. Biophys. Methods* **2001**, *49* (1–3), 455–465. https://doi.org/10.1016/S0165-022X(01)00213-5.

(153) Zordan, R. E.; Beliveau, B. J.; Trow, J. A.; Craig, N. L.; Cormack, B. P. Avoiding the Ends: Internal Epitope Tagging of Proteins Using Transposon Tn7. *Genetics* **2015**, *200* (1), 47–58. https://doi.org/10.1534/genetics.114.169482.

(154) Whitmore, L.; Wallace, B. A. DICHROWEB, an Online Server for Protein Secondary Structure Analyses from Circular Dichroism Spectroscopic Data. *Nucleic Acids Res.* **2004**, *32* (WEB SERVER ISS.), 668–673. https://doi.org/10.1093/nar/gkh371.

(155) Whitmore, L.; Wallace, B. A. Protein Secondary Structure Analyses from Circular Dichroism Spectroscopy: Methods and Reference Databases. *Biopolymers* **2008**, *89* (5), 392–400. https://doi.org/10.1002/bip.20853.

(156) Janes, R. W. Reference Datasets for Protein Circular Dichroism and Synchrotron Radiation Circular Dichroism Spectroscopic Analyses. *Adv. Biomed. Spectrosc.* **2009**, *1*, 183.

(157) Abraham, M. J.; Murtola, T.; Schulz, R.; Páll, S.; Smith, J. C.; Hess, B.; Lindah, E. Gromacs: High Performance Molecular Simulations through Multi-Level Parallelism from Laptops to Supercomputers. *SoftwareX* **2015**, *1–2*, 19–25. https://doi.org/10.1016/j.softx.2015.06.001.

(158) Semisotnov, G. V.; Rodionova, N. A.; Razgulyaev, O. I.; Uversky, V. N.; Gripas', A. F.; Gilmanshin, R. I. Study of the "Molten Globule" Intermediate State in Protein Folding by a Hydrophobic Fluorescent Probe. *Biopolymers* **1991**, *31* (1), 119–128. https://doi.org/10.1002/bip.360310111.

(159) Pantoliano, M. W.; Petrella, E. C.; Kwasnoski, J. D.; Lobanov, V. S.; Myslik, J.; Graf, E.; Carver, T.; Asel, E.; Springer, B. A.; Lane, P.; et al. High-Density Miniaturized Thermal Shift Assays as a General Strategy for Drug Discovery. *J. Biomol. Screen.* **2001**, *6* (6), 429–440. https://doi.org/10.1177/108705710100600609.

(160) Duan, Y.; Wu, C.; Chowdhury, S.; Lee, M. C.; Xiong, G.; Zhang, W.; Yang, R.; Cieplak, P.; Luo, R.; Lee, T.; et al. A Point-Charge Force Field for Molecular Mechanics Simulations of Proteins Based on Condensed-Phase Quantum Mechanical Calculations. *J. Comput. Chem.* **2003**, *24* (16), 1999–2012. https://doi.org/10.1002/jcc.10349.

(161) Duan, Y.; Wu, C.; Chowdhury, S.; Lee, M. C.; Xiong, G.; Zhang, W.; Yang, R.; Cieplak, P.; Luo, R.; Lee, T.; et al. A Point-Charge Force Field for Molecular Mechanics Simulations of Proteins Based on Condensed-Phase Quantum Mechanical Calculations. *J. Comput. Chem.* **2003**, *24* (16), 1999–2012. https://doi.org/10.1002/jcc.10349.

(162) Skyner, R. E.; McDonagh, J. L.; Groom, C. R.; Van Mourik, T.; Mitchell, J. B. O. A Review of Methods for the Calculation of Solution Free Energies and the Modelling of Systems in Solution. *Phys. Chem. Chem. Phys.* **2015**, *17* (9), 6174–6191. https://doi.org/10.1039/c5cp00288e.

(163) Atak, K.; Golnak, R.; Xiao, J.; Suljoti, E.; Pflüger, M.; Brandenburg, T.; Winter, B.; Aziz, E. F. Electronic Structure of Hemin in Solution Studied by Resonant X-Ray Emission Spectroscopy and Electronic Structure Calculations. *J. Phys. Chem. B* **2014**, *118* (33), 9938–9943. https://doi.org/10.1021/jp505129m.

(164) Sol, E. M.; Wagner, S. A.; Weinert, B. T.; Kumar, A.; Kim, H. S.; Deng, C. X.; Choudhary, C.; Imhof, A. Proteomic Investigations of Lysine Acetylation Identify Diverse Substrates of Mitochondrial Deacetylase Sirt3. *PLoS One* **2012**, *7* (12), 1–9. https://doi.org/10.1371/journal.pone.0050545.

(165) Olsen, J. V.; Vermeulen, M.; Santamaria, A.; Kumar, C.; Miller, M. L.; Jensen, L. J.; Gnad, F.; Cox, J.; Jensen, T. S.; Nigg, E. A.; et al. Quantitative Phosphoproteomics RevealsWidespread Full Phosphorylation Site Occupancy During Mitosis. *Cell cylcle* **2010**, *3* (104 ra3), 1–15.

(166) Yarm, F. R. Plk Phosphorylation Regulates the Microtubule-Stabilizing Protein TCTP. *Mol. Cell. Biol.* **2002**, *22* (17), 6209–6221. https://doi.org/10.1128/mcb.22.17.6209-6221.2002.

(167) Lewis, M. G.; Dafonseca, S.; Chomont, N.; Palamara, A. T.; Tardugno, M.; Mai, A.; Collins, M.; Wagner, W. L.; Yalley-Ogunro, J.; Greenhouse, J.; et al. Gold Drug Auranofin Restricts the Viral Reservoir in the Monkey AIDS Model and Induces Containment of Viral Load Following ART Suspension. *Aids* **2011**, *25* (11), 1347–1356. https://doi.org/10.1097/QAD.0b013e328347bd77.

APPENDIX A

Supplementary materials for Chapter Two – purification gels and mass spectrometry data

SDS-PAGE gels to check purification status

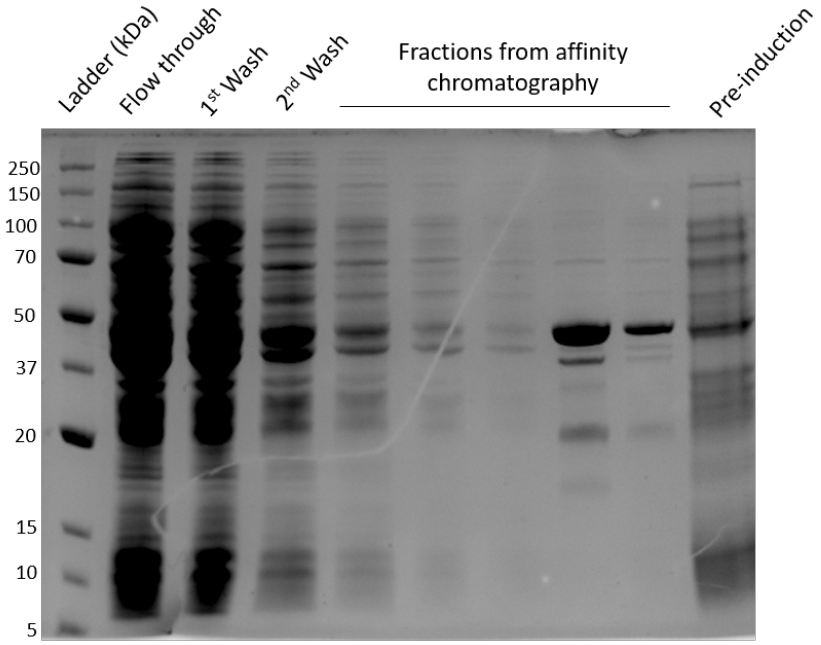

Figure A1. (GGS)0 purification. GST-fortilin can be seen at approximately 47 kDa.

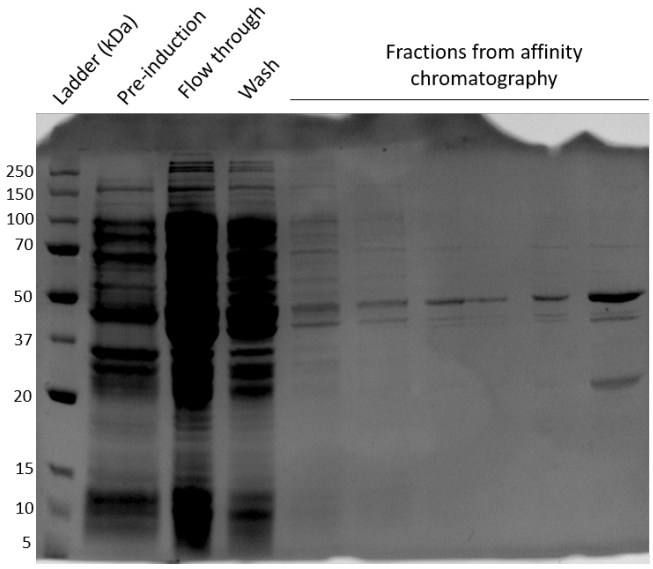

Figure A2. (GGS)1 purification. Pure GST-GGS-fortilin can be seen at 47 kDa.

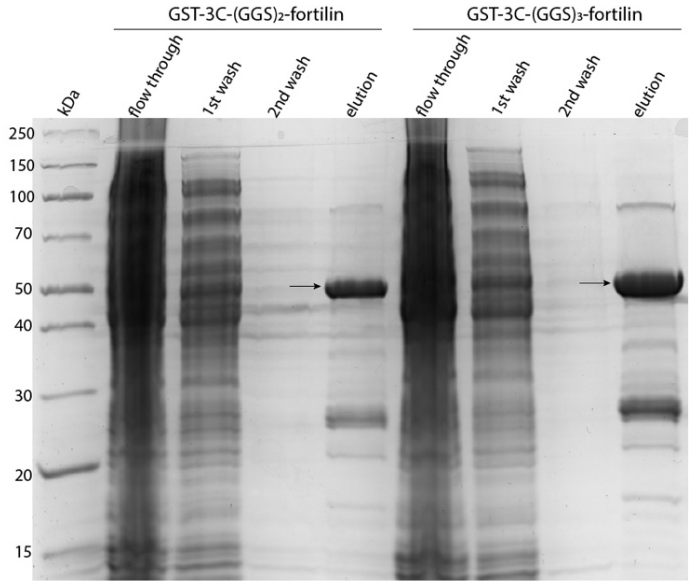

Figure A3. (GGS)2 and (GGS)3 purification. Arrows point to GST-(GGS)N-fortilin.

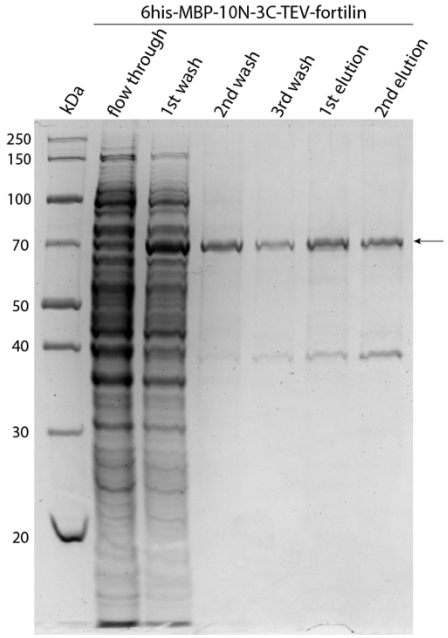

Figure A4. 6His-MBP-10N-3C-TEV-Fortilin purification. Arrow points to 6His-MBP-10N-3C-TEV-fortilin.

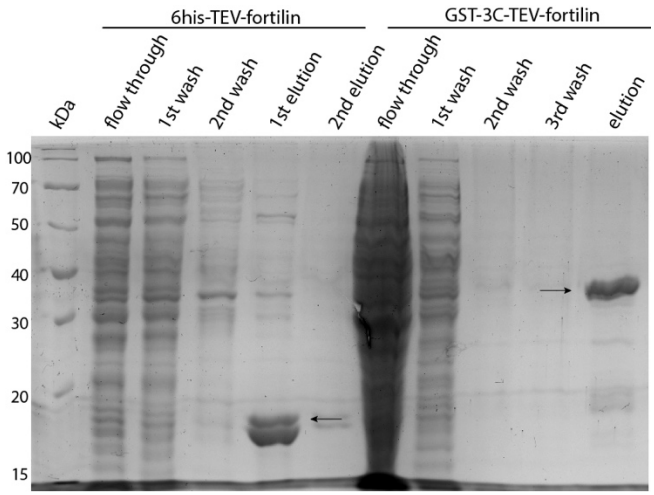

Figure A5. 6His-TEV-fortilin and GST-3C-TEV-fortilin purification. Arrows indicate purified 6His-TEV-fortilin (left) and GST-3C-TEV-fortilin (right).

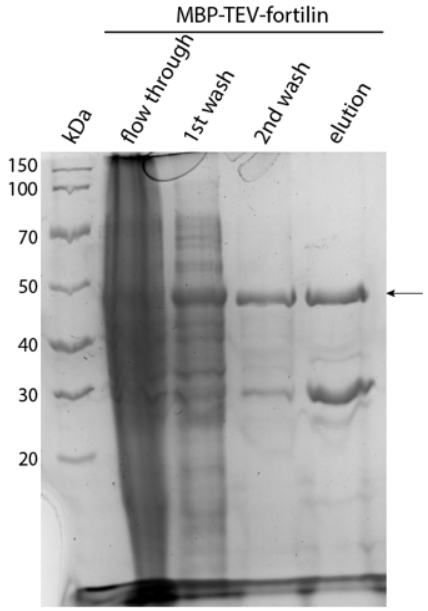

Figure A6. MBP-TEV-fortilin purification. Arrow indicates MBP-TEV-fortilin.

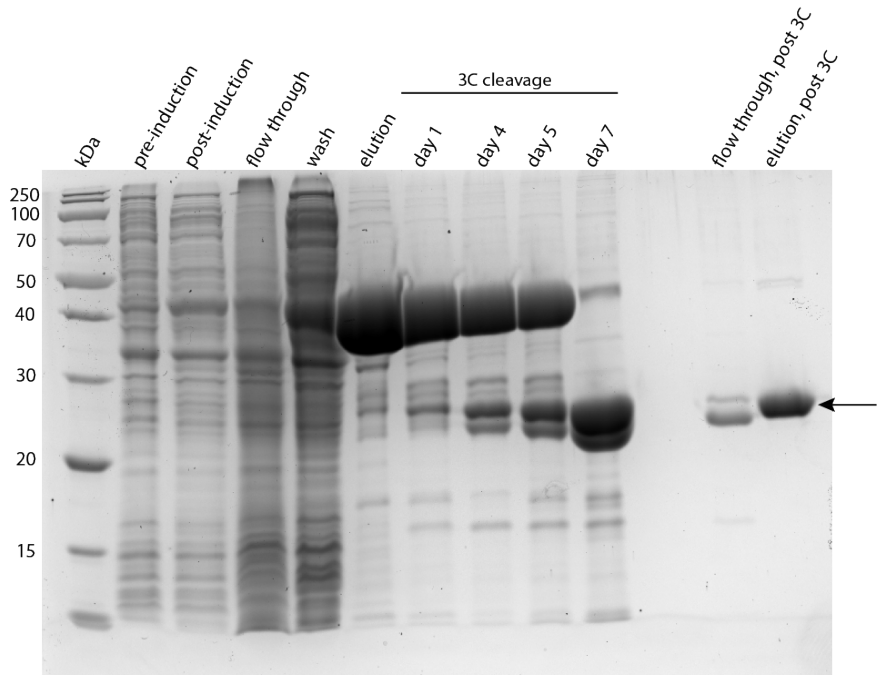

Figure A7. 15N-GGS-fortilin cleavage and purification. Arrow indicates pure GGS-fortilin after cleavage and subsequent purification on glutathione agarose. For this sample, not enough 3C protease was initially added (day 1 lane). On day 5, protease was added to a combined volume of 50 mL protease in the sample and ideal cleavage was observed on day 7.

Mass Spectrometry Analysis for Chapter Two.

Table A1. Sample names and sequences for mass spectrometry analysis. These data correspond to the following MS files in this section.

Sequence name	sample name	sample from what construct	expected sequence
MC1	MBP +ctrl	MBP-TEV-OSM	MKIEEGKLVI WINGDKGYNG LAEVGKKFEK DTGIKVTVEH PDKLEEKFPQ VAATGDGPDI IFWAHD RFGGYAQSGLLAEI TPDKAFQDKL YPFTWDAVRY NGKLIAYPIA VEALSLIYNK DLLPNPPKTW EEI PALDKEL KAKGKSALMF NLQEPYFTWP LIAADGGYAF KYENGKYDIK DVGVDNAGAKAGLTFLV DLI KNKHMNADTD YSIAEAAFNK GETAMTINGP WAWSNIDTSK VNYGVTVLPT FKGQPSKPFVGV LSAGINAA SPNKELAKEF LENYLLTDEG LEAVNKDKPL GAVALKSYEE ELAKDPRIAATMENAQKG EI MPNIPQMSAF WYAVRTAVIN AASGRQTVDE ALKDAQTNSS SNNNNNNNNN NLGIEGR ENLYFQ
MC2	OSM +ctrl	MBP-TEV-OSM	MGVLLTQRTLLSLVLALLFPSMASMAAIGSCSKEYRVLLGQLQK QTDLMQDTSRLLDPYI RIQGLDVPKLREHCRERPGAFPSEETLRGLGRRGFLQTLNATLGC VLHRLADLEQRLPKA QDLERSGLNIEDLEKLQMARPNILGLRNNIYCMAQLLDNSDTAE PTKAGRGASQPPTPTP ASDAFQRKLEGCRFLHGYHRFMHSVGRVFSKWGESPNRSRRHSP HQALRKGVRRTRPSRK GKRLMTRGQLPR
MC3	MBPTEV Fortilin TEV+ Day 1	MBP-TEV-Fortilin	MKTEEGKLVIWINGDKGYNGLAEVGKKFEKDTGIKVTVEHPDK LEEKFPQVAATGDGPDIIFWAHDRF GGYAQSGLLAEITPDKAFQDKLYPFTWDAVRYNGKLIAYPIAVE ALSLIYNKDLLPNPPKTWEEIPALD KELKAKGKSALMFNLQEPYFTWPLIAADGGYAFKYENGKYDIK DVGVDNAGAKAGLTFLVDLIKNKH MNADTDYSIAEAAFNKGETAMTINGPWAWSNIDTSKVNYGVTV LPTFKGQPSKPFVGVLSAGINAASP NKELAKEFLENYLLTDEGLEAVNKDKPLGAVALKSYEEELAKD PRIAATMENAQKGEIMPNIPQMSAF WYAVRTAVINAASGRQTVDEALKDAQTNFQGPMENLYFQGIIY RDLISHDEMFSDIYKIREIADGLCLE VEGKMVSRTEGNIDDSLIGGNASAEGPEGEGTESTVITGVDIVM NHHLQETSFTKEAYKKYIKDYMKS IKGKLEEQRPERVKPFMTGAAEQIKHILANFKNYQFFIGENMNPD GMVALLDYREDGVTPYMIFFKDG LEMEKCLE
MC3	MBPTEV Fortilin TEV- Day 1	MBP-TEV-Fortilin	MKTEEGKLVIWINGDKGYNGLAEVGKKFEKDTGIKVTVEHPDK LEEKFPQVAATGDGPDIIFWAHDR FGGYAQSGLLAEITPDKAFQDKLYPFTWDAVRYNGKLIAYPIAV EALSLIYNKDLLPNPPKTWEEIPAL DKELKAKGKSALMFNLQEPYFTWPLIAADGGYAFKYENGKYDI KDVGVDNAGAKAGLTFLVDLIKN KHMNADTDYSIAEAAFNKGETAMTINGPWAWSNIDTSKVNYG VTVLPTFKGQPSKPFVGVLSAGINA ASPNKELAKEFLENYLLTDEGLEAVNKDKPLGAVALKSYEEELA KDPRIAATMENAQKGEIMPNIPQ MSAFWYAVRTAVINAASGRQTVDEALKDAQTNFQGPMENLYF QGIIYRDLISHDEMFSDIYKIREIA DGLCLEVEGKMVSRTEGNIDDSLIGGNASAEGPEGEGTESTVITG VDIVMNHHLQETSFTKEAYKKY

			IKDYMKSIKGKLEEQRPERVKPFMTGAAEQIKHILANFKNYQFFI GENMNPDGMVALLDYREDGVTP YMIFFKDGLEMEKCLE
MC5	TEV Fortilin 3C+ Day 1	6His-MBP-10N-3C-TEV-Fortilin	MENLYFQGIIYRDLISHDEMFSDIYKIREIADGLCLEVEGKMVSR TEGNIDDSLIGGNASAEGPEGEGT ESTVITGVDIVMNHHLQETSFTKEAYKKYIKDYMKSIKGKLEEQ RPERVKPFMTGAAEQIKHILANFK NYQFFIGENMNPDGMVALLDYREDGVTPYMIFFKDGLEMEKC
MC5	TEV Fortilin from GST Day 1	GST-3C-TEV-Fortilin	MENLYFQGIIYRDLISHDEMFSDIYKIREIADGLCLEVEGKMVSR TEGNIDDSLIGGNASAEGPEGEGT ESTVITGVDIVMNHHLQETSFTKEAYKKYIKDYMKSIKGKLEEQ RPERVKPFMTGAAEQIKHILANFK NYQFFIGENMNPDGMVALLDYREDGVTPYMIFFKDGLEMEKC
MC7	GST3CTEV Fortilin -ctrl Day 1	GST-3C-TEV-Fortilin	MSPILGYWKIKGLVQPTRLLLEYLEEKYEEHLYERDEGDKWRN KKFELGLEFPNLPYYIDGDVKLTQS MAIIRYIADKHNMLGGCPKERAEISMLEGAVLDIRYGVSRIAYSK DFETLKVDFLSKLPEMLKMFEDRL CHKTYLNGDHVTHPDFMLYDALDVVLYMDPMCLDAFPKLVCF KKRIEAIPQIDKYLKSSKYIAWPLQ GWQATFGGGDHPPKSDLEVLFQGPMENLYFQGIIYRDLISHDEM FSDIYKIREIADGLCLEVEGKMVS RTEGNIDDSLIGGNASAEGPEGEGTESTVITGVDIVMNHHLQETS FTKEAYKKYIKDYMKSIKGKLEE QRPERVKPFMTGAAEQIKHILANFKNYQFFIGENMNPDGMVALL DYREDGVTPYMIFFKDGLEMEKC
MC7	GST3CTEV Fortilin 3C+ Day 1	GST-3C-TEV-Fortilin	MSPILGYWKIKGLVQPTRLLLEYLEEKYEEHLYERDEGDKWRN KKFELGLEFPNLPYYIDGDVKLTQS MAIIRYIADKHNMLGGCPKERAEISMLEGAVLDIRYGVSRIAYSK DFETLKVDFLSKLPEMLKMFEDR LCHKTYLNGDHVTHPDFMLYDALDVVLYMDPMCLDAFPKLVC FKKRIEAIPQIDKYLKSSKYIAWP LQGWQATFGGGDHPPKSDLEVLFQGPMENLYFQGIIYRDLISHD EMFSDIYKIREIADGLCLEVEGKM VSRTEGNIDDSLIGGNASAEGPEGEGTESTVITGVDIVMNHHLQE TSFTKEAYKKYIKDYMKSIKGKL EEQRPERVKPFMTGAAEQIKHILANFKNYQFFIGENMNPDGMVA LLDYREDGVTPYMIFFKDGLEM EKC
MC7	GST3CTEV Fortilin TEV+ Day 1	GST-3C-TEV-Fortilin	MSPILGYWKIKGLVQPTRLLLEYLEEKYEEHLYERDEGDKWRN KKFELGLEFPNLPYYIDGDVKLT QSMAIIRYIADKHNMLGGCPKERAEISMLEGAVLDIRYGVSRIAY SKDFETLKVDFLSKLPEMLKMFE DRLCHKTYLNGDHVTHPDFMLYDALDVVLYMDPMCLDAFPKL VCFKKRIEAIPQIDKYLKSSKYIA WPLQGWQATFGGGDHPPKSDLEVLFQGPMENLYFQGIIYRDLIS HDEMFSDIYKIREIADGLCLEVEG KMVSRTEGNIDDSLIGGNASAEGPEGEGTESTVITGVDIVMNHH LQETSFTKEAYKKYIKDYMKSIK GKLEEQRPERVKPFMTGAAEQIKHILANFKNYQFFIGENMNPDG MVALLDYREDGVTPYMIFFKDG LEMEKC
MC10	6HisMBP Fortilin -ctrl Day 1	6His-MBP-10N-3C-TEV-Fortilin	MHHHHHHKTEEGKLVIWINGDKGYNGLAEVGKKFEKDTGIKVT VEHPDKLEEKFPQVAATGDGPD IIFWAHDRFGGYAQSGLLAEITPDKAFQDKLYPFTWDAVRYNGK LIAYPIAVEALSLIYNKDLLPNP PKTWEEIPALDKELKAKGKSALMFNLQEPYFTWPLIAADGGYAF KYENGKYDIKDVGVDNAGAK AGLTFLVDLIKNKHMNADTDYSIAEAAFNKGETAMTINGPWAW SNIDTSKVNYGVTVLPTFKGQPS KPFVGVLSAGINAASPNKELAKEFLENYLLTDEGLEAVNKDKPL GAVALKSYEEELAKDPRIAATM

			ENAQKGEIMPNIPQMSAFWYAVRTAVINAASGRQTVDEALKDA QTNLEVLFNSSSNNNNNNNNNN LGIEGRISHMLEVLFQGPMENLYFQGIIYRDLISHDEMFSDIYKIR EIADGLCLEVEGKMVSRTEGNID DSLIGGNASAEGPEGEGTESTVITGVDIVMNHHLQETSFTKEAYK KYIKDYMKSIKGKLEEQRPERV KPFMTGAAEQIKHILANFKNYQFFIGENMNPDGMVALLDYRED GVTPYMIFFKDGLEMEKCLE
MC10	6HisMBP Fortilin 3C+ Day 1	6His-MBP-10N-3C-TEV-Fortilin	MHHHHHHKTEEGKLVIWINGDKGYNGLAEVGKKFEKDTGIKVT VEHPDKLEEKFPQVAATGDGP DIIFWAHDRFGGYAQSGLLAEITPDKAFQDKLYPFTWDAVRYNG KLIAYPIAVEALSLIYNKDLLP NPPKTWEEIPALDKELKAKGKSALMFNLQEPYFTWPLIAADGGY AFKYENGKYDIKDVGVDNAGA KAGLTFLVDLIKNKHMNADTDYSIAEAAFNKGETAMTINGPWA WSNIDTSKVNYGVTVLPTFKG QPSKPFVGVLSAGINAASPNKELAKEFLENYLLTDEGLEAVNKD KPLGAVALKSYEEELAKDPR IAATMENAQKGEIMPNIPQMSAFWYAVRTAVINAASGRQTVDE ALKDAQTNLEVLFNSSSNNN NNNNNNNLGIEGRISHMLEVLFQGPMENLYFQGIIYRDLISHDEM FSDIYKIREIADGLCLEVEGK MVSRTEGNIDDSLIGGNASAEGPEGEGTESTVITGVDIVMNHHL QETSFTKEAYKKYIKDYMKS IKGKLEEQRPERVKPFMTGAAEQIKHILANFKNYQFFIGENMNPD GMVALLDYREDGVTPYMIFF KDGLEMEKCLE
MC10	6HisMBP Fortilin TEV+ Day 1	6His-MBP-10N-3C-TEV-Fortilin	MHHHHHHKTEEGKLVIWINGDKGYNGLAEVGKKFEKDTGIKVT VEHPDKLEEKFPQVAATGDGPD IIFWAHDRFGGYAQSGLLAEITPDKAFQDKLYPFTWDAVRYNGK LIAYPIAVEALSLIYNKDLLPNPP KTWEEIPALDKELKAKGKSALMFNLQEPYFTWPLIAADGGYAF KYENGKYDIKDVGVDNAGAKAG LTFLVDLIKNKHMNADTDYSIAEAAFNKGETAMTINGPWAWSN IDTSKVNYGVTVLPTFKGQPSKP FVGVLSAGINAASPNKELAKEFLENYLLTDEGLEAVNKDKPLGA VALKSYEEELAKDPRIAATMEN AQKGEIMPNIPQMSAFWYAVRTAVINAASGRQTVDEALKDAQT NLEVLFNSSSNNNNNNNNNNL GIEGRISHMLEVLFQGPMENLYFQGIIYRDLISHDEMFSDIYKIREI ADGLCLEVEGKMVSRTEGNID DSLIGGNASAEGPEGEGTESTVITGVDIVMNHHLQETSFTKEAYK KYIKDYMKSIKGKLEEQRPER VKPFMTGAAEQIKHILANFKNYQFFIGENMNPDGMVALLDYRE DGVTPYMIFFKDGLEMEKCLE
MC10	6HisMBP 3C+ Day 1	6His-MBP-10N-3C-TEV-Fortilin	MHHHHHHKTEEGKLVIWINGDKGYNGLAEVGKKFEKDTGIKVT VEHPDKLEEKFPQVAATGDG PDIIFWAHDRFGGYAQSGLLAEITPDKAFQDKLYPFTWDAVRYN GKLIAYPIAVEALSLIYNKDLLP NPPKTWEEIPALDKELKAKGKSALMFNLQEPYFTWPLIAADGGY AFKYENGKYDIKDVGVDNAG AKAGLTFLVDLIKNKHMNADTDYSIAEAAFNKGETAMTINGPW AWSNIDTSKVNYGVTVLPTFK GQPSKPFVGVLSAGINAASPNKELAKEFLENYLLTDEGLEAVNK DKPLGAVALKSYEEELAKDPR IAATMENAQKGEIMPNIPQMSAFWYAVRTAVINAASGRQTVDE ALKDAQTNLEVLFNSSSNNNN NNNNNNLGIEGRISH
MC14	MBP TEV+ Day 1	6His-MBP-10N-3C-	MHHHHHHKTEEGKLVIWINGDKGYNGLAEVGKKFEKDTGIKVT VEHPDKLEEKFPQVAATGDG PDIIFWAHDRFGGYAQSGLLAEITPDKAFQDKLYPFTWDAVRYN GKLIAYPIAVEALSLIYNKDLL

		TEV-Fortilin	PNPPKTWEEIPALDKELKAKGKSALMFNLQEPYFTWPLIAADGG YAFKYENGKYDIKDVGVDN AGAKAGLTFLVDLIKNKHMNADTDYSIAEAAFNKGETAMTING PWAWSNIDTSKVNYGVTVLP TFKGQPSKPFVGVLSAGINAASPNKELAKEFLENYLLTDEGLEA VNKDKPLGAVALKSYEEELAK DPRIAATMENAQKGEIMPNIPQMSAFWYAVRTAVINAASGRQT VDEALKDAQT
MC14	MBP TEV-Day 1	6His-MBP-10N-3C-TEV-Fortilin	MHHHHHHKTEEGKLVIWINGDKGYNGLAEVGKKFEKDTGIKVT VEHPDKLEEKFPQVAATGDGP DIIFWAHDRFGGYAQSGLLAEITPDKAFQDKLYPFTWDAVRYNG KLIAYPIAVEALSLIYNKDLLP NPPKTWEEIPALDKELKAKGKSALMFNLQEPYFTWPLIAADGGY AFKYENGKYDIKDVGVDNAG AKAGL TFLVDLIKNKHMNADTDYSIAEAAFNKGETAMTINGPWAWSNI DTSKVNYGVTVLPTFKGQPS KPFVGVLSAGINAASPNKELAKEFLENYLLTDEGLEAVNKDKPL GAVALKSYEEELAKDPRIAAT MENAQKGEIMPNIPQMSAFWYAVRTAVINAASGRQTVDEALKD AQT
MC16	6HisTEV Fortilin TEV- Day 1	6His-TEV-Fortilin	MHHHHHHMENLYFQGIIYRDLISHDEMFSDIYKIREIADGLCLEV EGKMVSRTEGNIDDSLIGGNA SAEGPEGEGTESTVITGVDIVMNHHLQETSFTKEAYKKYIKDYM KSIKGKLEEQRPERVKPFMTG AAEQIKHILANFKNYQFFIGENMNPDGMVALLDYREDGVTPYMI FFKDGLEMEKCLE
MC16	6HisTEV Fortilin TEV+ Day 1	6His-TEV-Fortilin	MHHHHHHMENLYFQGIIYRDLISHDEMFSDIYKIREIADGLCLEV EGKMVSRTEGNIDDSLIGGN ASAEGPEGEGTESTVITGVDIVMNHHLQETSFTKEAYKKYIKDY MKSIKGKLEEQRPERVKPFM TGAAEQIKHILANFKNYQFFIGENMNPDGMVALLDYREDGVTP YMIFFKDGLEMEKCLE
MC18	15N(GGS)1-fortilin (this is 15N labeled)	GST-3C-(GGS)1-Fortilin	GGSMIIYRDLISHDEMFSDIYKIREIADGLCLEVEGKMVSRTEGNI DDSLIGGNASAEGPEGEGT ESTVITGVDIVMNHHLQE

Table A2. Results from the MS analysis for the cleavage of constructs used.

Sample name	Accession	Coverage [%]	# Peptides	# Unique Peptides	# AAs	MW [kDa]	calc. pI	Score Sequest HT	# Peptides
6His MBP 3C+	MC10	70	37	2	592	66	5.21	937.84	37
	MC3	72	36	1	553	61.5	5.02	880.75	36
	MC7	43	17	11	407	47	5.3	86.03	17
	A1AIF3	36	10	10	394	43.3	5.45	36.91	10
	B7NSH9	25	6	6	353	38	5.19	22.22	6
	P0C0V1	10	3	3	474	49.3	8.56	10.6	3
6His MBP Fortilin -ctrl	MC10	77	46	34	592	66	5.21	1510.32	46
	MC7	30	14	2	407	47	5.3	389.2	14
	P0AG67	10	5	5	557	61.1	4.98	16.45	5
	P08660	10	3	3	449	48.5	5.11	10.65	3
6His MBP Fortilin 3C+	MC10	74	40	31	592	66	5.21	740.78	40
	MC7	37	13	4	407	47	5.3	198.95	13
	P0AG67	18	8	8	557	61.1	4.98	27.72	8
6His MBP Fortilin TEV+	MC10	80	45	2	592	66	5.21	1334.5	45
	MC1	92	33	1	393	43.3	5.15	959.24	33
	MC7	30	13	2	407	47	5.3	336.29	13
	P0AG67	12	5	5	557	61.1	4.98	21.98	5
6His TEV Fort TEV+	MC10	58	27	16	592	66	5.21	838.13	27
	MC7	40	19	8	407	47	5.3	799.43	19
	MC18	45	4	1	83	9	4.36	464.2	4
	P0A6T6	34	6	6	222	24.8	7.33	29.16	6
	P0ACJ8	47	9	9	210	23.6	8.25	26.29	9
6His TEV Fort TEV-	MC3	48	20	10	553	61.5	5.02	490.22	20
	MC7	35	13	3	407	47	5.3	449.7	13
	P0A6T6	34	7	7	222	24.8	7.33	25.01	7
	A7ZSM6	2	2	2	601	66.4	6.68	10.4	2
GST 3C TEV Fort -ctrl	MC7	70	35	24	407	47	5.3	1620.44	35
	MC10	34	18	7	592	66	5.21	646.51	18
	P0A9G6	52	16	16	434	47.5	5.31	58.66	16
	A7ZML6	41	11	11	406	43.6	6.35	46.74	11
	P0A932	6	3	3	379	41.7	6.06	10.47	3
	A1AIF3	12	4	4	394	43.3	5.45	10.01	4
GST 3C TEV Fortilin +3C	MC7	64	33	22	407	47	5.3	1241.48	33
	MC10	54	24	13	592	66	5.21	674.25	24

	MC18	45	5	2	83	9	4.36	315.56	5
	P0A9G6	59	19	19	434	47.5	5.31	101.88	19
	A7ZML6	43	11	11	406	43.6	6.35	55.05	11
	A1AIF3	15	5	5	394	43.3	5.45	15.3	5
	B1XC35	15	4	4	446	49.9	4.98	13.47	4
GST 3C TEV Fortilin TEV+	MC7	66	38	26	407	47	5.3	1793.38	38
	MC10	28	16	4	592	66	5.21	634.19	16
	MC18	45	4	1	83	9	4.36	400.76	4
	P0A9G6	52	17	17	434	47.5	5.31	81.6	17
	A7ZML6	48	13	13	406	43.6	6.35	58.48	13
	A1AIF3	14	4	4	394	43.3	5.45	13.98	4
MBP +ctrl	MC3	74	42	36	553	61.5	5.02	1324.27	42
	MC7	28	9	3	407	47	5.3	38.16	9
	MC2	34	7	7	252	28.5	10.71	36.98	7
	B1X8Q8	30	5	5	172	19	6.57	19.28	5
	P03023	16	5	5	360	38.6	6.89	14.26	5
	P76083	8	2	2	475	51.7	5.91	11.34	2
MBP TEV Fort TEV-	MC3	77	37	29	553	61.5	5.02	819.19	37
	MC7	32	11	3	407	47	5.3	207.07	11
MBP TEV Fortilin TEV+	MC3	79	40	2	553	61.5	5.02	852.73	40
	MC10	76	40	2	592	66	5.21	842.68	40
	MC7	30	12	2	407	47	5.3	206.49	12
MBP TEV-	MC10	64	37	5	592	66	5.21	770.37	37
	P0AEX9	82	33	1	396	43.4	5.71	767.19	33
	P02931	43	17	17	362	39.3	4.96	141.84	17
	B1XC35	17	4	4	446	49.9	4.98	14.73	4
MBP TEV+	MC3	77	44	2	553	61.5	5.02	1152.63	44
	P0AEX9	83	37	1	396	43.4	5.71	1101.93	37
	P02931	52	17	17	362	39.3	4.96	166.63	17
	MC7	23	7	1	407	47	5.3	54.65	7
	B1XC35	34	10	10	446	49.9	4.98	46.22	10
	P10384	11	4	4	446	48.5	5.3	12.86	4
OSM +ctrl	MC2	21	5	5	252	28.5	10.71	20.12	5
TEV Fortilin 3C+	MC10	53	28	17	592	66	5.21	336.42	28
	MC7	52	26	14	407	47	5.3	334.93	26
	MC5	67	13	1	179	20.4	4.87	257.77	13
	B7LA77	24	4	4	234	24.7	9.64	12.68	4

	B1LHD4	23	3	3	209	22.2	9.91	11.17	3
	B7LHZ8	20	3	3	206	23.5	10.05	10.32	3
TEV Fortilin from GST 3C+	MC7	61	30	19	407	47	5.3	549.13	30
	MC10	33	17	7	592	66	5.21	247.95	17
	MC5	67	12	1	179	20.4	4.87	220.44	12
	P0A9D2	46	8	8	201	22.9	6.21	69.67	8
	B1IPZ4	50	8	8	177	18.9	9.7	25.09	8
	P0AA25	39	3	3	109	11.8	4.88	15.87	3
	B7LHZ8	21	4	4	206	23.5	10.05	14.28	4
	P0A9G6	12	3	3	434	47.5	5.31	11	3

APPENDIX B

Supplementary materials for Chapter Three – purification gels of protein expressions

SDS-PAGE to check purification status of proteins

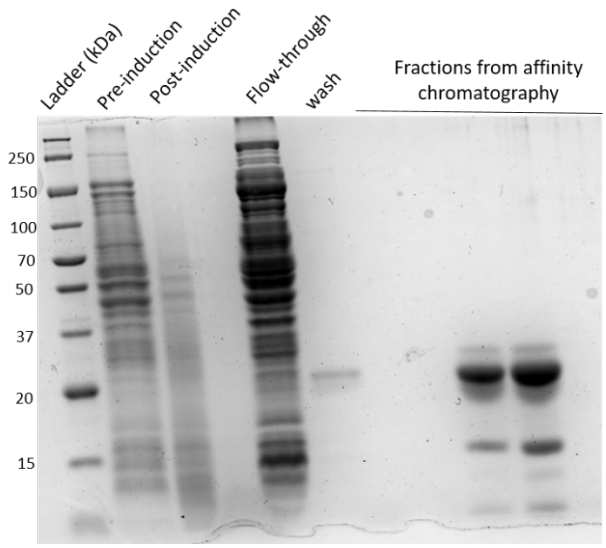

Figure B1. Purification gel of NGly56 mutant fortilin construct.

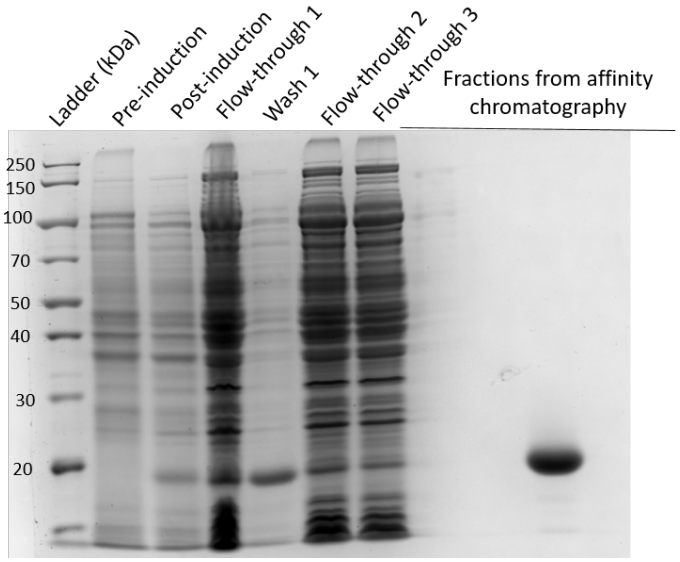

Figure B2. Purification gel of CGly56 mutant fortilin construct.

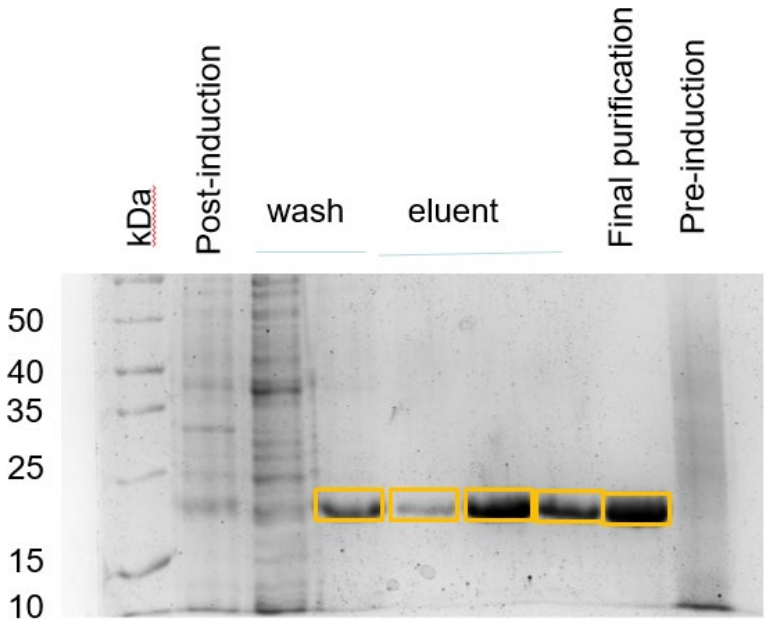

Figure B3. Purification gel of NSer46 mutant fortilin construct.

APPENDIX C

Protein amino acid & plasmid DNA sequence

Protein amino acid sequences

WT Fortilin, No Tag (Uniprot.com)

>sp|P13693|TCTP_HUMAN Translationally controlled tumor protein OS=Homo sapiens OX=9606 GN=TPT1 PE=1 SV=1

MIIYRDLISHDEMFSDIYKIREIADGLCLEVEGKMVSRTEGNIDDSLIGGNASAEGPEGEGTESTVITGVDIVMNHHLQETSFTKEAYKKYIKDYMKSIKGKLEEQRPERVKPFMTGAAEQIKHILANFKNYQFFIGENMNPDGMVALLDYREDGVTPYMIFFKDGLEMEKC

# of amino acids – 172

Mass – 19595.32 Da

mI – 4.84

Extinction coefficients are in units of M^{-1} cm^{-1}, at 280 nm measured in water.

Ext. coefficient 12045

Abs 0.1% (=1 g/l) 0.615, assuming all pairs of Cys residues form cystines

Ext. coefficient 11920

Abs 0.1% (=1 g/l) 0.608, assuming all Cys residues are reduced

6His-TEV-Fortilin

>HHHHHHENLYFQMIIYRDLISHDEMFSDIYKIREIADGLCLEVEGKMVSRTEGNIDDSLIGGNASAEGPEGEGTESTVITGVDIVMNHHLQETSFTKEAYKKYIKDYMKSIKGKLEEQRPERVKPFMTGAAEQIKHILANFKNYQFFIGENMNPDGMVALLDYREDGVTPYMIFFKDGLEMEKC

# of amino acids – 184

Mass – 21213.05 Da

pI – 5.24

Ext. coefficient 13535

Abs 0.1% (=1 g/l) 0.638, assuming all pairs of Cys residues form cystines

Ext. coefficient 13410

Abs 0.1% (=1 g/l) 0.632, assuming all Cys residues are reduced

MBP-TEV-Fortilin

>MKIEEGKLVI WINGDKGYNG LAEVGKKFEK DTGIKVTVEH PDKLEEKFPQ VAATGDGPDI IFWAHDRFGG YAQSGLLAEI TPDKAFQDKL YPFTWDAVRY NGKLIAYPIAVEALSLIYNK DLLPNPPKTW EEIPALDKEL KAKGKSALMF NLQEPYFTWP LIAADGGYAF KYENGKYDIK DVGVDNAGAK AGLTFLVDLI KNKHMNADTD YSIAEAAFNK GETAMTINGP WAWSNIDTSK VNYGVTVLPT FKGQPSKPFV GVLSAGINAA SPNKELAKEF LENYLLTDEG LEAVNKDKPL GAVALKSYEE ELAKDPRIAA TMENAQKGEI MPNIPQMSAF WYAVRTAVIN AASGRQTVDEALKDAQTNSSSNNNNNNNNNNLGIEGRENLYFQMIIYRDLISHD EMFSDIYKIREIADGLCLEVEGKMVSRTEGNIDDSLIGGNASAEGPEGEGTESTVI TGVDIVMNHHLQETSFTKEAYKKYIKDYMKSIKGKLEEQRPERVKPFMTGAAEQ IKHILANFKNYQFFIGENMNPDGMVALLDYREDGVTPYMIFFKDGLEMEKC

# of amino acids – 565

Mass – 62854.17 Da

pI – 4.95

Ext. coefficient 79885

Abs 0.1% (=1 g/l) 1.271, assuming all pairs of Cys residues form cystines

Ext. coefficient 79760

Abs 0.1% (=1 g/l) 1.269, assuming all Cys residues are reduced

6His-MBP-10N-3C-TEV-Fortilin

>HHHHHHMKIEEGKLVI WINGDKGYNG LAEVGKKFEK DTGIKVTVEH PDKLEEKFPQ VAATGDGPDI IFWAHDRFGG YAQSGLLAEI TPDKAFQDKL YPFTWDAVRY NGKLIAYPIAVEALSLIYNK DLLPNPPKTW EEIPALDKEL KAKGKSALMF NLQEPYFTWP LIAADGGYAF KYENGKYDIK DVGVDNAGAK AGLTFLVDLI KNKHMNADTD YSIAEAAFNK GETAMTINGP WAWSNIDTSK VNYGVTVLPT FKGQPSKPFV GVLSAGINAA SPNKELAKEF LENYLLTDEG LEAVNKDKPL GAVALKSYEE ELAKDPRIAA TMENAQKGEI MPNIPQMSAF WYAVRTAVIN AASGRQTVDE ALKDAQTNSS SNNNNNNNNN NLGIEGRNNNNNNNNNNLEVLFQENLYFQMIIYRDLISHDEMFSDIYKIREIADGL CLEVEGKMVSRTEGNIDDSLIGGNASAEGPEGEGTESTVITGVDIVMNHHLQETS FTKEAYKKYIKDYMKSIKGKLEEQRPERVKPFMTGAAEQIKHILANFKNYQFFIG ENMNPDGMVALLDYREDGVTPYMIFFKDGLEMEKC

# of amino acids – 587

Mass – 65547.93

pI – 5.12

Ext. coefficient 79885

Abs 0.1% (=1 g/l) 1.219, assuming all pairs of Cys residues form cystines

Ext. coefficient 79760

Abs 0.1% (=1 g/l) 1.217, assuming all Cys residues are reduced

GST-3C-TEV-Fortilin

>MSPILGYWKIKGLVQPTRLLLEYLEEKYEEHLYERDEGDKWRNKKFEL
GLEFPNLPYYIDGDVKLTQSMAIIRYIADKHNMLGGCPKERAEISMLEGAVLDIR
YGVSRIAYSKDFETLKVDFLSKLPEMLKMFEDRLCHKTYLNGDHVTHPDFMLY
DALDVVLYMDPMCLDAFPKLVCFKKRIEAIPQIDKYLKSSKYIAWPLQGWQATF
GGGDHPPKLEVLFQENLYFQMIIYRDLISHDEMFSDIYKIREIADGLCLEVEGKMV
SRTEGNIDDSLIGGNASAEGPEGEGTESTVITGVDIVMNHHLQETSFTKEAYKKYI
KDYMKSIKGKLEEQRPERVKPFMTGAAEQIKHILANFKNYQFFIGENMNPDGMV
ALLDYREDGVTPYMIFFKDGLEMEKC

# of amino acids – 402

Mass – 46600.74 Da

Ext. coefficient 56645

Abs 0.1% (=1 g/l) 1.216, assuming all pairs of Cys residues form cystines

Ext. coefficient 56270

Abs 0.1% (=1 g/l) 1.207, assuming all Cys residues are reduced

GST-3C-Fortilin

>MSPILGYWKIKGLVQPTRLLLEYLEEKYEEHLYERDEGDKWRNKKFEL
GLEFPNLPYYIDGDVKLTQSMAIIRYIADKHNMLGGCPKERAEISMLEGAVLDIR
YGVSRIAYSKDFETLKVDFLSKLPEMLKMFEDRLCHKTYLNGDHVTHPDFMLY
DALDVVLYMDPMCLDAFPKLVCFKKRIEAIPQIDKYLKSSKYIAWPLQGWQATF
GGGDHPPKLEVLFQMIIYRDLISHDEMFSDIYKIREIADGLCLEVEGKMVSRTEGN
IDDSLIGGNASAEGPEGEGTESTVITGVDIVMNHHLQETSFTKEAYKKYIKDYMK

SIKGKLEEQRPERVKPFMTGAAEQIKHILANFKNYQFFIGENMNPDGMVALLDY

REDGVTPYMIFFKDGLEMEKC

# of amino acids – 396

pI – 5.25

Ext. coefficient 55155

Abs 0.1% (=1 g/l) 1.204, assuming all pairs of Cys residues form cystines

Ext. coefficient 54780

Abs 0.1% (=1 g/l) 1.196, assuming all Cys residues are reduced

GST-3C-GGS-Fortilin

>MSPILGYWKIKGLVQPTRLLLEYLEEKYEEHLYERDEGDKWRNKKFEL

GLEFPNLPYYIDGDVKLTQSMAIIRYIADKHNMLGGCPKERAEISMLEGAVLDIR

YGVSRIAYSKDFETLKVDFLSKLPEMLKMFEDRLCHKTYLNGDHVTHPDFMLY

DALDVVLYMDPMCLDAFPKLVCFKKRIEAIPQIDKYLKSSKYIAWPLQGWQATF

GGGDHPPKLEVLFQGGSMIIYRDLISHDEMFSDIYKIREIADGLCLEVEGKMVSRT

EGNIDDSLIGGNASAEGPEGEGTESTVITGVDIVMNHHLQETSFTKEAYKKYIKD

YMKSIKGKLEEQRPERVKPFMTGAAEQIKHILANFKNYQFFIGENMNPDGMVAL

LDYREDGVTPYMIFFKDGLEMEKC

# of amino acids – 399

Mass – 46007.06

pI – 0.525

Ext. coefficient 55155

Abs 0.1% (=1 g/l) 1.199, assuming all pairs of Cys residues form cystines

Ext. coefficient 54780

Abs 0.1% (=1 g/l) 1.191, assuming all Cys residues are reduced

GST-3C-GGSGGS-Fortilin

>MSPILGYWKIKGLVQPTRLLLEYLEEKYEEHLYERDEGDKWRNKKFEL
GLEFPNLPYYIDGDVKLTQSMAIIRYIADKHNMLGGCPKERAEISMLEGAVLDIR
YGVSRIAYSKDFETLKVDFLSKLPEMLKMFEDRLCHKTYLNGDHVTHPDFMLY
DALDVVLYMDPMCLDAFPKLVCFKKRIEAIPQIDKYLKSSKYIAWPLQGWQATF
GGGDHPPKLEVLFQGGSGGSMIIYRDLISHDEMFSDIYKIREIADGLCLEVEGKM
VSRTEGNIDDSLIGGNASAEGPEGEGTESTVITGVDIVMNHHLQETSFTKEAYKK
YIKDYMKSIKGKLEEQRPERVKPFMTGAAEQIKHILANFKNYQFFIGENMNPDG
MVALLDYREDGVTPYMIFFKDGLEMEKC

# of amino acids – 402

pI – 5.25

Ext. coefficient 55155

Abs 0.1% (=1 g/l) 1.194, assuming all pairs of Cys residues form cystines

Ext. coefficient 54780

Abs 0.1% (=1 g/l) 1.186, assuming all Cys residues are reduced

GST-3C-GGSGGSGGS-Fortilin

>MSPILGYWKIKGLVQPTRLLLEYLEEKYEEHLYERDEGDKWRNKKFEL
GLEFPNLPYYIDGDVKLTQSMAIIRYIADKHNMLGGCPKERAEISMLEGAVLDIR
YGVSRIAYSKDFETLKVDFLSKLPEMLKMFEDRLCHKTYLNGDHVTHPDFMLY
DALDVVLYMDPMCLDAFPKLVCFKKRIEAIPQIDKYLKSSKYIAWPLQGWQATF
GGGDHPPKLEVLFQGGSGGSGGSMIIYRDLISHDEMFSDIYKIREIADGLCLEVEG
KMVSRTEGNIDDSLIGGNASAEGPEGEGTESTVITGVDIVMNHHLQETSFTKEAY

KKYIKDYMKSIKGKLEEQRPERVKPFMTGAAEQIKHILANFKNYQFFIGENMNPD

GMVALLDYREDGVTPYMIFFKDGLEMEKC

# of amino acids – 405

Mass – 46409.42

pI – 5.25

Ext. coefficient 55155

Abs 0.1% (=1 g/l) 1.188, assuming all pairs of Cys residues form cystines

Ext. coefficient 54780

Abs 0.1% (=1 g/l) 1.180, assuming all Cys residues are reduced

GGS-Fortilin

>GGSMIIYRDLISHDEMFSDIYKIREIADGLCLEVEGKMVSRTEGNIDDSLI

GGNASAEGPEGEGTESTVITGVDIVMNHHLQETSFTKEAYKKYIKDYMKSIKGK

LEEQRPERVKPFMTGAAEQIKHILANFKNYQFFIGENMNPDGMVALLDYREDGV

TPYMIFFKDGLEMEKC

# of amino acids – 175

Mass – 19796.52 Da

pI – 4.84

Extinction coefficients are in units of M^{-1} cm^{-1}, at 280 nm measured in water. No Trp residues means there can be 10% or more in error.

Ext. coefficient 12045

Abs 0.1% (=1 g/l) 0.608, assuming all pairs of Cys residues form cystines

Ext. coefficient 11920

Abs 0.1% (=1 g/l) 0.602, assuming all Cys residues are reduced

Fortilin-Strep (C-terminal StrepTactin® fusion tag)

>MIIYRDLISHDEMFSDIYKIREIADGLCLEVEGKMVSRTEGNIDDSLIGGN
ASAEGPEGEGTESTVITGVDIVMNHHLQETSFTKEAYKKYIKDYMKSIKGKLEEQ
RPERVKPFMTGAAEQIKHILANFKNYQFFIGENMNPDGMVALLDYREDGVTPY
MIFFKDGLEMEKCWSHPQFEK

# of amino acids - 180

Mass – 20,635.48 Da

pI – 4.93

Extinction coefficients are in units of M^{-1} cm^{-1}, at 280 nm measured in water.

Ext. coefficient 17545

Abs 0.1% (=1 g/l) 0.850, assuming all pairs of Cys residues form cystines

Ext. coefficient 17420

Abs 0.1% (=1 g/l) 0.844, assuming all Cys residues are reduced

Fortilin-Strep CSer46

>MIIYRDLISHDEMFSDIYKIREIADGLCLEVEGKMVSWSHPQFEKSLIGGN
ASAEGPEGEGTESTVITGVDIVMNHHLQETSFTKEAYKKYIKDYMKSIKGKLEEQ
RPERVKPFMTGAAEQIKHILANFKNYQFFIGENMNPDGMVALLDYREDGVTPY
MIFFKDGLEMEKC

# of amino acids – 172

Mass – 19374.58 Da

pI – 5.07

Extinction coefficients are in units of M^{-1} cm^{-1}, at 280 nm measured in water.

Ext. coefficient 17545Abs 0.1% (=1 g/l) 0.889, assuming all pairs of Cys residues form cystines

Ext. coefficient 17420

Abs 0.1% (=1 g/l) 0.883, assuming all Cys residues are reduced

Fortilin-Strep NSer46

>MIIYRDLISHDEMFSDIYKIREIADGLCLEVEGKMVSWSHPQFEKSLIGGN ASAEGPEGEGTESTVITGVDIVMNHHLQETSFTKEAYKKYIKDYMKSIKGKLEEQ RPERVKPFMTGAAEQIKHILANFKNYQFFIGENMNPDGMVALLDYREDGVTPY MIFFKDGLEMEKC

# of amino acids - 172

Mass – 19734.58 Da

pI – 5.07

Extinction coefficients are in units of M^{-1} cm^{-1}, at 280 nm measured in water.

Ext. coefficient 17545

Abs 0.1% (=1 g/l) 0.889, assuming all pairs of Cys residues form cystines

Ext. coefficient 17420

Abs 0.1% (=1 g/l) 0.883, assuming all Cys residues are reduced

Fortilin-Strep CGly56

>MIIYRDLISHDEMFSDIYKIREIADGLCLEVEGKMVSRTEGNIDDSLIGGN ASAEGWSHPQFEKTVITGVDIVMNHHLQETSFTKEAYKKYIKDYMKSIKGKLEE QRPERVKPFMTGAAEQIKHILANFKNYQFFIGENMNPDGMVALLDYREDGVTPY MIFFKDGLEMEKC

# of amino acids – 172

Mass – 19848.73 Da

pI – 5.16

Extinction coefficients are in units of M^{-1} cm^{-1}, at 280 nm measured in water.

Ext. coefficient 17545

Abs 0.1% (=1 g/l) 0.884, assuming all pairs of Cys residues form cystines

Ext. coefficient 17420

Abs 0.1% (=1 g/l) 0.878, assuming all Cys residues are reduced

Fortilin-Strep NGly56

>MIIYRDLISHDEMFSDIYKIREIADGLCLEVEGKMVSRTEGNIDDSLWSHP
QFEKGPEGEGTESTVITGVDIVMNHHLQETSFTKEAYKKYIKDYMKSIKGKLEEQ
RPERVKPFMTGAAEQIKHILANFKNYQFFIGENMNPDGMVALLDYREDGVTPY
MIFFKDGLEMEKC

# of amino acids – 172

Mass – 19935.77 Da

pI – 4.99

Extinction coefficients are in units of M^{-1} cm^{-1}, at 280 nm measured in water.

Ext. coefficient 17545

Abs 0.1% (=1 g/l) 0.880, assuming all pairs of Cys residues form cystines

Ext. coefficient 17420

Abs 0.1% (=1 g/l) 0.874, assuming all Cys residues are reduced

Plasmid DNA sequences

pASG-IBA3 vector (IBA LifeSciences)

Figure C1. Plasmid vector map from IBA Lifesciences (iba-lifesciences.com/details/product/5-4003-001.html)

DNA sequence:

>TCACGGATCTCCACGCGCCCTGTAGCGGCGCATTAAGCGCGGCGGGTGTGGTGGTTACGCGCAG

CGTGACCGCTACACTTGCCAGCGCCCTAGCGCCCGCTCCTTTCGCTTTCTTCCCTTCCTTTCTCGCCACGT

TCGCCGGCTTTCCCCGTCAAGCTCTAAATCGGGGGCTCCCTTTAGGGTTCCGATTTAGTGCTTTACGGCAC

CTCGACCCCAAAAAACTTGATTAGGGTGATGGTTCACGTAGTGGGCCATCGCCCTGATAGACGGTTTTTCG

CCCTTTGACGTTGGAGTCCACGTTCTTTAATAGTGGACTCTTGTTCCAAACTGGAACAACACTCAACCCTA

TCTCGGTCTATTCTTTTGATTTATAAGGGATTTTGCCGATTTCGGCCTATTGGTTAAAAAATGAGCTGATT

TAACAAAAATTTAACGCGAATTTTAACAAAATATTAACGCTTACAATTTCAGGTGGCACTTTTCGGGGAAA

TGTGCGCGGAACCCCTATTTGTTTATTTTTCTAAATACATTCAAATATGTATCCGCTCATGAGACAATAAC

CCTGATAAATGCTTCAATAATATTGAAAAAGGAAGAGTATGAGTATTCAACATTTCCGTGTCGCCCTTATT

CCCTTTTTTGCGGCATTTTGCCTTCCTGTTTTTGCTCACCCAGAAACGCTGGTGAAAGTAAAAGATGCTGA

AGATCAGTTGGGTGCACGAGTGGGTTACATCGAACTGGATCTCAACAGCGGTAAGATCCTTGAGAGTTTTC

GCCCCGAAGAACGTTTTCCAATGATGAGCACTTTTAAAGTTCTGCTATGTGGCGCGGTATTATCCCGTATT

GACGCCGGGCAAGAGCAACTCGGTCGCCGCATACACTATTCTCAGAATGACTTGGTTGAGTACTCACCAGT

CACAGAAAAGCATCTTACGGATGGCATGACAGTAAGAGAATTATGCAGTGCTGCCATAACCATGAGTGATA

ACACTGCGGCCAACTTACTTCTGACAACGATCGGAGGACCGAAGGAGCTAACCGCTTTTTTGCACAACATG

GGGGATCATGTAACTCGCCTTGATCGTTGGGAACCGGAGCTGAATGAAGCCATACCAAACGACGAGCGTGA

CACCACGATGCCTGTAGCAATGGCAACAACGTTGCGCAAACTATTAACTGGCGAACTACTTACTCTAGCTT

CCCGGCAACAATTGATAGACTGGATGGAGGCGGATAAAGTTGCAGGACCACTTCTGCGCTCGGCCCTTCCG

GCTGGCTGGTTTATTGCTGATAAATCTGGAGCCGGTGAGCGTGGCTCTCGCGGTATCATTGCAGCACTGGG

GCCAGATGGTAAGCCCTCCCGTATCGTAGTTATCTACACGACGGGGAGTCAGGCAACTATGGATGAACGAA

ATAGACAGATCGCTGAGATAGGTGCCTCACTGATTAAGCATTGGTAGGAATTAATGATGTCTCGTTTAGAT

AAAAGTAAAGTGATTAACAGCGCATTAGAGCTGCTTAATGAGGTCGGAATCGAAGGTTTAACAACCCGTAA

ACTCGCCCAGAAGCTAGGTGTAGAGCAGCCTACATTGTATTGGCATGTAAAAAATAAGCGGGCTTTGCTCG

ACGCCTTAGCCATTGAGATGTTAGATAGGCACCATACTCACTTTTGCCCTTTAGAAGGGGAAAGCTGGCAA

GATTTTTTACGTAATAACGCTAAAAGTTTTAGATGTGCTTTACTAAGTCATCGCGATGGAGCAAAAGTACA

TTTAGGTACACGGCCTACAGAAAAACAGTATGAAACTCTCGAAAATCAATTAGCCTTTTTATGCCAACAAG

GTTTTTCACTAGAGAATGCATTATATGCACTCAGCGCAGTGGGGCATTTTACTTTAGGTTGCGTATTGGAA

GATCAAGAGCATCAAGTCGCTAAAGAAGAAAGGGAAACACCTACTACTGATAGTATGCCGCCATTATTACG

ACAAGCTATCGAATTATTTGATCACCAAGGTGCAGAGCCAGCCTTCTTATTCGGCCTTGAATTGATCATAT

GCGGATTAGAAAAACAACTTAAATGTGAAAGTGGGTCTTAAAAGCAGCATAACCTTTTTCCGTGATGGTAA

CTTCACTAGTTTAAAAGGATCTAGGTGAAGATCCTTTTTGATAATCTCATGACCAAAATCCCTTAACGTGA

GTTTTCGTTCCACTGAGCGTCAGACCCCGTAGAAAAGATCAAAGGATCTTCTTGAGATCCTTTTTTTCTGC

GCGTAATCTGCTGCTTGCAAACAAAAAAACCACCGCTACCAGCGGTGGTTTGTTTGCCGGATCAAGAGCTA

CCAACTCTTTTTCCGAAGGTAACTGGCTTCAGCAGAGCGCAGATACCAAATACTGTCCTTCTAGTGTAGCC

GTAGTTAGGCCACCACTTCAAGAACTCTGTAGCACCGCCTACATACCTCGCTCTGCTAATCCTGTTACCAG

TGGCTGCTGCCAGTGGCGATAAGTCGTGTCTTACCGGGTTGGACTCAAGACGATAGTTACCGGATAAGGCG

CAGCGGTCGGGCTGAACGGGGGGTTCGTGCACACAGCCCAGCTTGGAGCGAACGACCTACACCGAACTGAG

ATACCTACAGCGTGAGCTATGAGAAAGCGCCACGCTTCCCGAAGGGAGAAAGGCGGACAGGTATCCGGTAA

GCGGCAGGGTCGGAACAGGAGAGCGCACGAGGGAGCTTCCAGGGGGAAACGCCTGGTATCTTTATAGTCCT

GTCGGGTTTCGCCACCTCTGACTTGAGCGTCGATTTTTGTGATGCTCGTCAGGGGGGCGGAGCCTATGGAA

AAACGCCAGCAACGCGGCCTTTTTACGGTTCCTGGCCTTTTGCTGGCCTTTTGCTCACATGACCCGACACC

ATCGAATGGCCAGATGATTAATTCCTAATTTTTGTTGACACTCTATCATTGATAGAGTTATTTTACCACTC

CCTATCAGTGATAGAGAAAAGTGAAATGAATAGTTCGACAAAAATCTAGAAATAATTTTGTTTAACTTTAA

GAAGGAGATATACAAATGAGAGACGCTGCAGCCCAATACGCAAACCGCCTCTCCCCGCGCGTTGGCCGATT

CATTAATGCAGCTGGCACGACAGGTTTCCCGACTGGAAAGCGGGCAGTGAGCGCAACGCAATTAATGTGAG

TTAGCTCACTCATTAGGCACCCCAGGCTTTACACTTTATGCTTCCGGCTCGTATGTTGTGTGGAATTGTGA

GCGGATAACAATTTCACACAGGAAACAGCTATGACCATGATTACGCCAAGCTCGAAATTAACCCTCACTAA

AGGGAACAAAAGCTGGAGCTCCACCGCGGTGGCGGCCGCTCTAGAACTAGTGGATCCCCCGGGCTGCAGGA

ATTCGATATCAAGCTTATCGATACCGTCGACCTCGAGGGGGGGCCCGGTACCCAATTCGCCCTATAGTGAG

TCGTATTACAATTCACTGGCCGTCGTTTTACAACGTCGTGACTGGGAAAACCCTGGCGTTACCCAACTTAA

TCGCCTTGCAGCACATCCCCCTTTCGCCAGCTGGCGTAATAGCGAAGAGGCCCGCTCCTTTCGCTTTCTTC

CCTTCCTTTCTCGCCACGTTCGCCGGCTTTCCCCGTCAAGCTCTAAATCGGGGGCTCCCTTTAGGGTTCCG

ATTTAGTGCTTTACGGCACCTCGACCCCAAAAAACTTGATTAGGGTGATGGTTCACCTCGAGCGTCTCAGG

GAGCGCTTGGAGCCACCCGCAGTTCGAAAAATAAGGGAGCCACCCGCAAGCTTGACCTGTGAAGTGAAAAA

TGGCGCACATTGTGCGACATTTTTTTTGTCTGCCGTTTACCGCTACTGCG

pD441-SR Vector (ATUM)

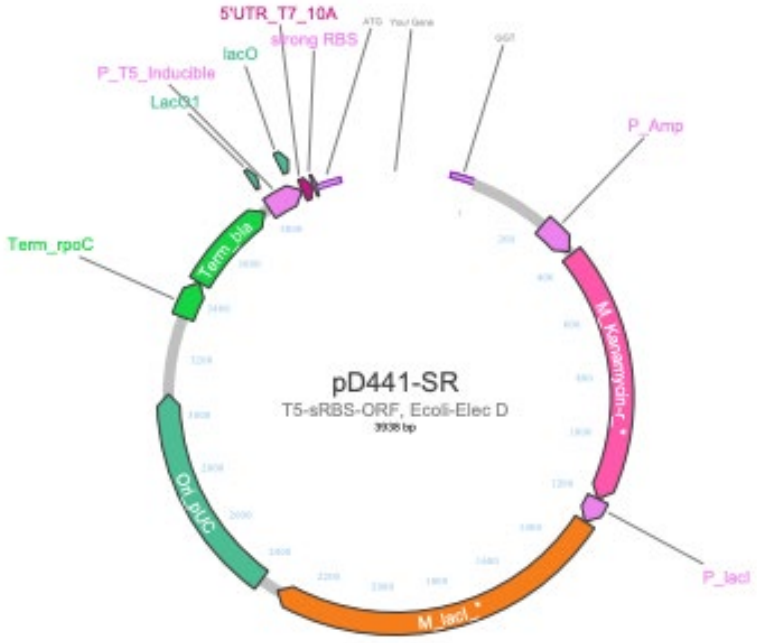

Figure C2. pD441-SR plasmid vector map from ATUM (https://www.atum.bio/eCommerce/catalog/datasheet/117).

DNA sequence:

```
> 1 CCCGTAGAAA AGATCAAAGG ATCTTCTTGA GATCCTTTTT TTCTGCGCGT AATCTGCTGC

    61 TTGCAAACAA AAAAACCACC GCTACCAGCG GTGGTTTGTT TGCCGGATCA

AGAGCTACCA

    121 ACTCTTTTTC CGAAGGTAAC TGGCTTCAGC AGAGCGCAGA TACCAAATAC

TGTTCTTCTA

    181 GTGTAGCCGT AGTTAGCCCA CCACTTCAAG AACTCTGTAG CACCGCCTAC

ATACCTCGCT

    241 CTGCTAATCC TGTTACCAGT GGCTGCTGCC AGTGGCGATA AGTCGTGTCT

TACCGGGTTG

    301 GACTCAAGAC GATAGTTACC GGATAAGGCG CAGCGGTCGG GCTGAACGGG

GGGTTCGTGC
```

361 ACACAGCCCA GCTTGGAGCG AACGACCTAC ACCGAACTGA GATACCTACA GCGTGAGCTA

421 TGAGAAAGCG CCACGCTTCC CGAAGGGAGA AAGGCGGACA GGTATCCGGT AAGCGGCAGG

481 GTCGGAACAG GAGAGCGCAC GAGGGAGCTT CCAGGGGGAA ACGCCTGGTA TCTTTATAGT

541 CCTGTCGGGT TTCGCCACCT CTGACTTGAG CGTCGATTTT TGTGATGCTC GTCAGGGGGG

601 CGGAGCCTAT GGAAAAACGC CAGCAACGCG GCCTTTTTAC GGTTCCTGGC CTTTTGCTGG

661 CCTTTTGCTC ACATGTTCTT TCCTGCGTTA TCCCCTGATT CTGTGGATAA CCGTATTACC

721 GCCTTTGAGT GAGCTGATAC CGCTCGCCGC AGCCGAACGA CCGAGCGCAG CGAGTCAGTG

781 AGCGAGGAAG CGGAAGGCGA GAGTAGGGAA CTGCCAGGCA TCAAACTAAG CAGAAGGCCC

841 CTGACGGATG GCCTTTTTGC GTTTCTACAA ACTCTTTCTG TGTTGTAAAA CGACGGCCAG

901 TCTTAAGCTC GGGCCCCCTG GGCGGTTCTG ATAACGAGTA ATCGTTAATC CGCAAATAAC

961 GTAAAAACCC GCTTCGGCGG GTTTTTTTAT GGGGGGAGTT TAGGGAAAGA GCATTTGTCA

1021 GAATATTTAA GGGCGCCTGT CACTTTGCTT GATATATGAG AATTATTTAA CCTTATAAAT

1081 GAGAAAAAAG CAACGCACTT TAAATAAGAT ACGTTGCTTT TTCGATTGAT GAACACCTAT

1141 AATTAAACTA TTCATCTATT ATTTATGATT TTTTGTATAT ACAATATTTC TAGTTTGTTA

1201 AAGAGAATTA AGAAAATAAA TCTCGAAAAT AATAAAGGGA AAATCAGTTT
TTGATATCAA

1261 AATTATACAT GTCAACGATA ATACAAAATA TAATACAAAC TATAAGATGT
TATCAGTATT

1321 TATTATGCAT TTAGAATAAA TTTTGTGTCG CCCTTAATTG TGAGCGGATA
ACAATTACGA

1381 GCTTCATGCA CAGTGAAATC ATGAAAAATT TATTTGCTTT GTGAGCGGAT
AACAATTATA

1441 ATATGTGGAA TTGTGAGCGC TCACAATTCC ACAACGGTTT CCCTCTAGAA
ATAATTTTGT

1501 TTAACTTTTA AGGAGGTAAA AAATGATTAT CTACCGTGAT TTGATTAGCC
ACGACGAAAT

1561 GTTTAGCGAT ATCTACAAGA TCCGCGAGAT CGCAGACGGC CTGTGCCTCG
AAGTTGAGGG

1621 TAAAATGGTG TCTCGTACCG AAGGCAATAT CGACGATTCC CTGATCGGCG
GCAATGCGAG

1681 CGCCGAGGGT TGGAGCCATC CGCAAGGTCA GAAAACCGTT ATCACGGGTG
TCGATATTGT

1741 CATGAACCAC CATCTGCAGG AAACCAGCTT TACTAAAGAG GCGTACAAAA
AGTACATTAA

1801 AGACTACATG AAAAGCATTA AGGGCAAACT GGAAGAACAG CGCCCAGAGC
GTGTGAAGCC

1861 GTTTATGACC GGTGCGGCAG AGCAAATCAA GCACATTCTG GCTAACTTTA
AGAACTATCA

1921 ATTCTTCATT GGTGAGAACA TGAATCCGGA CGGTATGGTT GCGCTGCTGG
ATTATCGTGA

1981 GGACGGTGTG ACGCCGTATA TGATTTTCTT CAAAGATGGC CTGGAAATGG
AAAAGTGTTA

2041 ATAAGGTTGA CCCCAAGGGC GACACCCCCT AATTAGCCCG GGCGAAAGGC
CCAGTCTTTC

2101 GACTGAGCCT TTCGTTTTAT TTGATGCCTG GCAGTTCCCT ACTCTCGCAT
GGGGAGTCCC

2161 CACACTACCA TCGGCGCTAC GGCGTTTCAC TTCTGAGTTC GGCATGGGGT
CAGGTGGGAC

2221 CACCGCGCTA CTGCCGCCAG GCAAACAAGG GGTGTTATGA GCCATATTCA
GGTATAAATG

2281 GGCTCGCGAT AATGTTCAGA ATTGGTTAAT TGGTTGTAAC ACTGACCCCT
ATTTGTTTAT

2341 TTTTCTAAAT ACATTCAAAT ATGTATCCGC TCATGAGACA ATAACCCTGA
TAAATGCTTC

2401 AATAATATTG AAAAAGGAAG AATATGAGCC ATATTCAACG GGAAACGTCG
AGGCCGCGAT

2461 TAAATTCCAA CATGGATGCT GATTTATATG GGTATAAATG GGCTCGCGAT
AATGTCGGGC

2521 AATCAGGTGC GACAATCTAT CGCTTGTATG GGAAGCCCGA TGCGCCAGAG
TTGTTTCTGA

2581 AACATGGCAA AGGTAGCGTT GCCAATGATG TTACAGATGA GATGGTCAGA
CTAAACTGGC

2641 TGACGGAATT TATGCCACTT CCGACCATCA AGCATTTTAT CCGTACTCCT
GATGATGCAT

2701 GGTTACTCAC CACTGCGATC CCCGGAAAAA CAGCGTTCCA GGTATTAGAA
GAATATCCTG

2761 ATTCAGGTGA AAATATTGTT GATGCGCTGG CAGTGTTCCT GCGCCGGTTG
CACTCGATTC

2821 CTGTTTGTAA TTGTCCTTTT AACAGCGATC GCGTATTTCG CCTCGCTCAG
GCGCAATCAC

2881 GAATGAATAA CGGTTTGGTT GATGCGAGTG ATTTTGATGA CGAGCGTAAT GGCTGGCCTG

2941 TTGAACAAGT CTGGAAAGAA ATGCATAAAC TTTTGCCATT CTCACCGGAT TCAGTCGTCA

3001 CTCATGGTGA TTTCTCACTT GATAACCTTA TTTTTGACGA GGGGAAATTA ATAGGTTGTA

3061 TTGATGTTGG ACGAGTCGGA ATCGCAGACC GATACCAGGA TCTTGCCATC CTATGGAACT

3121 GCCTCGGTGA GTTTTCTCCT TCATTACAGA AACGGCTTTT TCAAAAATAT GGTATTGATA

3181 ATCCTGATAT GAATAAATTG CAGTTTCATT TGATGCTCGA TGAGTTTTTC TAAGCGGCGC

3241 GCCATCGAAT GGCGCAAAAC CTTTCGCGGT ATGGCATGAT AGCGCCCGGA AGAGAGTCAA

3301 TTCAGGGTGG TGAATATGAA ACCAGTAACG TTATACGATG TCGCAGAGTA TGCCGGTGTC

3361 TCTTATCAGA CCGTTTCCCG CGTGGTGAAC CAGGCCAGCC ACGTTTCTGC GAAAACGCGG

3421 GAAAAAGTGG AAGCGGCGAT GGCGGAGCTG AATTACATTC CCAACCGCGT GGCACAACAA

3481 CTGGCGGGCA AACAGTCGTT GCTGATTGGC GTTGCCACCT CCAGTCTGGC CCTGCACGCG

3541 CCGTCGCAAA TTGTCGCGGC GATTAAATCT CGCGCCGATC AACTGGGTGC CAGCGTGGTG

3601 GTGTCGATGG TAGAACGAAG CGGCGTCGAA GCCTGTAAAG CGGCGGTGCA CAATCTTCTC

3661 GCGCAACGCG TCAGTGGGCT GATCATTAAC TATCCGCTGG ATGACCAGGA TGCCATTGCT

3721 GTGGAAGCTG CCTGCACTAA TGTTCCGGCG TTATTTCTTG ATGTCTCTGA CCAGACACCC

3781 ATCAACAGTA TTATTTTCTC CCATGAGGAC GGTACGCGAC TGGGCGTGGA GCATCTGGTC

3841 GCATTGGGTC ACCAGCAAAT CGCGCTGTTA GCGGGCCCAT TAAGTTCTGT CTCGGCGCGT

3901 CTGCGTCTGG CTGGCTGGCA TAAATATCTC ACTCGCAATC AAATTCAGCC GATAGCGGAA

3961 CGGGAAGGCG ACTGGAGTGC CATGTCCGGT TTTCAACAAA CCATGCAAAT GCTGAATGAG

4021 GGCATCGTTC CCACTGCGAT GCTGGTTGCC AACGATCAGA TGGCGCTGGG CGCAATGCGC

4081 GCCATTACCG AGTCCGGGCT GCGCGTTGGT GCGGATATCT CGGTAGTGGG ATACGACGAT

4141 ACCGAAGATA GCTCATGTTA TATCCCGCCG TTAACCACCA TCAAACAGGA TTTTCGCCTG

4201 CTGGGGCAAA CCAGCGTGGA CCGCTTGCTG CAACTCTCTC AGGGCCAGGC GGTGAAGGGC

4261 AATCAGCTGT TGCCAGTCTC ACTGGTGAAA AGAAAAACCA CCCTGGCGCC CAATACGCAA

4321 ACCGCCTCTC CCCGCGCGTT GGCCGATTCA TTAATGCAGC TGGCACGACA GGTTTCCCGA

4381 CTGGAAAGCG GGCAGTGACT CATGACCAAA ATCCCTTAAC GTGAGTTACG CGCGCGTCGT

4441 TCCACTGAGC GTCAGAC

APPENDIX D

Filenames and parameters for NMR experiments

Table D1. Filenames and parameters for NMR experiments.

Filename	B_0	ns	td1	td2	d1	T
15N_fortilin_20mMTrisHCl_Ca_18102019_MSC	600	8	2048	400	1	308
15N_fortilin_50mMNaCl_Hemin_21012020_MSC	600	16	2048	400	1	308
15N_fortilin_50mMNaCl_Hemin11CO9_24012020	600	8	2048	400	1	308
15N_fortilin_50mMNaCl_HeminDHA_22012020_MSC	600	8	2048	400	1	308
15N_fortilin007_A26A3Titr_10May2021_MSC	600	16	2048	400	1	298
15N_fortilinstrep004_ArtTitr_03May2021_MSC	600	16	2048	400	1	298
15Nfortilin50mMNaCl_DHA_17092019mc	600	8	2048	400	1	308
Lisa_004-TCTP_210427	800	16	2048	400	1	298

B0 – static magnetic field strength in MHz

ns – number of scans

td1 – number of FID points in proton frequency

td1 – number of FID points in nitrogen frequency

d1 – interscan delay

T – temperature (K)